Elite Master Course
Theoretical and Mathematical Physics

LMU LUDWIG-MAXIMILIANS-UNIVERSITÄT MÜNCHEN

Master's Thesis

Finding Stationary States by Interacting Quantum Worlds

Hannes Herrmann

Elite Master Course
Theoretical and Mathematical Physics

LMU LUDWIG-MAXIMILIANS-UNIVERSITÄT MÜNCHEN

Ludwig-Maximilians-Universität München

Finding Stationary States by Interacting Quantum Worlds

Vorgelegt von:
Hannes Herrmann
geboren in Öhringen
Matrikelnummer 10359262

Betreuer:
Dr. Dirk-André Deckert

München, den 22. Dezember 2016

Contents

1. Introduction

Since the beginning of quantum theory in the early 20th century, quantum mechanics has proven to be one of the most fruitful theories within physics. From calculating atomic orbitals to describing superconducting magnets, its practical usage today cannot be overestimated. Besides its broad practical applications, quantum mechanics has revolutionized the way we think about nature, and raised new fundamental questions. Many of them are still a controversial topic in physics.

Despite its huge success, obtaining solutions for the fundamental equation of quantum mechanics, the Schrödinger equation, remains surprisingly hard. Only in simple situations analytic solutions are known and numerical computations are limited to a small number of particles. In fact, whole fields in physics and chemistry have been developed to find useful approximations to solutions of the Schrödinger equation or to develop much simpler effective descriptions of quantum systems in order to avoid solving the full Schrödinger equation. One prominent field is quantum chemistry, which focuses on the description of atoms and molecules and is in particular interested in solutions of the stationary Schrödinger equation and their respective energy levels.

For example, for the study of stationary states of many-electron systems such as molecules, the Hartree-Fock method or density functional theory are commonly employed and often provide good predictions in quantum chemistry. Yet, these kind of approximation methods only work well in certain regimes as main parts of the electron interactions including entanglement are neglected. In other regimes where these interactions become important and the full Schrödinger equation has to be considered, conventional methods already reach their limit when calculating systems of three particles. Thus, finding new numerical methods for such cases is of high interest for both chemistry and physics and has even led to new approaches beyond the usage of conventional computers, such as quantum computers. In fact, the goal of solving many particle quantum systems has been one of the driving forces behind the development of quantum computing.

In this thesis we investigate a new computational approach to obtaining solutions for the stationary Schrödinger equation by modeling quantum systems with many interacting quantum worlds (MIW), a concept which was introduced by Hall, Deckert and Wiseman [1] in 2014. They proposed a fully mechanical theory of finitely many "particles" called *worlds* in configuration space $\mathbb{R}^{3n}$ of n physical particles in order to model quantum phenomena without any reference to a wave function. Instead of a wave function, quantum effects are modeled by a direct interaction between these worlds called *interworld interaction*. Statistical properties of the quantum system such as expectation values are obtained by ensemble averages over a finite number of worlds, and for an infinite number ordinary quantum mechanics is recovered as a continuum limit.

For computational modeling of quantum systems such a purely mechanical model is supposed to have significant advantages, since only world positions and velocities have to be saved in order to represent the quantum system. By modifying the number of worlds this approach should give fine grained control over the approximation to a full quantum system. Even further, Hall et al. [1] hope

that the exponential scaling of naive grid methods in the number of physical particles n could be avoided.

Although Hall et al. could reproduce some generic quantum mechanical effects, such as Ehrenfest's theorem, dispersion, barrier tunneling, and zero-point energy, only a one-dimensional model was introduced explicitly, leaving the question of the general strategy to find approximate solutions of the Schrödinger equation, in particular for higher spatial dimensions, open.

The objective of this thesis is to examine different interworld interaction models for the computation of stationary states of quantum systems, for which explicit solutions are accessible to do qualitative error analysis. For the one-dimensional case it is demonstrated how this approach can be used to compute not only ground states, as originally proposed in [1], but also excited states. Furthermore, it is attempted to generalize the developed techniques to two spatial dimensions, however, with only qualitative and no quantitative results. A detailed discussion of the difficulties in this extension to higher dimensions is provided.

This thesis is structured as follows. In this first chapter we will introduce the fundamental concepts of modeling quantum systems by many interacting worlds. But to tell the full story we will start with examining general difficulties in solving the Schrödinger equation numerically. This will lead us to the notion of quantum trajectories, and their useful property equivariance, which can be exploited to improve conventional grid methods used by numerical integrators of the Schrödinger equation. From there we will outline a systematic way of how to construct a fully mechanical theory modeling quantum phenomena without any explicit integration of fields or a wave function. Subsequently, an algorithm for the calculation of ground states is provided.

Chapter 2 will continue with the explicit construction of interworld interaction models in one dimension. First, we will reexamine the one-dimensional toy model proposed by Hall et al. [1] and calculate the ground state of a simple quantum system in order to familiarize ourselves with the basic notions of a MIW model. Afterwards, we will construct and examine alternative models with potential generalizations to higher dimensions and compare them to the original MIW approach. Besides calculating ground states, also a detailed analysis of excited states is provided, for which an extension to the ground state algorithm, presented in this chapter, will be developed.

In chapter 3 we will continue with generalizations to the higher dimensional case. There, different natural candidates for an interworld interaction in two dimensions will be introduced and the conceptual differences to the one-dimensional case will be discussed. Due to arising difficulties in two dimensions, we will analyze the problems of the different models under consideration, and try to identify possible routes to reconcile them.

1.1. The challenge of solving the Schrödinger equation

In order to illustrate the computational challenges, we consider the Schrödinger equation[1] of n spinless particles in d dimensions with a generic time-independent interaction potential V [2]

$$\mathrm{i}\partial_t \Psi_t(\mathbf{x_1}, \dots, \mathbf{x_n}) = \left(\sum_{i=1}^{n} -\frac{\Delta_i}{2} + V(\mathbf{x_1}, \dots, \mathbf{x_n}) \right) \Psi_t(\mathbf{x_1}, \dots, \mathbf{x_n}) \,. \tag{1.1}$$

For the full dynamical problem, the object of interest is the calculation of the time dependent wave function $\Psi_t \in \mathcal{L}^2(\mathbb{R}^{dn})$, which solves equation (1.1) for a given initial wave faction Ψ_0. If V is not of a particular simple form, explicit solutions are intractable and the objective is to find numerical approximations. For partial differential equations, such as the Schrödinger equation, there are in general many integration schemes available. They usually involve a discretization of time and space coordinates and discrete approximation of differential operators. For example in one dimension with a discretization of space in form of a uniform grid

$$\begin{aligned} &\psi(x) \longrightarrow \psi_i = \psi(x_i) \\ &x_i = x_0 + ih \quad i = 1, \dots, N \\ &\Delta\psi(x_i) \approx \frac{\psi_{i+1} + \psi_{i-1} - 2\psi_i}{h^2} \end{aligned} \tag{1.2}$$

could be used to represent the wave function and differential operators as finite differences. A standard method to solve the time-dependent Schrödinger equation in this manner is given by the Crank-Nickolson method [2], which can be seen as an implicit Runge-Kutta method of second order in time.

In order to have a feasible approximation to the continuum case, the resolution of the wave function has to be high enough. That is, the number of grid points N has to be sufficiently large and the distance between grid points h has to be sufficiently small. For one particle in one dimension this poses no problem, since computational resources are more than sufficient to achieve a good enough resolution. However, considering higher dimensions or an increasing number n of particles, the number of necessary grid points explodes as N^{nd}, because it scales exponentially with the number of particles n and dimension d. This scaling behaviour is due to the fact that the wave function is a field on configuration space $\mathbb{R}^{nd}$, which even after discretization remains a very high dimensional object. Classical fields, like the electric field, are much easier to represent, since they are fields on physical space, which is only a three-dimensional space.

With this scaling one easily runs into limitations of available computer memory. For example, for a system of $n = 3$ particles in $d = 3$ dimensions, a resolution of $N = 100$ grid points in each dimension of configuration space corresponds to a total amount of 1.45×10^7 Tbytes using double precision. For comparison the SuperMuc of the Leibniz Supercomputing Centre in Garching, one of the fastest supercomputers in Europe, has 540 Tbyte of memory space available in total [3], clearly insufficient for this system. In contrast, only $2dn = 18$ phase space coordinates would be sufficient to represent a similar system in classical mechanics, which corresponds to only 144 Bytes.

[1] For now we will consider the full dynamical problem, because it allows for a straightforward approach to a many interacting worlds model. Yet, the computational difficulties, discussed in the following, also apply to the stationary Schrödinger equation.

[2] Throughout this thesis we use $m = \hbar = 1$.

Nevertheless, many useful predictions can be obtained by reducing the full n-particle Schrödinger equation to the one-particle case. This usually involves some approximation of the interaction potential, for example neglecting electron-electron interactions in atomic orbitals or a mean-field approximation such as in the Hartree-Fock case.

Although for many situations there are sufficient approximation methods to solutions of the Schrödinger equation, there exist certain regimes for which these methods fail. This is typical the case when quantum entanglement or superposition plays a significant role as it is the case for numerous examples in quantum chemistry such as binding modes of molecules. In these situations it is desirable to obtain estimates considering the full Schrödinger equation.

1.2. Bohmian grids

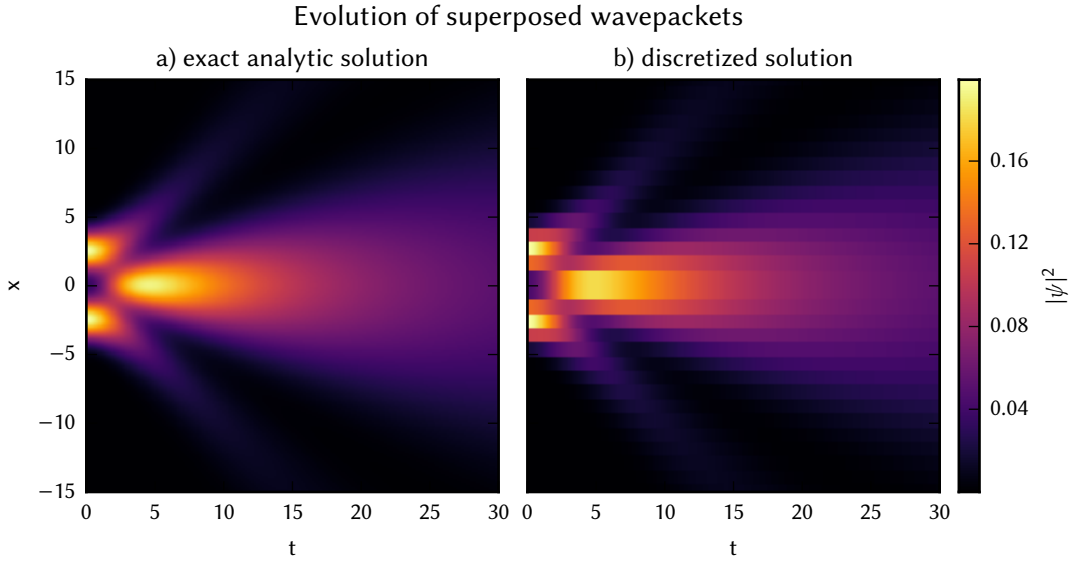

Figure 1.1.: a) Exact analytic solution of two superposed Gaussian wave packets under free time evolution. b) Manually discretized version of the analytic solution in space according to Equation (1.2) with $N = 30$ grid points. The evenly spaced grid points sample the wave function very inefficiently. In regions of high density the resolution is very crude, whereas a lot of grid points are wasted to sample regions of very low density.

Until now we only discussed a very naive approach of an evenly spaced grid in configuration space. Figure 1.1 illustrates such an approach for the evolution of two superposed Gaussian wave packets in one dimension and compares the continuum Schrödinger evolution with a discretized version. The left plot shows the exact analytic free time evolution and for the right plot the discretization procedure of (1.2) has been applied in a very coarse manner to illustrate the loss in accuracy by moving to an evenly spaced grid in space. In order to focus on discretization issues in space, the time variable has not been discretized.

For regions of interest, i.e. regions of high density, the resolution of the wave function is very coarse. Details around the maximum of the constructive interference around $x = 0$ are lost, whereas a lot

of grid points lie in regions of very low density (black regions). In order to improve the resolution in the center, one is forced to introduce a lot of grid points in regions of very low density, which are physically not interesting. This is especially bad if the domain of interest in physical space is very big, as it is the case for long-time simulations such as scattering situations. Due to the bad scaling behaviour in higher dimensions, the number of grid points is also strongly limited, such that these systems cannot be handled.

In other words, the evenly spaced fixed grid wastes a lot of grid points for regions of low density, and thereby samples the wave function in a very inefficient way. Of course, one could try to refine the fixed grid manually in order to focus on regions of high density. However, such a refined fixed grid would have to be adjusted repeatedly to the current state of the density in order to ensure good resolution, which does not significantly improve the situation. The question arises, if there are better ways to sample the wave function. That is, if there is a more flexible "comoving" grid, which adapts itself automatically to the wave function in order to focus on regions of higher density.

1.2.1. Short introduction to Bohmian trajectories

The question of a better suited comoving grid has been addressed by Wyatt et al. [4]. They introduced the idea of using Bohmian trajectories, a concept from Bohmian mechanics, as a candidate for such a grid, since these trajectories tend to stay in regions of high density very naturally.

In contrast to ordinary quantum mechanics, Bohmian mechanics is a mechanical quantum theory in the sense that it describes n particles and their motion in Galilean space time. This motion is governed by a vector field which is a functional of the wave function. We will investigate different properties of these particle trajectories and use them to construct a grid that adapts itself to the wave function. But first a very short introduction to the theory is in order; a more detailed description can be found in [5].

For n spin-less particles in d dimensions $\mathbf{q}_1, \dots, \mathbf{q}_n \in \mathbb{R}^d$ the set of all particle positions is denoted by $\mathbf{Q} = (\mathbf{q}_1, \dots, \mathbf{q}_n) \in \mathbb{R}^{dn}$.[3] The dynamics of the particles is governed by a wave function

$$\begin{array}{rccc} \Psi_t & : & \mathbb{R}^{dn} & \longrightarrow & \mathbb{C} \\ & & (\mathbf{x}_1, \dots, \mathbf{x}_n) & \longmapsto & \Psi_t(\mathbf{x}_1, \dots, \mathbf{x}_n) \end{array},$$

which defines a vector field

$$\mathbf{v}^{\Psi_t}(\mathbf{X}) = \Im \frac{\nabla \Psi_t}{\Psi_t}(\mathbf{X}) \tag{1.3}$$

on configuration space. The wave function in turn obeys the Schrödinger equation. Thus the dynamics of the whole system is given by

$$\mathrm{i}\partial_t \Psi_t(\mathbf{X}) = \left(\sum_{i=1}^{n} -\frac{\Delta_i}{2} + V(\mathbf{X}) \right) \Psi_t(\mathbf{X}) \tag{1.4}$$

$$\dot{\mathbf{Q}}(t) = \mathbf{v}^{\Psi_t}(\mathbf{Q}(t)) = \Im \frac{\nabla \Psi_t}{\Psi_t}(\mathbf{Q}(t)), \tag{1.5}$$

[3] In contrast to the actual particle position, arguments of functions on configurations space will be denoted by $\mathbf{X} = (\mathbf{x}_1, \dots, \mathbf{x}_n) \in \mathbb{R}^{dn}$.

where equation (1.5) is called the Bohmian guiding law.

An important aspect of equation (1.5) is that it is an ODE of first order. Consequently, given a solution of the Schrödinger equation Ψ_t, sufficient initial conditions for the particle motions are given by an initial configuration $\mathbf{Q}_0$ at $t = 0$, whereas in classical mechanics the initial momenta of the particles also have to be specified. Hence, the "state" of the system is uniquely specified by all its particle positions alone. This is the motivation for introducing the term *world* for the set $\mathbf{Q}$ of all realized particle positions in physical space and *world trajectory* for a solution $(t \to \mathbf{Q}(t))_{t\in\mathbb{R}}$, which incorporates all particle trajectories of the n-particle system. A world $\mathbf{Q}$ represents all particle positions as one point in configuration space, in a similar way as a point in phase space specifies the state of a system in classical mechanics, which could be called "classical world".

Another consequence of the first order ODE is that different solutions of (1.5), i.e. solutions of different initial conditions $\mathbf{Q}_0$, *cannot cross* in configuration space[4]. To see this, consider two trajectories solving (1.5) with different initial conditions at $t_0 = 0$, but crossing each other at some point in time $t_1 > t_0$. If one started the dynamics from this point in time, both trajectories would have the same initial condition for the ODE (1.5) at t_1 and thus coincide for all other times due to uniqueness of solutions contradicting the different initial conditions at t_0. That is, two trajectories cannot cross each other, otherwise they would have to be the same solution to the guiding law. Although this seems trivial, this non-crossing of world trajectories in configuration space is an important property, which has to be respected when introducing numerical approximations.

The second important property of world trajectories is the notion of *equivariance*, which originates from statistical analysis of Bohmian mechanics. In short, equivariance means that if an *ensemble of worlds*[5] $\mathbf{Q}_1(t_0), \dots, \mathbf{Q}_N(t_0)$ is distributed with respect to the $|\Psi_{t_0}|^2$-measure in configuration space at some initial time t_0 and their trajectories obey the Bohmian guiding law, then the ensemble $\mathbf{Q}_1(t), \dots, \mathbf{Q}_N(t)$ stays $|\Psi_t|^2$ distributed for all times t. Due to its significance a proof can be found in appendix A.1.

As an example, figure 1.2 a) shows an ensemble of different world trajectories for the simple one-dimensional system of two superposed wave packets, the same system as in figure 1.1. Since the worlds are $|\Psi|^2$-distributed at $t = 0$, the worlds stay $|\Psi|^2$-distributed for all times due to the equivariance property. This guarantees that world trajectories stay in regions, where the density is high and regions of a very low density $|\Psi|^2$ tend to be neglected. Additionally, the non-crossing behaviour of world trajectories can be observed.

Now the idea is to use the property of equivariance to sample the wave function along world trajectories in contrast to the naive approach of an evenly spaced grid. Figure 1.2 b) illustrates this procedure. It shows the exact analytic free time evolution of figure 1.1 manually discretized along Bohmian trajectories. Note how the same number of trajectories as grid points in figure 1.1, $N = 30$, is able to capture a lot more details and the grid has a good resolution in regions of high density, especially in regions around the maximum at $x = 0$.

[4] Of course particle trajectories in physical space can still cross.
[5] not to be confused with an ensemble of particles in physical space

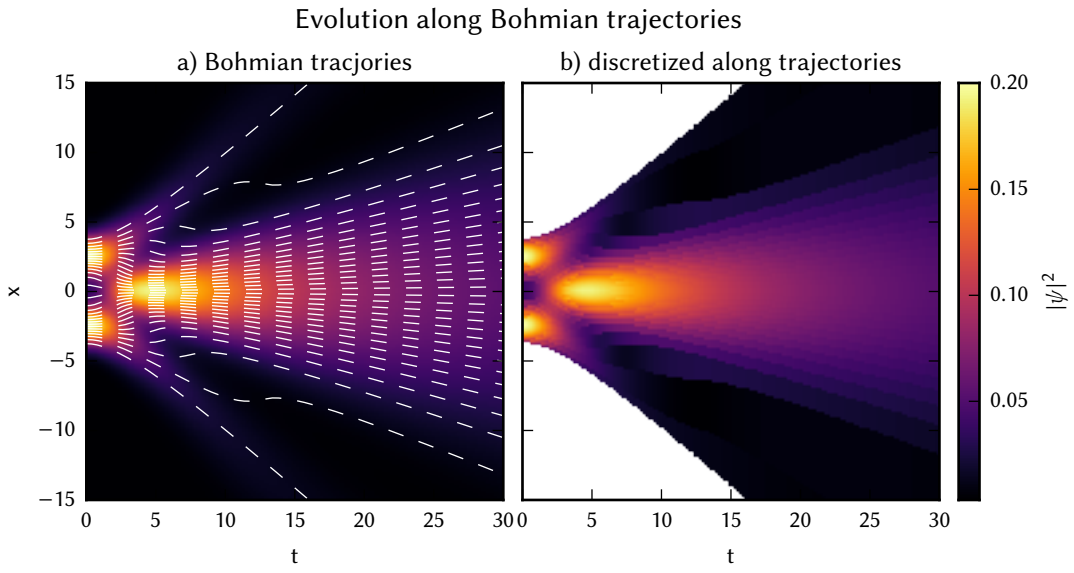

Figure 1.2.: a) Density plot of two superposed one-dimensional Gaussian wave packets under free time evolution with corresponding Bohmian world trajectories. b) Manually discretized version of the analytic solution along the Bohmian trajectories. Since worlds are $|\Psi|^2$-distributed at the beginning, due to equivariance they stay $|\Psi|^2$-distributed for all times. They stay in regions, where density is high and therefore sample the wave function in a more efficient way. In both plots $N = 30$ worlds were used, the same for the even grid in figure 1.1.

1.2.2. Hydrodynamical formulation of Bohmian mechanics

So far we argued why quantum trajectories could be a useful tool for solving the Schrödinger equation numerically and examined their properties within Bohmian mechanics. However, in order to solve for world trajectories, the Bohmian guiding law (1.5) has to be reformulated, because it already requires a solution of the Schrödinger equation. In contrast, we seek a formulation, which allows us to calculate both world trajectories and wave function "on the fly". Wyatt et al. [4] call this the *synthetic approach*.

First we introduce two real functions, probability density P_t and phase S_t with the help of the modulus and the argument of the wave function,

$$\begin{aligned} P_t(\mathbf{X}) &:= |\Psi_t(\mathbf{X})|^2 \\ S_t(\mathbf{X}) &:= \arg\left(\Psi_t(\mathbf{X})\right) \end{aligned} \tag{1.6}$$

to rewrite Ψ in *polar form*

$$\Psi_t = P_t^{1/2} \exp \mathrm{i} S_t \,. \tag{1.7}$$

Using the Schrödinger equation and sorting by real and imaginary part, we get two coupled partial differential equations

$$\partial_t P_t(\mathbf{X}) = -\nabla(P_t(\mathbf{X})\nabla S_t(\mathbf{X})) \tag{1.8}$$

$$\partial_t S_t(\mathbf{X}) = -\frac{1}{2}(\nabla S_t(\mathbf{X}))^2 - V(\mathbf{X}) - U_t(\mathbf{X})\,, \tag{1.9}$$

where U is the *quantum potential* given by

$$U_t = -\frac{1}{2} P_t^{-1/2} \Delta P_t^{1/2} \tag{1.10}$$

$$= -\frac{1}{4}\left[\frac{\Delta P_t}{P_t} - \frac{1}{2}\frac{\nabla P_t \cdot \nabla P_t}{P_t^2}\right]. \tag{1.11}$$

Equation (1.8) is the well-known continuity equation, whereas equation (1.9) is very similar to the Hamilton-Jacobi formulation of classical mechanics. The only difference is introduced by the additional quantum potential U. Furthermore, the Bohmian guiding law reduces to the gradient of the phase function

$$\dot{\mathbf{Q}}(t) = \nabla S_t(\mathbf{Q}(t)). \tag{1.12}$$

Taking time derivatives along world trajectories gives

$$\begin{aligned}
\tfrac{\mathrm{d}}{\mathrm{d}t} P_t(\mathbf{Q}(t)) &= \nabla P_t(\mathbf{Q}(t))\dot{\mathbf{Q}}(t) + \partial_t P_t(\mathbf{Q}(t)) \\
&= \nabla P_t(\mathbf{Q}(t))\dot{\mathbf{Q}}(t) - \nabla(P_t(\mathbf{X})\nabla S_t(\mathbf{X}))\Big|_{\mathbf{X}=\mathbf{Q}(t)} \\
&= \nabla P_t(\mathbf{Q}(t))\dot{\mathbf{Q}}(t) - \nabla P_t(\mathbf{Q}(t))\nabla S_t(\mathbf{Q}(t)) - P_t(\mathbf{Q}(t))\Delta S_t(\mathbf{Q}(t)) \\
&= -P_t(\mathbf{Q}(t))\Delta S_t(\mathbf{Q}(t))
\end{aligned} \tag{1.13}$$

$$\begin{aligned}
\tfrac{\mathrm{d}}{\mathrm{d}t} S_t(\mathbf{Q}(t)) &= \nabla S_t(\mathbf{Q}(t))\dot{\mathbf{Q}}(t) + \partial_t S_t(\mathbf{Q}(t)) \\
&= \nabla S_t(\mathbf{Q}(t))\dot{\mathbf{Q}}(t) - \frac{1}{2}(\nabla S_t(\mathbf{Q}(t)))^2 - V(\mathbf{Q}(t)) - U_t(\mathbf{Q}(t)) \\
&= \frac{1}{2}(\dot{\mathbf{Q}}(t))^2 - V(\mathbf{Q}(t)) - U_t(\mathbf{Q}(t)),
\end{aligned} \tag{1.14}$$

which together with (1.12) can readily be integrated numerically.

To this end we introduce an ensemble of world trajectories $\mathbf{Q}_1(t), \dots, \mathbf{Q}_N(t)$ with appropriate initial conditions, i.e. $\mathbf{Q}_1(t_0), \dots, \mathbf{Q}_N(t_0)$ are P_{t_0} distributed at some initial time t_0, to discretize the fields P and S along these trajectories

$$\begin{aligned}
P_t(\mathbf{Q}(t)) &\to P_i(t) := P_t(\mathbf{Q}_i(t)) \\
S_t(\mathbf{Q}(t)) &\to S_i(t) := S_t(\mathbf{Q}_i(t)).
\end{aligned}$$

This new dynamical grid, given by the ensemble of worlds, is called *Bohmian grid*, and due to equivariance has the desired property that grid points stay in regions of large density $|\Psi_t|^2$.

Using standard time integration methods the coupled equations (1.12-1.14) can readily be integrated, as it was done by Wyatt [4]. Although integrating this system of equations seems to be very straightforward, problems arise with approximations of spatial derivatives in configuration space, such as ∇S or ΔP. In contrast to structured grids, where derivatives can be approximated by a finite differences scheme, the situation on unstructured grids, such as the Bohmian grid, is significantly more difficult. Standard techniques use polynomial least square fitting to estimate the spatial derivatives. However, problems arise with regard to the repulsiveness of the quantum potential, such that world trajectories of the ensemble can cross each other.

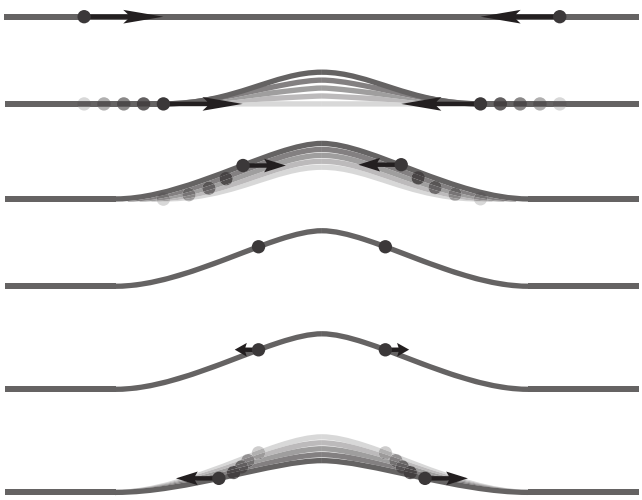

Figure 1.3.: Illustration of the repulsiveness of the quantum potential. If two worlds approach each other and become closer to each other than to the rest of the worlds, the corresponding density develops a small bump between the worlds in accordance with the equivariance property. This bump in turn exhibits a repulsive force via the quantum potential (1.11), such that the worlds slow down until they change their direction and move apart from each other. Consequently, the bump in the density vanishes and also the repulsive force. (Source of illustration: [6])

1.2.3. Repulsiveness of the quantum potential

One important property of the quantum potential is its repulsive nature, which is illustrated in figure 1.3. It ensures that in the second order formulation the non-crossing behaviour of the worlds is preserved. If two worlds approach each other and become closer to each other than to all other worlds, the movement must coincide with a bump developing in the density P due to equivariance. The curvature of this bump in turn causes a repelling force via the quantum potential (1.11) between the worlds, such that the worlds change their direction and do not cross each other.

Using a Bohmian grid, the non-crossing behaviour of the grid points has to be ensured. Otherwise the numerical approximation clearly violates the exact time evolution given by the hydrodynamical formulation. In this context Deckert, Dürr and Pickl [7] showed that least square methods used by Wyatt tend to oversmooth the density such that this repulsive mechanism via the quantum potential breaks down. In other words, the microstructure with small bumps in the density on the scale of world distances is smoothed out, resulting in a too flat density estimate which is incapable of repelling the worlds enough to prevent crossings.

1.3. From Bohmian grids to many interacting worlds

Although a Bohmian grid samples the wave function better than naive grid methods, these approaches have difficulties reproducing an interaction, which is sufficiently repulsive between worlds. Besides the difficulties of estimating correct derivatives of the density, numerical integrating P on the fly can delay the buildup of bumps and can also cause crossing world trajectories. Therefore, we will now go a step further and seek a model incorporating the repulsiveness by a direct interaction

between the worlds avoiding any integration of the fields P and S. The main motivation is given by the following observations:

Reconsidering the system of equations (1.12-1.14), the information about P seems to be redundant if we assume that equivariance still holds for the integrated world trajectories. If this is the case, all statistical information can be recovered from world positions alone. Thus, instead of integrating P, we introduce a new model, where we omit equation (1.13) and recover P from an ensemble of worlds in configuration space alone. That is, we seek a method to reconstruct the density from the distribution of finitely many worlds in configuration space:

$$P(\mathbf{X}) \to P(\mathbf{X}; \mathbf{Q}_1, \dots, \mathbf{Q}_N) \approx N^{-1} \sum_{i=1}^{N} \delta\left(\mathbf{X} - \mathbf{Q}_i\right) . \tag{1.15}$$

Furthermore, by taking another time derivative of equation (1.12) and using (1.14)

$$\ddot{\mathbf{Q}}(t) = \underbrace{-\nabla V(\mathbf{Q}(t))}_{\mathbf{F}_{\text{classical}}} - \nabla U_t(\mathbf{Q}(t)) , \tag{1.16}$$

the Bohmian guiding law (1.12) can be reformulated in terms of forces without any reference to a field S. In addition to the classical force this defines a new force

$$\begin{aligned} \mathbf{r}_t(\mathbf{X}) &:= -\nabla U_t(\mathbf{X}) && (1.17)\\ &= \frac{1}{2}\nabla(P_t^{-1/2}\Delta P_t^{1/2})(\mathbf{X}) && (1.18)\\ &= \frac{1}{4}\left[\frac{\nabla(\Delta P_t)}{P_t} - \frac{\Delta P_t}{P_t^2}\nabla P_t + \frac{(\nabla P_t \cdot \nabla P_t)}{P_t^3}\nabla P_t - \frac{1}{2}\frac{\nabla(\nabla P_t \cdot \nabla P_t)}{P_t^2}\right] , && (1.19) \end{aligned}$$

which is called *Bohmian force*.

Equation (1.16) is the original formulation of the guiding law introduced by Bohm [8], and looks very similar to a classical Newtonian system. Indeed, all quantum effects are described by the Bohmian force or the quantum potential alone, which depend on the density $P = |\Psi|^2$ and the classical limit is very naturally obtained in the case of a vanishing force $\mathbf{r}$. More precisely, the classical limit is reached if the Bohmian force $\mathbf{r} \sim \hbar^2$ is negligible compared to the classical force.

From a theoretical standpoint, however, the second order differential equation is to be considered artificial, because it still retains its first order nature in terms of initial conditions for the worlds velocities

$$\dot{\mathbf{Q}}(0) \stackrel{!}{=} \nabla S_0(\mathbf{Q}(0)) , \tag{1.20}$$

which is hidden in the second order formulation. Though, Hall et al. [1] argue that for arbitrary initial world velocities, one could always construct a corresponding field S fulfilling (1.20); in other words, choosing specific initial velocities is identical to choosing an initial wave function up to a global phase factor.

In any case it is remarkable that equation (1.16) is independent of the field S, and *depends only on the density P* in configuration space. Hence, given an ensemble of worlds in configuration space and an appropriate procedure for estimating the density P similarly to (1.15) or a direct approximation of the

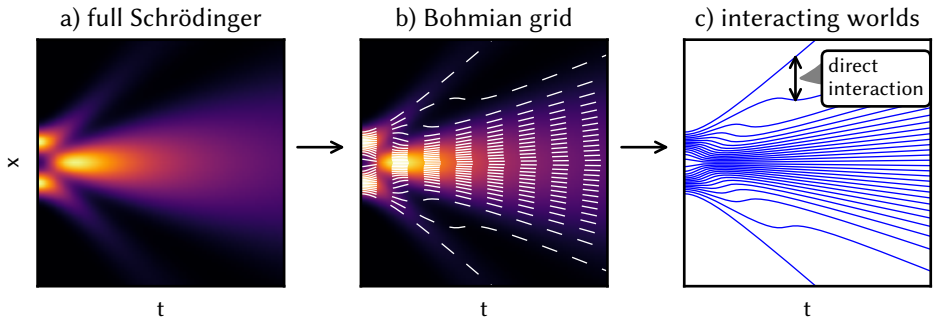

Figure 1.4.: In summary we started with the full Schrödinger picture, and argued that Bohmian grids have significant advantages over naive grid methods. We then went a step further by formulating a fully mechanical theory, where worlds only interact with each other.

quantum potential or the Bohmian force, one could approximate the same dynamics as obtained from the discretized versions of equations (1.12-1.14) without integrating any fields, and subsequently one would arrive at a purely mechanical model.

In the end the aim is to find a purely mechanical theory of N worlds $\{\mathbf{Q}_1(t), \dots, \mathbf{Q}_N(t)\}$, whose dynamics is given in terms of forces

$$\ddot{\mathbf{Q}}_i(t) = -\nabla V(\mathbf{Q}_i(t)) + \mathbf{r}_t(\mathbf{Q}_i; \mathbf{Q}_1, \dots, \mathbf{Q}_N)\,, \tag{1.21}$$

where in addition to the classical force the interworld interaction force $\mathbf{r}_t(\mathbf{Q}_i; \mathbf{Q}_1, \dots, \mathbf{Q}_N)$ models all quantum effects.

The statistical properties of ordinary quantum mechanics should be recovered in the continuum limit $N \to \infty$ worlds. Since all empirical predictions of ordinary quantum mechanics are calculated via the $|\Psi_t|^2$-measure in configuration space, this is sufficient to compute all quantum predictions. That is, for any smooth function φ on configuration space, expectation values with respect to the $|\Psi_t|^2$ measure should be recovered by for a large enough number of worlds:

$$\left\langle \varphi(\mathbf{X}) \right\rangle_{\Psi_t} = \int \varphi(\mathbf{X}) |\Psi_t(\mathbf{X})|^2 \, \mathrm{d}X \tag{1.22}$$

$$= \lim_{N\to\infty} \frac{1}{N} \sum_{i=0}^{N} \varphi(\mathbf{Q}_i(t))\,. \tag{1.23}$$

This rather radical viewpoint of describing quantum phenomena with a purely mechanical theory by many interacting worlds has been introduced by Hall, Deckert, and Wiseman [1]. From a numerical point of view, a purely mechanical model, which still entails the property of equivariance of Bohmian grids, could have significant advantages in computational modeling of quantum systems. As mentioned before, equivariance would imply a much more efficient way of approximating Schrödinger dynamics, and by modifying the number of worlds N, such a mechanical model could offer fine grained control over the approximation to a full quantum system. Even further, Hall et al. [1] also hope that the exponential scaling of naive grid methods could be avoided. However, it should be noted that this new approach of modeling quantum systems is still in a very conceptual stage and strongly depends on the quality of the density estimate (1.15). In fact, it is the crucial

step of finding a many interacting worlds model with good agreement with ordinary quantum mechanics. Thus, the main focus of this thesis will be the analysis of different density estimates for the construction of a many worlds interaction via the quantum potential (1.11) and will be discussed in detail in the following chapters.

At this point the step (1.15) and a corresponding approximation of the Bohmian force without an explicit model remains rather vague. An explicit toy model of an interworld interaction in one dimension and a corresponding density estimate in the form of (1.15) is given by Hall et al. [1]. They also show that this one-dimensional toy model can reproduce generic quantum mechanical phenomena, such as wave packet spreading, barrier tunneling and zero-point energy of the harmonic oscillator. We will discuss this model in detail in the next chapter and also investigate other approximations of the one-dimensional case in order to find generalizations to higher dimensions.

Figure 1.4 summarizes the steps we have taken so far. We started from the exact quantum dynamics given by the Schrödinger equation, and explained why Bohmian trajectories could be used as an adapted comoving grid in contrast to standard discretization of configuration space. Then we introduced the idea of a fully mechanical theory of many interacting worlds in order to model quantum phenomena without any integration of fields.

1.4. Finding stationary states

Until now we have considered both the fully dynamical case and the stationary case. Since interworld interaction models are still in a rather conceptual stage, we shift the focus to the simpler problem: finding stationary solutions, i.e. eigenfunctions and eigenvalues of the Hamilton operator $\mathcal{H} := \sum_{i=1}^{n} -\frac{\Delta_i}{2} + V$.

From the perspective of a many interacting worlds model, these systems are simpler, because for every eigenvalue of $\mathcal{H}$ we can find an eigenstate Ψ, such that the Bohmian vector field (1.5) vanishes. Thus, for these states worlds do not move in configuration space.

Claim Let $\Psi \in \mathcal{L}^2(\mathbb{R}^{dn})$ be an eigenstate of $\mathcal{H}$ with eigenvalue $E \in \mathbb{R}$. Then there exists an eigenstate $\tilde{\Psi}$, such that the Bohmian vector field (1.5) vanishes.

Proof This very simple proof relies on the well-known fact that any eigenstate Ψ can be chosen to be real without loss of generality.

Since $\mathcal{H}$ is self-adjoint, it follows that also the complex conjugate Ψ^* is an eigenfunction of $\mathcal{H}$ with eigenvalue E. This also holds for every linear combination of Ψ and Ψ^*. Thus, $\tilde{\Psi} := \Psi^* + \Psi$ is an eigenfunction with eigenvalue E, which is real. Consequently $\frac{\nabla\tilde{\Psi}}{\tilde{\Psi}} \in \mathbb{R}$ and plugging this into the Bohmian guiding law (1.5), we immediately see that the vector field $\mathbf{v}^{\tilde{\Psi}}$ vanishes.[6] □

In the language of many interacting worlds this means that velocities vanish and the interworld force $\mathbf{r}$ cancels the classical force

$$\dot{\mathbf{Q}}_i \stackrel{!}{=} 0 \qquad \ddot{\mathbf{Q}}_i = \mathbf{F}_{\text{classical}}(\mathbf{Q}_i) + \mathbf{r}(\mathbf{Q}_i; \mathbf{Q}_1, \dots, \mathbf{Q}_N) \stackrel{!}{=} 0 \qquad \forall i = 1, \dots, N\,. \tag{1.24}$$

[6] However, there are stationary states with non-vanishing vector field, such as the $2p_x$ orbital of the hydrogen atom.

Thus, in order to solve the stationary Schrödinger equation, we seek world configurations such that the respective forces cancel each other. Since one is usually interested in the lowest energy eigenstate, we will use an algorithm which also minimizes the energy of the system. This is achieved by introducing an additional damping effect into the dynamics such that world trajectories can settle down into the ground state of the system.

Ground state algorithm In order to solve equation (1.24), we use the following simple algorithm. In the beginning we specify the positions of a finite set of N worlds $\mathbf{Q}_1, \dots, \mathbf{Q}_N$ in configuration space. For simplicity they can be uniformly distributed[7], but of course a good guess of the solution can accelerate the algorithm greatly.

Choosing a step size $\mathrm{d}t \in \mathbb{R}^+$, we do one integration step with velocities set to zero:

$$\mathbf{Q}_i \leftarrow \mathbf{Q}_i + \frac{1}{2}\mathrm{d}t^2 \left(\mathbf{F}_{\text{classical}} + \mathbf{r}(\mathbf{Q}_i; \mathbf{Q}_1, \dots, \mathbf{Q}_N)\right) \qquad \forall i = 1, \dots, N \tag{1.25}$$

We then repeat this step until convergence of the world positions.

In physical terms, we repeatedly accelerate the worlds for small time step $\mathrm{d}t$ by doing one Euler[8] integration step and immediately decelerate the worlds by setting the velocities to zero, thereby removing all kinetic energy from the system.[9] Thus, the resulting world trajectories are artificially damped, such that they can settle down into stationary states. This damping effect depends on the choice of integration time step $\mathrm{d}t$. Smaller time steps increase the damping effect, as kinetic energy is removed more often. Alternatively, an additional force in form of friction could be used to damp the world trajectories.

In this scenario of damped trajectories it is reasonable to assume that the system converges to a fixed world configuration and therefore is expected to be much more robust in the face of numerical errors. Furthermore, calculating stationary states is a good benchmark of finding good candidates for the interworld interaction. Essential features and arising difficulties of constructing an interworld interaction can already be seen in this simplified perspective, which we will see in the following chapters.

As we have now established the most important aspects of the many interacting worlds approach, we will continue with the construction of explicit interworld interaction models in one dimension. In the beginning of the next chapter we will first introduce a simple MIW toy model established by Hall et al. [1] and familiarize ourselves with its basic features. Then, we will continue with a more detailed discussion about density estimation techniques to solve the problem of equation (1.15). This will allow us to construct alternative interaction models, which we will benchmark with given exact solutions in one dimension. In addition to the original MIW approach by Hall et al. [1], also the problem of finding excited states will be discussed, for which an extension to the original approach will be introduced.

[7] or in any other way

[8] This is sufficient, because we are only interested in the final stationary state and not the time evolution of the system, where errors could accumulate.

[9] This can also be seen as a gradient descent method to minimize the total energy.

2. Models in one dimension

In this chapter we will examine different one dimensional models for the interworld interaction. First we will identify different ways of constructing a corresponding interworld interaction potential or force. For pedagogical reasons we will then continue with the one dimensional toy model of Hall et al. [1] and familiarize ourselves with its basic repulsive nature. Afterwards, we will examine other models and compare them to the original MIW approach [1] focussing on excited states and their possible generalizations to higher dimensions.

2.1. General route to an interworld interaction

To find an interworld interaction we use the Bohmian force (1.19) or the quantum potential (1.11) as a guide. These allow different routes of deriving an interworld interaction, which we want to sketch first. However, the approaches discussed here are far from complete and a good interworld force is yet to be found, especially in higher dimensions. Difficulties arise particularly in the context of estimating derivatives at the world positions and reproducing the repulsiveness of interworld interaction.

But we postpone the discussions of these problems, since they will become more clear, when we implement explicit models of an interworld interaction. Here, the objective is to give only a general idea, what a rigorous derivation of an interworld interaction should look like. Nonetheless working examples in one dimension do exist and can be used for simple classical potentials.

Step 1: Finding an a-priori density estimate

The construction of an interworld interaction consists essentially of two steps. Since both the Bohmian force and the quantum potential are functionals of the exact density, the first essential step is to address the problem of (1.15). That is, a procedure $Q \mapsto P_Q$ to find a density estimate P_Q from a given ensemble of $|\Psi|^2$-distributed worlds $Q \coloneqq \{\mathbf{Q}_i, \dots, \mathbf{Q}_N\}$, which comes as close to their original $|\Psi|^2$-distribution as possible. Yet, instead of estimating the full density in one go, we also want to consider rougher estimators which are not defined on all of configuration space or cannot be differentiated as it is the case for discrete estimators. We will call this preliminary density estimate an *a-priori density estimate*.

Nonetheless, in general we aim to find a good estimate on all of configuration space, but we are most interested in the behaviour of P_Q in the neighbourhood of the worlds themselves, because we want to use this density estimate to find an approximation to the Bohmian force *only at the worlds positions* Q. Thus as a minimal requirement we have to define a discrete estimate at the worlds positions $P_Q(\mathbf{Q}_i)$ for all $i = 1, \dots, N$. Other requirements such as differentiability depend on the

subsequent step used to construct the interworld force. In section 2.3.1, an overview of different density estimation techniques can be found.

Step 2: Constructing the interworld force

direct approach with a differentiable density estimate

Given an a-priori density estimate, the most straightforward approach to an interworld force is given by the form of the Bohmian force (1.19). We simply replace the exact density by our density estimate P_Q, which leads to the interworld force

$$\mathbf{r}(\mathbf{Q}_i; Q) = \frac{1}{2}\nabla \left(P_Q^{-1/2} \Delta P_Q^{1/2} \right) \Big|_{\mathbf{X}=\mathbf{Q}_i} , \tag{2.1}$$

whereas the quantum potential is similarly approximated by

$$U(\mathbf{Q}_i; Q) = -\frac{1}{2} P_Q^{-1/2} \Delta P_Q^{1/2} \Big|_{\mathbf{X}=\mathbf{Q}_i} . \tag{2.2}$$

For these equations to hold, we need a density estimate which is at least three times differentiable. This requirement is considerably more difficult to fulfill than the minimal requirement of a discrete density estimate at the world's position. Although this is challenging, the main advantage is that if such a model is found, taking derivatives in arbitrary dimensions is trivial and thus poses a very simple route to an interworld interaction in more than one dimension.

If only discrete density values are given, an interpolation method can be used to estimate the derivatives. Since simple polynomial interpolation techniques has proven unreliable, we will introduce another interpolation method based on Gaussian functions. Alternatively, one can introduce discrete approximations to the derivatives such as finite differences. However, the latter approach involves further difficulties as density values are given on an unstructured grid, where it is not clear how to define discrete approximations to derivatives.

Constructing a potential via the energy expectation value

This alternative route to an interworld interaction was proposed by Hall et.al.[1]. Instead of approximating the Bohmian force directly they assumed that the interworld force $\mathbf{r}$ is conservative and thus is given by an interworld interaction potential $U(Q)$

$$\mathbf{r}(\mathbf{Q}_i; Q) = -\nabla_{\mathbf{Q}_i} U(Q) . \tag{2.3}$$

Given the momenta $\mathbf{P}_i = \dot{\mathbf{Q}}_i$, the corresponding dynamics is then generated by the Hamiltonian

$$\mathcal{H}(X, P) = \sum_{i=1}^{N} \frac{1}{2}\mathbf{P}_i^2 + \sum_{i=1}^{N} V(\mathbf{Q}_i) + U(Q) . \tag{2.4}$$

Hall et al. then compare the energy expectation value of the many worlds model

$$\langle E\rangle_Q = \frac{1}{N}\mathcal{H}(Q,P) \tag{2.5}$$

$$= \frac{1}{N}\sum_{i=1}^{N}\left(\frac{1}{2}\mathbf{P}_i^2 + V(\mathbf{Q}_i)\right) + \frac{1}{N}U(Q) \tag{2.6}$$

to the quantum mechanical expectation value $\langle E\rangle_\Psi$. In the hydrodynamical formulation of Bohmian mechanics $\Psi = P^{1/2}\exp(\mathrm{i}S)$ the expectation value is given by (see Hall et al. [1] and Bohm [8])

$$\langle E\rangle_\Psi = \int P(\mathbf{X})\left[\frac{1}{2}\left(\nabla S(\mathbf{X})\right)^2 + V(\mathbf{X}) - \frac{1}{2}\frac{\Delta P^{1/2}(\mathbf{X})}{P^{1/2}(\mathbf{X})}\right] \tag{2.7}$$

$$\overset{i.b.p.}{=} \int P(\mathbf{X})\left[\frac{1}{2}\left(\nabla S(\mathbf{X})\right)^2 + V(\mathbf{X}) + \frac{1}{8}\left(\frac{\nabla P(\mathbf{X})}{P(\mathbf{X})}\right)^2\right] \tag{2.8}$$

$$\approx \frac{1}{N}\sum_{i=1}^{N}\left[\frac{1}{2}\left(\nabla S(\mathbf{Q}_i)\right)^2 + V(\mathbf{Q}_i) + \frac{1}{8}\left(\frac{\nabla P(\mathbf{Q}_i)}{P(\mathbf{Q}_i)}\right)^2\right], \tag{2.9}$$

where the last term in (2.8) reduces by one derivative after integration by parts and (2.9) is to be understood in the limit of large N. By comparison with equation (2.6) and using the density estimate P_Q from step 1 Hall et al. [1] identify U to be of the form

$$U(Q) = \frac{1}{8}\sum_{i=1}^{N}\left(\frac{\nabla P_Q(\mathbf{Q}_i)}{P_Q(\mathbf{Q}_i)}\right)^2. \tag{2.10}$$

The main advantage of this construction is that the density dependency is reduced by one derivation in comparison to the direct approach. Hence, the requirements on our density estimate are weaker than in the direct approach, but we still face the difficulty of finding a good approximation to derivatives up to second order of our density estimate.

In order to familiarize ourselves with this construction, we will now discuss a simple toy model in one dimension, before we consider more general approaches with potential generalizations to higher dimensions.

2.2. A simple MIW toy model

Hall et al. [1] introduced a toy model with a very simple interworld potential. Many interesting features, especially its repulsiveness, can easily be understood, which is why we start with this model.

We begin with the a-priori density estimate P_Q. Let us assume that the true probability density is given by some unknown density P_Ψ with $\mathrm{supp}P_\Psi = \overline{(a,b)} \subset \mathbb{R}$,[1] where $a, b \in \mathbb{R}\cup\{-\infty,\infty\}$. This guarantees that the cumulative distribution function

$$\begin{array}{rccl} F & : & (a,b) & \longrightarrow & (0,1) \\ & & x & \longmapsto & \displaystyle\int_{-\infty}^{x} P_\Psi(t)\,\mathrm{d}t \end{array} \tag{2.11}$$

[1] It still allows for nodes, i.e. points x in $[a,b]$ with $P_\Psi(x) = 0$.

is bijective. For $i = 1, \dots, N$ we then demand

$$F_i \equiv F(Q_i) = \int_a^{Q_i} P_\Psi(x)\,\mathrm{d}x \stackrel{!}{=} \frac{1}{N}\left(i - \frac{1}{2}\right) \tag{2.12}$$

to specify the world positions with respect to the cumulative distribution function. This also implies that we fix the order of worlds, i.e. $a < Q_1 < Q_2 < \cdots < Q_N < b$.

To see why this is the right choice, consider a smooth function $\varphi : \mathbb{R} \to \mathbb{R}$ on configuration space. By a simple change of variables $y = F(x)$ we see that its expectation value with respect to P_Ψ is given by

$$\begin{aligned}
\big\langle \varphi \big\rangle_\Psi &= \int_{-\infty}^{\infty} \varphi(x) P_\Psi(x)\,\mathrm{d}x && (2.13)\\
&= \int_0^1 \varphi \circ F^{-1}(y)\,\mathrm{d}y && (2.14)\\
&= \lim_{N\to\infty} \frac{1}{N} \sum_{i=1}^{N} \varphi \circ F^{-1}\left(\frac{1}{N}\left(i - \frac{1}{2}\right)\right) && (2.15)\\
&= \lim_{N\to\infty} \frac{1}{N} \sum_{i=1}^{N} \varphi(Q_i)\,, && (2.16)
\end{aligned}$$

where in equation (2.15) the definition of the Riemann integral in terms of a midpoint rule has been used, which is called middle sum. Thus by the choice of (2.12) we guarantee that (2.16) holds, which is our desired statistical property for the worlds expectation value in the continuum limit.

An error estimate for the approximation of (2.16) by a finite sum can be found in [9, p.54]. For $\varphi \circ F^{-1} \in C^2[-1, 1]$ $\exists\, \xi \in (0, 1)$ such that the error is given by

$$\left| \int_{-\infty}^{\infty} \varphi(x) P_\Psi(x)\ \mathrm{d}x - \frac{1}{N} \sum_{i=1}^{N} \varphi \circ F^{-1}\left(\frac{1}{N}\left(i - \frac{1}{2}\right)\right) \right| = \frac{1}{24N^2} \frac{\mathrm{d}^2}{\mathrm{d}y^2} (\varphi \circ F^{-1}) \Big|_{y=\xi}\ . \tag{2.17}$$

Thus, the error decreases quadratically with the number of worlds.

Finally we arrive at our a-priori density estimate by approximating $P_\Psi(x) = F'(x)$ in terms of finite differences. This results in a forward and backward density

$$\begin{aligned}
P_i^+ \equiv P_Q^+(Q_i) &:= \frac{F(Q_{i+1}) - F(Q_i)}{Q_{i+1} - Q_i} = \frac{1}{N(Q_{i+1} - Q_i)}\\
P_i^- \equiv P_Q^-(Q_i) &:= \frac{F(Q_i) - F(Q_{i-1})}{Q_i - Q_{i-1}} = \frac{1}{N(Q_i - Q_{i-1})}\,,
\end{aligned} \tag{2.18}$$

with which we define our density estimate

$$P_Q(x) = \begin{cases} 0, & \text{for } x \le a, x \ge b \\ P_i^+ & \text{for } Q_i < x < Q_{i+1} \\ \frac{1}{2}(P_i^+ + P_i^-) & \text{for } x = Q_i \end{cases}\ . \tag{2.19}$$

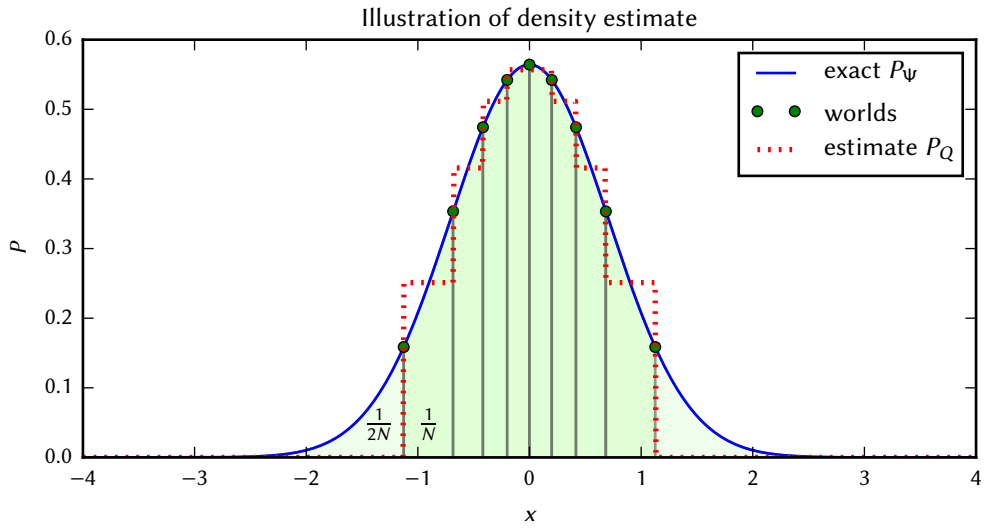

Figure 2.1.: Illustration of the density estimate of the MIW toy model. The world position are chosen, such that the inner areas below the exact density density P_Ψ, indicated by green color, integrate to $1/N$.

The estimate and its construction is illustrated in figure 2.1. This density can also be understood in a slightly different view. Since the order of worlds is conserved we can consider the worlds as a parameterization of a partition of configuration space into succeeding intervals

$$\mathbb{R} = \bigcup_{i=0}^{N} \overline{(Q_i, Q_{i+1})} \tag{2.20}$$

where we set $Q_0 = -\infty, Q_{N+1} = \infty$. The density estimate (2.19) then corresponds to assigning each interval $I_i := (Q_0, Q_i)$ the density $1/(N|I_i|)$. Hence by definition of (2.12), it is ensured that the integrated probability density over the interval I_i, $\int_{I_i} P_Q(X)\,\mathrm{d}X = 1/N$ is conserved. This view becomes important when we consider generalizations of this density estimate to two dimensions.

As a next step we have to approximate the Bohmian force in terms of our density estimate. To this end we need to take spatial derivatives up to third order of our density estimate; in our case discrete approximations of them. Due to our unstructured grid in terms of worlds positions, usual finite differences schemes cannot be applied directly. Yet recalling definition (2.12) we see that the world positions represent an evenly spaced grid in terms of the cumulative distribution function F. Rewriting derivatives with respect to F

$$\frac{\mathrm{d}}{\mathrm{d}F} = \frac{\mathrm{d}x}{\mathrm{d}F(x)}\frac{\mathrm{d}}{\mathrm{d}x} = \frac{1}{P_\Psi}\frac{\mathrm{d}}{\mathrm{d}x}, \tag{2.21}$$

we can express spatial derivatives in terms of derivatives with respect to the cumulative distribution function.

Indeed, an easy calculation [1] shows that the Bohmian force r_t in the one dimensional case can be

rewritten as

$$r_t(x) = \frac{1}{4}\left[\frac{1}{P_\Psi(x)}\frac{\mathrm{d}}{\mathrm{d}x}\right] P_\Psi(x)^2 \left[\frac{1}{P_\Psi(x)}\frac{\mathrm{d}}{\mathrm{d}x}\right]^2 P_\Psi(x) \tag{2.22}$$

$$r_t = \frac{1}{4}\frac{\mathrm{d}}{\mathrm{d}F}\ P_\Psi^2\ \frac{\mathrm{d}^2}{\mathrm{d}F^2}\ P_\Psi\,, \tag{2.23}$$

where derivatives apply to all terms on the right side and arguments have been suppressed in the last line. The operator $\frac{\mathrm{d}}{\mathrm{d}F}$ can now easily be approximated by forward and backward differences

$$D_F^+\varphi_i := N(\varphi_{i+1} - \varphi_i) \tag{2.24}$$

$$D_F^-\varphi_i := N(\varphi_i - \varphi_{i-1})\,, \tag{2.25}$$

where $\varphi_i := \varphi(Q_i)$ is the discretized version of some function φ on configuration space.

At last these approximations together with (2.23) lead to the interworld interaction force r_{miw} proposed by [1]

$$r_{\mathrm{miw}}(Q_i; Q) := \frac{1}{4}D_F^+\left[(P_i^-)^2 D_F^+ D_F^- P_i^-\right] \tag{2.26}$$

$$= \frac{N^3}{4}\left\{P_i^{+2}\left(P_{i+1}^+ - 2P_i^+ + P_{i-1}^+\right) - P_i^{-2}\left(P_{i+1}^- - 2P_i^- + P_{i-1}^-\right)\right\} \tag{2.27}$$

$$= \frac{1}{4}\Bigg\{\frac{1}{(Q_{i+1}-Q_i)^2}\left(\frac{1}{Q_{i+2}-Q_{i+1}} - \frac{2}{Q_{i+1}-Q_i} + \frac{1}{Q_i - Q_{i-1}}\right) - \frac{1}{(Q_i - Q_{i-1})^2}\left(\frac{1}{Q_{i+1}-Q_i} - \frac{2}{Q_i - Q_{i-1}} + \frac{1}{Q_{i-1}-Q_{i-2}}\right)\Bigg\}, \tag{2.28}$$

where forward and backward differences and densities have been arranged in such way that the resulting force is symmetric.

2.2.1. Repulsiveness of the interworld interaction

It is difficult to develop an intuition about this interaction when looking at the force directly. In contrast, with the corresponding potential

$$U_{\mathrm{miw}}(Q) = \frac{1}{8}\sum_{i=1}^{N}(D_F^+ P_i^-)^2 = \frac{1}{8}\sum_{i=1}^{N}\left[\frac{1}{Q_{i+1}-Q_i} - \frac{1}{Q_i - Q_{i-1}}\right]^2 \tag{2.29}$$

the interaction is much easier to understand. In fact, Hall et al. [1] used a slightly different derivation of the interaction, where they first derived this potential and then introduced the interaction force (2.28). However, the form of (2.27) makes the dependence on our density estimate much clearer. For simplicity we do set the boundary densities $P_1^- = P_N^+ = 0$, or equivalently placing "boundary" worlds $Q_0 = -\infty$ $Q_{N+1} = \infty$ at infinity.

In contrast to common classical potentials, U_{miw} includes also three-body terms. Expanding the sum, we see that a chain of five subsequent worlds interact directly with each other. This part is illustrated in figure 2.2, where only the world at the center of the chain is varied and the outer worlds are kept fixed. Potential and force become singular when two neighbouring worlds approach each other,

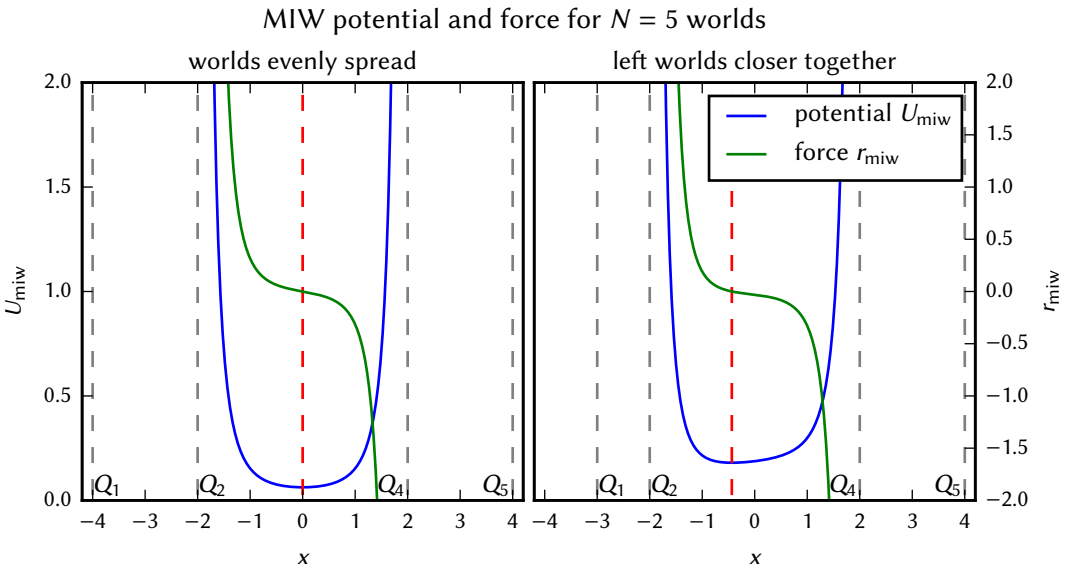

Figure 2.2.: MIW potential U_{miw} and force $r_{\text{miw}}(Q_3; Q)$ for $N = 5$ worlds, varying the inner world Q_3, and keeping the outer worlds fixed at different positions. Given outer worlds positions are illustrated by gray lines, whereas the red line indicates the world position for Q_3 where the force acting on Q_3 vanishes. Generally, for Q_3 approaching one of its neighbours Q_2 and Q_4 the potential becomes singular resulting in an overall repulsive force. For evenly spaced outer worlds (left plot) the force vanishes at $Q_3 = 0$ such that neighbouring world distances and thus densities equalize. In the right plot, where $Q_1 = -3$ is closer to Q_2 than Q_4 to Q_5, the equilibrium point of vanishing force moves to the left. In this case distances do not equalize, but minimizes the local curvature of the density.

resulting in an overall repulsive force. The repulsive nature ensures that world trajectories cannot cross each other, which is the desired property we should preserve from Bohmian mechanics. This also implies that the ordering of worlds is conserved.

Due to the repulsiveness the corresponding dynamics tends to "flatten" the density. Keeping the outer worlds Q_1 and Q_N fixed, the potential is minimal when distances between neighbouring worlds are equal, as illustrated by the left plot of figure 2.2. By equation (2.29) this is equivalent to a constant density. The case of different distances of the corresponding outer two worlds is depicted on the right hand side of figure 2.2. Keeping all worlds except Q_3 fixed with $Q_2 - Q_1 < Q_5 - Q_4$, the equilibrium point moves to the left and consequently increasing the density estimate between Q_2 and Q_3. This minimizes the curvature of the density estimate, hence "flattens" the density.

This toy model already incorporates many features of the original Bohmian quantum potential, but also incorporates some nice numerical features. The interworld interaction force is of very simple form and therefore leads to a quite fast calculation. Furthermore the flattening effect tends to stabilize worlds with respect to numerical inaccuracies of their positions during the ground state algorithm and spreads them evenly in configuration space.

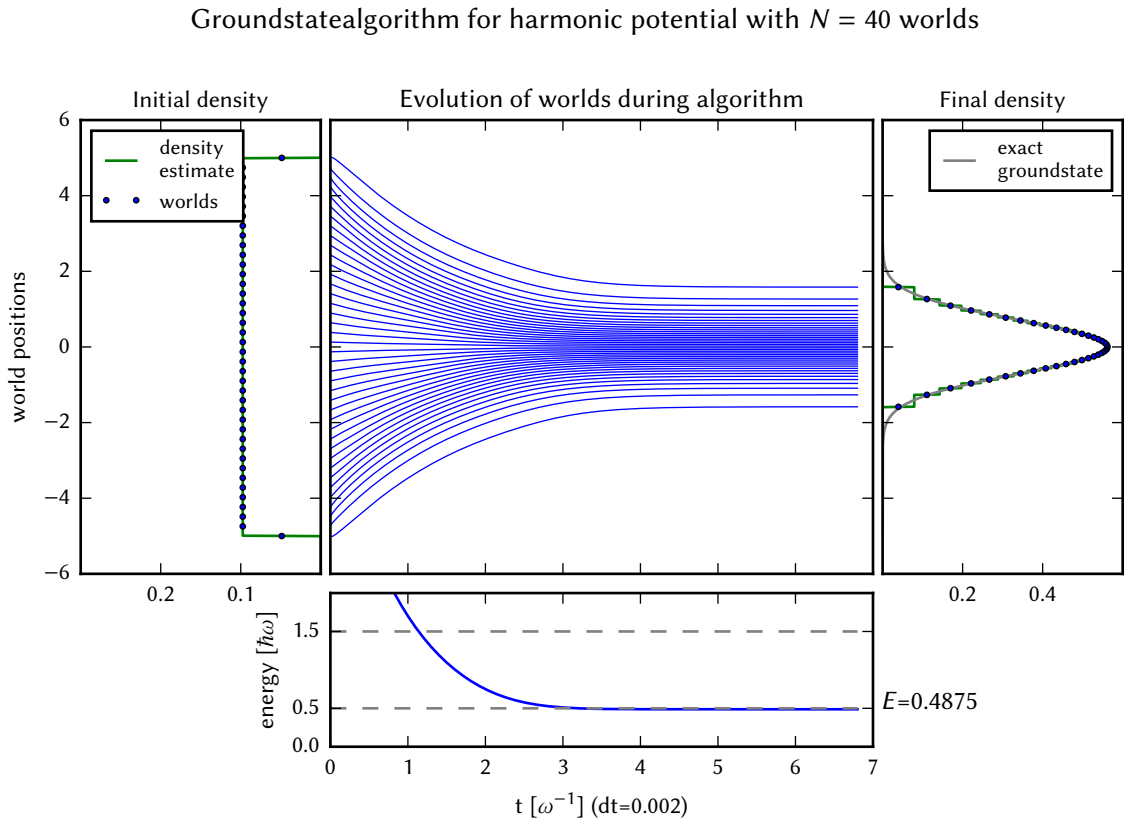

Figure 2.3.: Illustration of the ground state algorithm for the harmonic potential with given interworld force $\mathbf{r}_{\text{miw}}$. We start with a uniform distribution (upper left plot) of worlds in configuration space. The green line represents our established density estimate P_Q of equation (2.19). The central plot shows the evolution of world positions during the ground state algorithm. Worlds do not cross each other and move to the center attracted by the harmonic force until the interworld force r_{miw} cancels the harmonic force. The final configuration and density are shown in the upper right plot. The density estimate given by world positions converges to the exact ground state density given by a Gaussian function. Additionally the average energy $\langle E\rangle_Q = N^{-1}\sum_{i=1}^{N} V(Q_i) + N^{-1}U_{\text{miw}}(Q)$ in the lower plot shows convergence to a value slightly below the exact ground state energy of the harmonic oscillator $\langle E\rangle_{\Psi_0} = 1/2$.

2.2.2. Ground state of the harmonic oscillator

This model can readily be used for the ground state algorithm to find stationary states as described in section 1.4. To illustrate this, we shortly consider the case of the harmonic classical potential $V(x) = 1/2x^2$.[2] The ground state is given by a Gaussian distribution around the center with energy $\langle E\rangle_{\Psi_0} = 1/2$

Figure 2.3 shows the simulation for $N = 40$ worlds. Starting from a uniform distribution the ground state algorithm applied to our model converges to the exact analytic density. Note that no crossings of worlds occur during the algorithm, i.e. the integration step dt has been chosen small enough. The resulting average energy lies slightly below the analytic value as predicted by Hall et al. [1], but

[2] $\omega = m = 1$

captures the right energy level compared to the known first excited state at $E = 1.5$.

The biggest errors originate from the tails of the distribution, where the sampling is low. In the case of the harmonic potential these errors are especially bad.

Since we now have seen a simple example of an interworld interaction model and its application to the ground state algorithm, we will now come back to the question of alternative more general models, for which we will introduce different density estimating techniques in the following.

2.3. More generic models

Although the MIW toy model in section 2.2 is already capable of reproducing many generic quantum effects, it has shortcomings when considering excited stationary states (see section 2.5.1). Most significant, it is not clear how to generalize the model to higher dimensions than one, since there is no useful integral transformation as in equation (2.14) in terms of a cumulative density function.

Therefore we take a step back and consider alternative interaction models in this section. We will stay in the one dimensional case, which we use to benchmark our models with exact solutions available there. However, the objective is to focus on models that will later allow for generalizations to the two dimensional case.

For this purpose we have to reconsider the problem (1.15) of finding a density estimate P_Q given a worlds distribution Q in configuration space which can be generalized to higher dimensions. Since reconstructing the density from an observed is a common question in statistics, a huge number of such techniques already exists. In the following, we will introduce some of the most common methods and investigate if they can be utilized for the construction of an interworld interaction.

2.3.1. Standard density estimation techniques

The most difficult step in the construction of an interworld interaction is finding a "smooth enough" density estimate, when the true density P_ψ is encoded only in the distribution of worlds $\{\mathbf{Q}_1, \dots, \mathbf{Q}_N\}$ in configuration space.

Estimating the density P without any prior knowledge of its functional form from an observed data set is a common problem within statistics. Such methods are called *non-parametric density estimation*, and a plethora of different models and techniques exist to address this problem. A nice overview of these techniques can be found in [10] and [11] or [12].

Though, choosing the optimal technique strongly depends on the problem considered, which is the main difficulty when applying such methods. Additionally, good estimates are only guaranteed if the sample size N is very large. By contrast, we are interested in good estimates which require minimal number of worlds to find more efficient algorithms than standard grid techniques. Thus at first glance it seems like a hopeless endeavour recovering the full density from such little information.

On the other hand our primary aim is to estimate the density correctly only in the close neighbourhood of the corresponding worlds, i.e. estimating the density correctly up to derivatives of third

order. Additionally our data set given by the worlds is not truly random and can be designed to be more regular and fit our needs as we did in the MIW toy model. Hence the statistical methods introduced in this section should rather be seen as an inspiration for finding a good density model and have to be adapted further. In the following some basic notions of non-parametric density estimation are introduced. Later, in section 2.3.3, these are used to construct an interworld interaction alternative to the MIW toy model.

Nearest neighbour estimates

We start with nearest neighbour estimates. Let $Q = \{\mathbf{Q}_1, \dots, \mathbf{Q}_N\}$ be a set of data points drawn from the distribution P. According to Silverman [10] the k-th nearest neighbour estimate $P_Q^{nn_k}$ is then defined as

$$P_Q^{nn_k}(\mathbf{X}) := \frac{k}{N c_d r_k(\mathbf{X})^d}\,, \tag{2.30}$$

where $r_k(\mathbf{X})$ is the euclidean distance in configuration space from $\mathbf{X}$ to the k-th nearest neighbour in the point set Q; c_d is the volume of the unit ball in d dimensions, i.e. $c_1 = 2$, $c_2 = \pi$.

To understand this definition we simple bring the numerator to the other side

$$N\, P_Q^{nn_k}(\mathbf{X}) \underbrace{c_d r_k(\mathbf{X})^d}_{\mathrm{vol}_k(\mathbf{x})} = k\,, \tag{2.31}$$

where $\mathrm{vol}_k(\mathbf{X})$ is the volume of the d-dimensional sphere centered at $\mathbf{X}$, such that it contains exactly k data points of the set Q. Hence the nearest neighbour estimate is defined in a way, such that in the volume $\mathrm{vol}_k(\mathbf{X})$ we expect exactly k data points to occur. This is illustrated in the left plot of figure Figure 2.4.

The main advantage of this estimator is its simple form and that it is fast to calculate if the nearest neighbour structure is already known.[3] On the other hand it shows some significant shortcoming when it comes to estimating derivatives of the density. Although it is continuous for $k >= 2$, it is not differentiable at the points where the kth nearest neighbour switches. The right hand side of figure 2.4 also suggests that it is a bad estimate for the derivative, because it fluctuates strongly between the worlds. According to Silverman [10] it is also prone to local noise in the observed data in general. Due to its $\sim 1/r^d$ dependence, the estimate also has too heavy tails and therefore is not normalizable.

Furthermore, the estimator depends on the choice of k, and becomes smoother with higher values of k. The right choice of k is a common subject for discussion (see [10, p.96]). For finding an estimate at the data points themselves, only $k \geq 2$ are valid choices.

Nevertheless, for $k \geq 2$ it is quite possible to estimate the density at the data points themselves as can be seen in the right plot of figure 2.4. Additionally, in our case we have some control over our data, and can design world positions as in (2.12) to sample the density in a regular way. For this case

[3] Finding nearest neighbours is a difficult problem in very high dimensions and not necessarily faster to do than simply doing the search by brute force.

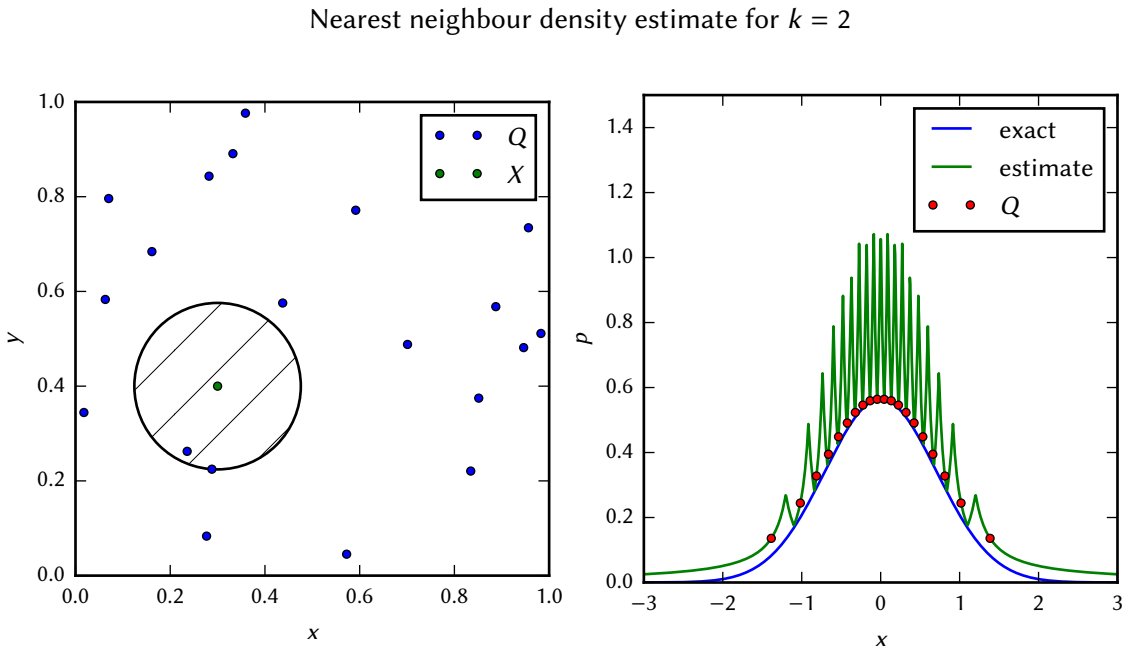

Figure 2.4.: Nearest neighbour density estimate for the case $k = 2$. The left plot illustrates the estimate (2.30) in the 2d dimensional case. In order to estimate the density at point X, one constructs a circle such that it contains $k = 2$ points of the data set. The density then is inverse proportional to the area of the circle. The right plot illustrates the one dimensional case, where our given data Q is defined by equation (2.12) given a Gaussian distribution (blue). The density estimate (2.30) is depicted by the green line, whereas the red points indicate the estimate at the given data points Q.

the lowest value $k = 2$ has proven to be most appropriate. In fact for $k = 2$ in one dimension the estimate at a data point reduces to

$$P_Q^{nn}(Q_i) = \frac{1}{|Q_i - Q_{nn(i)}|}, \tag{2.32}$$

where $nn(i)$ is the nearest neighbour of world Q_i. Compared to the toy model in section 2.2 and equation (2.18) it is equivalent to the maximum of left and right density estimate. The $1/r$ dependency between neighbouring worlds very naturally incorporates the repulsiveness of the quantum potential, as the density diverges when neighbouring worlds approach each other.

Summarising, the nearest neighbour method is not a good overall estimate of the density, but can be used to estimate the density at world positions. Thus it is a good candidate for an a-priori density estimate at the world themselves. In order to estimate derivatives, other methods must be used.

Kernel density estimation

Kernel density estimation is a more general approach to non-parametric density estimation. The central idea is to place small bump functions, so called *kernel functions*, centered at the data points, which in sum model the overall density estimate. This approach is fairly general and many different

density estimation methods can be reformulated in terms of an kernel density estimate. This also applies to the nearest neighbour estimate.

Let $h \in \mathbb{R}^+$ and $Q = \{Q_1, \dots, Q_N\}$ be a set of data points drawn from the distribution P. The simplest kernel density estimate P_Q^K given the *kernel function* K is defined by

$$P_Q^K(X) := \frac{1}{Nh} \sum_{i=1}^{N} K\left(\frac{X - Q_i}{h}\right). \tag{2.33}$$

The kernel function K can in principle be any probability density. Hence it has to be positive and normalized

$$K(X) \geq 0 \quad \forall X, \qquad \int K(X)\, \mathrm{d}X = 1\,. \tag{2.34}$$

A typical choice for K is the normal distribution

$$K(x) = \frac{1}{\sqrt{2\pi}} \exp\left(-\frac{1}{2}x^2\right), \tag{2.35}$$

but a lot of other kernel functions have been considered. Other common choices can be found in [10, p.43].

The resulting density estimate is well defined on configuration space and by definition normalized. All properties of the kernel function are inherited by the estimate. This is the main advantage of this method, since it gives a lot of control over the estimate's properties. In our case we only allow kernel functions, which are at least three times differentiable. In practice we only consider the normal distribution, which has proven to be most reliable when taking derivatives.

The parameter h is normally referred to as the *bandwidth* of the kernel function. It is introduced to have some control over how smooth the resulting density estimate will be. The estimate strongly depends on the choice of h, as figure 2.5 illustrates. Too large values of h tend to oversmooth the estimate and details in regions with a higher number of data points can get lost. This is especially bad as we need this microstructure between worlds, to model the repulsiveness of the interworld interaction correctly. On the other hand, choosing h too small, the bumps around the data points get too sharp resulting in a fluctuating density estimate. This would result in a very bad estimate for the derivatives and therefore for the interaction as well.

However, numerical simulations have shown that a universal choice of h for the density estimate is too rigid and cannot be used to achieve sufficient smoothing while retaining accurate derivative approximations. Therefore we continue to introduce a more generalized model.

Adaptive kernel estimates

The kernel density estimation in its simple form as of section 2.3.1 has proven to be inaccurate for our interworld interaction. A more flexible density estimate is given by the adaptive kernel density estimate, in which we allow individual bandwidths for every contributing kernel function. In full

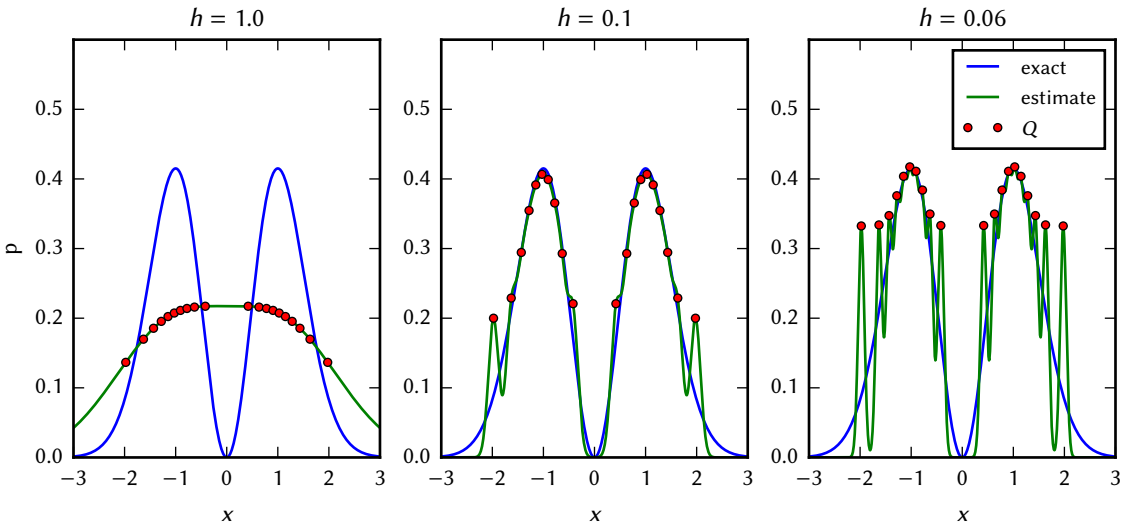

Figure 2.5.: Kernel density estimate for various choices of bandwidths h. For $h = 1.0$ the bandwidth of the individual Gaussians is too broad such that the estimate screens out the bimodal structure of the original density. Decreasing to $h = 0.1$, the bimodal structure reappears in the estimate. However, in regions of low density such as the tails, the density estimate oscillates around the true density, as the bandwidth at worlds in this region is too low. This effect becomes more visible when further decreasing h.

generality this amounts to a bandwidth function $h(X; Q)$ given the worlds configuration Q. The corresponding adaptive kernel density estimate is then given by the density

$$P_Q^A(X) := \frac{1}{N} \sum_{i=1}^{N} \frac{1}{h_i} K\left(\frac{X - Q_i}{h_i}\right), \tag{2.36}$$

where $h_i := h(Q_i; Q)$.

The idea is to allow for varying bandwidths adapted to the given data set, to choose the right bandwidths in regions of high and low density. I.e. higher values (broader kernels), where observed data is only sparse and the tail behaviour is better captured by broader kernels and lower values (sharper peaked kernels), where a lot of observed data points are present and the finer structure of the density should be resolved.

This adaptive kernel density estimate still exhibits the nice properties as in the simple case. The challenge, however, is to specify the right bandwidth function h. In fact the problem of finding a good density estimate has only been shifted to finding the appropriate bandwidth function h. Finding the right bandwidth functions is a research topic on its own. Nevertheless some simple choices exist; for example a common choice [12] is given by a nearest neighbour distance

$$h(X, Q) = r_k(X; Q), \tag{2.37}$$

where r_k is the distance to the k-th nearest point in the given sample Q.[4]

[4]For $k = 1$ $r_k(Q_i, ; Q) = 0$ since Q_i is in the point set Q.

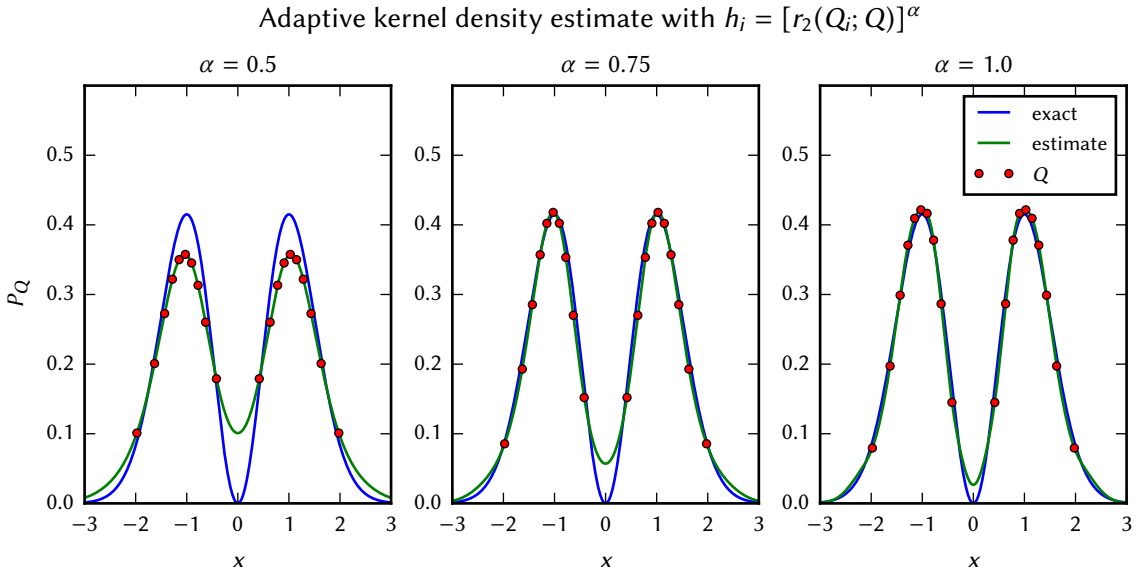

Figure 2.6.: Adaptive kernel estimate with a bandwidth function as a power law of the nearest neighbour distance. For all different power laws the density estimate shows significant improvements over the simple kernel density estimators as both in the tails and in region of high density sufficient smoothing can be achieved.

Figure 2.6 shows different density estimates for bandwidths function in form of a power law of the nearest neighbour distances. In comparison to the simple density estimate, all considered power laws show better smoothing properties for both the tails and regions of high density. Although the choice of $\alpha = 1$ models the density best in figure 2.6, the choice of

$$h_i = r_2(Q_i; Q)^{-1/2} \tag{2.38}$$

has proven more useful in practice. This square root dependence has been investigated before by Abramson [13], who suggests that it has a better convergence rate to the exact density. Simulations with different power laws also suggest that it reduces fluctuations in the density estimate and thus gives better estimates of its derivatives, which result in a more stable interworld interaction. For this reason we will include the adaptive kernel density estimate with bandwidths given by the square root law in the comparison of different interaction models, which will be benchmarked in section 2.4.

An alternative kernel density estimate can be constructed by allowing a global bandwidth function, which varies with the point at which the density estimate is evaluated

$$P_Q^A(X) := \frac{1}{N\, h(X; Q)} \sum_{i=1}^{N} K\left(\frac{X - Q_i}{h(X; Q)}\right) . \tag{2.39}$$

However, this estimate does not guarantee to be a proper probability estimate since depending on the choice of h it can be non-normalizable. This approach has not been thoroughly investigated and could be an ansatz for alternative density estimation models.

2.3.2. Error estimate of interaction model

In order to compare different interaction models, different error measures can be considered. Since our interaction model strongly depends on the density estimates of our model it seems natural to compare the estimated density with the exact one if it is known.

To this end there exist different error estimates within the field of non-parametric density estimation. There these methods are primarily used to find optimal parameters of the model under consideration by minimizing the chosen error. In this context world positions $Q = \{Q_1, \dots, Q_N\}$ are considered as random variables, each distributed with respect to a given distribution P.

A common choice is the L^2 approach, where the squared distance between the density P_Q and the original density P is considered. This error is called the mean integrated square error [11]

$$\mathrm{MISE} = \mathbb{E}_Q \int \left[P_Q(X) - P(X)\right]^2 \mathrm{d}X\,, \tag{2.40}$$

where the expectation value is taken with respect to the random variables Q. Similarly one can consider the L^1 distance, which defines the mean integrated absolute error

$$\mathrm{MIAE} = \mathbb{E}_Q \int \left|P_Q(X) - P(X)\right| \mathrm{d}X\,. \tag{2.41}$$

From a physical point of view the L^1 approach seems to be the most natural one, because the L^2 norm is the right choice on the level of the wave function. Izenman [11] also indicates that the L^1 norm should be a better choice, as errors in the tails of the distribution can be underestimated in the L^2 case.

In our case, we are interested in an error, where an explicit realization of world positions is already given. Since many density estimates only involve values at the world positions, a pointwise comparison is desirable.

As a naive approach one can simply sum the absolute errors

$$\mathrm{AE} \coloneqq \frac{1}{N} \sum_{i=1}^{N} \left|P_Q(Q_i) - P(Q_i)\right|\,. \tag{2.42}$$

However, this does not seem to be the right choice, because errors in the tails of the distribution are underestimated. A more natural estimate is given by the L^1 norm. Since we always assume our worlds to be P-distributed in the sense of (1.23), we can formulate a pointwise error estimate by reformulating the L^1 distance

$$\int \left|P_Q(X) - P(X)\right| \mathrm{d}X = \int P(X) \left|\frac{P_Q(X)}{P(X)} - 1\right| \mathrm{d}X \approx \frac{1}{N} \sum_{i=1}^{N} \left|\frac{P_Q(Q_i)}{P(Q_i)} - 1\right| \tag{2.43}$$

This motivates the absolute relative error estimate

$$\mathrm{ARE} = \frac{1}{N} \sum_{i=1}^{N} \left|\frac{P_Q(Q_i)}{P(Q_i)} - 1\right| \tag{2.44}$$

which focuses on the relative error and seems to be a better choice when considering the tails of the distribution.

Yet, both proposals are insensitive with respect to errors in the derivatives of the density estimate, which play a crucial role in the interworld interaction. Additionally the Bohmian force and quantum potential are invariant under the transformation $P \to \alpha P$. Thus, the corresponding error method should incorporate the same invariance, which is not the case for the former error proposals.

In order to incorporate both scaling-invariance and derivatives, it seems natural to consider the dynamical physical quantities themselves, such as the energy or the force, to give an error for the interaction model under consideration. As we focus on stationary states, where worlds are at rest and the force vanishes, we compare the energy expectation values with the exact analytic solution

$$\Delta E = \left\langle U_Q + V \right\rangle_Q - E_{\text{exact}} \,. \tag{2.45}$$

It should be noted that this error only makes sense if a world configuration at rest is considered. Thus before calculating the error, one uses the ground state algorithm to find a stationary solution of the interaction model.

In total, using the energy based error measure (2.45) seems to be most appropriate to our case of calculating stationary states as calculating energy levels is one of its key aspects. Thus, the energy based error measure does not only allow for a direct comparison to the exact energy values, but is also a good indicator for the quality of the considered interworld interaction model.

At this point we have discussed different density estimation techniques and possible error estimates. Although the adaptive kernel density estimate can be used to construct an interworld interaction, its application to the ground state algorithm shows mixed result as we will see in section 2.4. Therefore, another model is introduced in the following, which combines aspects of the MIW toy model and the kernel density estimators.

2.3.3. New interaction model via Gaussinterpolation

Since direct approaches with the adaptive kernel estimates prove to be quite cumbersome (see section 2.4), we introduce an additional interaction model in this section. For the adaptive kernel estimates a bandwidth function with reliable estimates for a general setting is quite difficult to find. In many cases the corresponding repulsive effects of the interworld interaction cannot be balanced correctly. In contrast, the density of the MIW toy model (2.19) has proven to be quite reliable. Thus, the main motivation for the construction of the model of this section is to combine the density estimate of the MIW toy model with the nice smooth properties of an adaptive kernel density estimate.

As described in section 1.2.3, the density estimate has to develop a small bump between two approaching worlds, in order to create a force repelling the corresponding worlds. Using an adaptive kernel estimate, the leading contribution to this bump originates from the two kernel functions placed at the two approaching worlds. This process is very sensitive to the chosen bandwidths. Given too small bandwidths, the bump in between the worlds and its repulsive effects can develop too late within in the discretized time evolution and when the bump finally builds up it may result in a strong repulsive force, which can produce crossings with other worlds due to numerical errors.

On the other hand if the bandwidths are too broad, a repulsive bump may not build up at all, even when worlds are very close and therefore crossings can easily occur.

The new idea of this model is to use a kernel density estimate, which places the kernels not at the worlds but between them, such that repulsive bumps can be modeled directly. In order to choose the bandwidths of these kernel functions we use the discrete a-priori density estimate of the MIW toy model in section 2.2 and assign it to the interval between the worlds.

Given the world positions $\{Q_i\}_{i=1,..N}$, we define $Q_{i+1/2} := \frac{1}{2}(Q_{i+1} + Q_i)$ to be the middle position between two subsequent worlds. The discrete density estimate *between* the worlds is then given by

$$p_{i+1/2} \equiv p(Q_{i+1/2}) := \frac{1}{N+1} \frac{1}{Q_{i+1} - Q_i} . \tag{2.46}$$

Smoothing with adaptive kernel estimate

The smooth density model is given by an adaptive kernel density estimate

$$P_Q(x) = \frac{1}{C} \sum_{i=1}^{N-1} \frac{1}{h_i} K\left(\frac{x - Q_{i+1/2}}{h_i}\right) , \tag{2.47}$$

where the kernel function K is a normalized Gaussian, placed at the middle position between the worlds with a bandwidth h_i each. In contrast to standard kernel density estimates, only $N-1$ kernels are used. The constant C is such that P is normalized. In the standard case with no additional constraints on the density it is set to $C = N - 1$

The bandwidths are then determined by fitting the adaptive kernel density estimate to the discrete values. This is achieved by enforcing the smooth model to coincide with the discrete estimate, i.e.

$$P(Q_{i+1/2}) \stackrel{!}{=} p_{i+1/2} \quad \forall i = 1...N-1 . \tag{2.48}$$

Though, this set of equations cannot be solved explicitly for the bandwidths h_i, but numerical solutions can be obtained by a simple recursion relation, which is given by

$$h_i \leftarrow h_i \frac{P(Q_{i+1/2})}{p_{i+1/2}} . \tag{2.49}$$

For this to work it is crucial that the adaptive kernel density estimate is normalized correctly. The Bohmian force can then easily be calculated by differentiating P_Q analytically, thus completing the interaction model.

One can see this method as an interpolation method of the discrete a-priori density estimate (2.46), which is illustrated in figure 2.7. At each middle position a Gaussian bump is pinpointed and kept fixed. By applying the recursion relation for the bandwidths, the individual Gaussians are spread out in such a way that the smooth estimate coincides with the discrete density values.

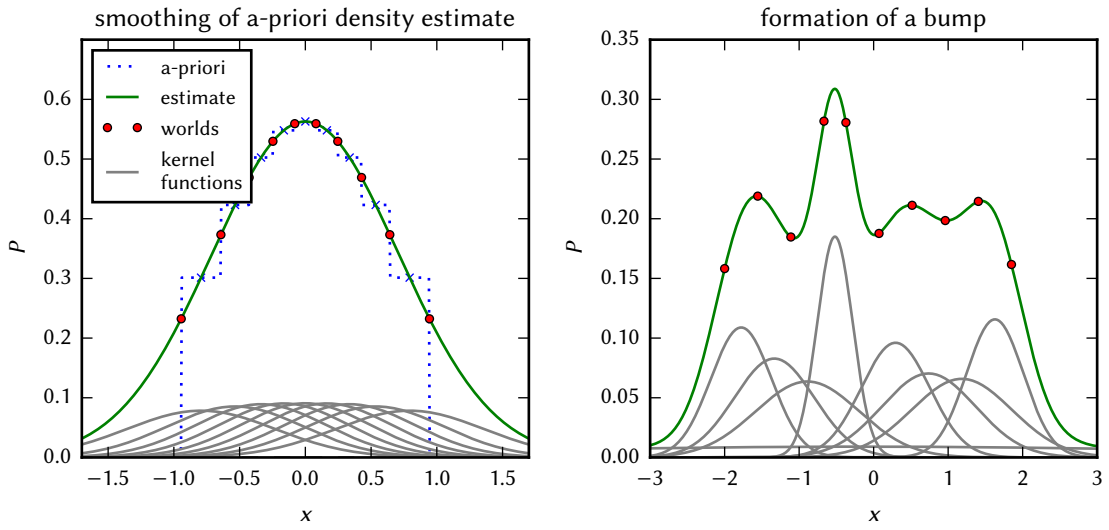

Figure 2.7.: The left plot illustrates the interpolation of the a-priori density estimate (2.46) with an adaptive kernel estimate, where kernel functions are placed in between the worlds. The right plot shows, how the kernel function placed between two worlds, which have approached each other, very naturally develops a bump between the worlds in the density estimate.

Some remarks about the Gaussinterpolation model

Placing the bump functions in between the worlds, models the repulsiveness of approaching worlds very naturally. If two neighbouring worlds are very close in comparison to the rest of the worlds, the discrete a-priori density estimate $\sim 1/\text{dist}$ will be increased. Consequently this produces a small bandwidth of the corresponding kernel at this position in order to coincide with this increased density estimate. Hence a bump between the worlds is produced in very natural way, which is illustrated in the right hand side of figure 2.7.

Although the Gaussinterpolation model uses the same a-priori density estimate as the MIW toy model, its interworld interaction is of a different type. All worlds interact with all other worlds simultaneously, whereas in the MIW toy model only five neighbouring worlds interact directly. Yet, the influence of distant worlds falls off exponentially $\sim \exp(-\frac{1}{2}((Q_i - Q_j)/h_i)^2)$.

2.3.4. Summary of computational aspects

Up to this point we have introduced three interworld interaction models: the MIW toy model of section 2.2, the adaptive kernel density estimate 2.3.1 with bandwidths given by a square root dependence on the nearest neighbour distances, and the Gaussinterpolation model 2.3.3. Before we will benchmark these models with simple quantum systems in the next section, some general remarks can be made.

Computationally, both the Gaussinterpolation model and the adaptive kernel density estimate have significant disadvantages in comparison to the MIW model. First of all, naive implementations of the

sum in the smooth kernel estimate lead to the worse scaling behaviour $O(N^2)$ compared to the linear scaling of the MIW toy model. Furthermore, calculations of the exponential function in the normal distribution are numerically expensive. These effects are especially bad for the Gaussinterpolation model, because the recursion relation (2.49) to find the bandwidths h_i involves repeated calculations of the density, further slowing down the algorithm. Yet, not many iterations are necessary to calculate the bandwidths up to sufficient accuracy, because the density will only vary slightly during the ground state algorithm.

There are different modifications, which could overcome some of these shortcomings. For example, it is clear that in order to carry out the sum in the smooth kernel estimates, not every term has to be considered, since the normal distribution function falls off very rapidly. Hence for a specific point only nearby Gaussian functions with broad enough bandwidths could be considered. In fact, Ahmed Elgammal, Ramani Duraiswami and Larry S. Davis [14] claim that for Gaussian kernel functions the calculation can be improved to scale linearly.

Alternatively, the Gaussian kernel functions could be replaced with functions of compact support, which would also reduce the number of kernel functions contributing to the density when considering singular points. Yet, finding functions with compact support, which are still smooth enough, has proven to be difficult. Especially in combination with the recursion algorithm to find the bandwidths h_i, using the Gaussian kernel functions has been superior.

Furthermore, calculating the bandwidths of the Gaussinterpolation model by a recursion relation is also unsatisfactory and seems to be a little bit artificially constructed. A direct law for the bandwidths, as in the case of the adaptive kernel density estimate, would not only speedup the algorithm but also pose a much more elegant model.

Now we have set the stage for benchmarking our three different interaction models. To this end we will use two simple quantum system, the harmonic oscillator and the Pöschl-Teller potential, and calculate the ground state via the ground state algorithm comparing the energy values of the respective interaction models with the exact analytic values.

2.4. Survey of different potentials

In this section we use our interaction models, the MIW toy model, an adaptive kernel estimate and the Gaussinterpolation to calculate the ground states of simple systems, where the analytic solutions are already known. Even though these systems are very simple to solve, they are a good benchmark for the constructed interaction models and problems can already be seen for such simple systems.

In all cases we start from a uniform distribution of worlds, i.e. worlds with equal distance to their nearest neighbour. Then, the ground state algorithm explained in section 1.4 is applied. Given a world configuration Q with velocities set to zero, the world positions are integrated for a small time step $\mathrm{d}t$, accelerated by the classical force and the interworld force. Then the velocities are reset to zero, thereby removing all kinetic energy from the system. This is repeated until the world configuration converges. It should be kept in mind that the resulting trajectories do not follow the time evolution of the interaction model, but represent the artificially damped trajectories. Thus, physical interpretations of these trajectories should be made with caution.

Before performing the ground state algorithm the right value of parameter $\mathrm{d}t$ has to be considered. In principle the largest possible value is desired, because it allows the worlds to move by greater distances in each iteration such that the algorithm converges faster. On the other hand if $\mathrm{d}t$ is too big, single worlds can jump too far during one iteration step and can cross other worlds before a repulsive effect of the interworld interaction has built up. Since in one dimension the order of worlds has to be preserved by the non-crossing property, this can easily be checked on the fly during the execution of the algorithm and defines an upper bound for the integration step $\mathrm{d}t$.

2.4.1. Harmonic potential

We start with the simplest of all non-trivial classical potentials with bound states, the harmonic potential. Finding stationary states for this potential is a standard task in any introductory course to quantum mechanics. Nevertheless the exact solutions can be found in appendix A.2.1.

Figures 2.8 and 2.9 show the damped trajectories and their energy values of the ground state algorithm for $N = 20$ worlds. Worlds start from a uniform distribution and are drawn to the center by the harmonic force. The worlds come closer together which increases the repulsive quantum force until it cancel the harmonic force and a stationary configuration is reached. Figure 2.8 clearly shows that all considered models are capable of reaching a good estimate of the exact ground state density. Only the Gaussinterpolation model has problems to reach a stationary configuration and oscillates slightly around the ground state of the system. This problem is probably an artifact of the recursion relation to calculate the bandwidths h_i.

The energy expectation values in figure 2.9 match the evolution of the worlds. The configurations of uniformly distributed worlds in the beginning correspond to a higher energy expectation value, which then reduces during the algorithm, when the worlds converge to the ground state configuration. In the end all energy values coincide with the exact value within an relative error of $2 \cdot 10^{-1}$. The oscillatory behaviour of the Gaussinterpolation model is also present in the energy expectation value. This is no surprise, because the worlds, which oscillate the most in figure 2.8, are the two outer boundary worlds. Since the harmonic potential increases quadratically, oscillations in the outer world positions propagate predominately into the energy expectation value, which explains the huge oscillations there.

In comparison the adaptive kernel estimate and the Gaussinterpolation model converge similarly fast to the ground state of the system, but faster in comparison to the MIW toy model. This indicates that the MIW toy model exhibits a stronger repulsive force in off-state configurations compared to the other to models. This could become important when considering the full dynamical situation.

2.4.2. Pöschl-Teller potential

It is no surprise that using density estimates with Gaussian kernel functions work at least qualitatively in the harmonic case, since the ground state itself is of this form. It has to be checked if the methods also work for other classical potentials which exhibit another ground state than a Gaussian. To this end we repeat the calculations for the Pöschl-Teller potential

$$V(x) = -\frac{\lambda(\lambda+1)}{2}\frac{1}{\cosh^2(x)}\,. \tag{2.50}$$

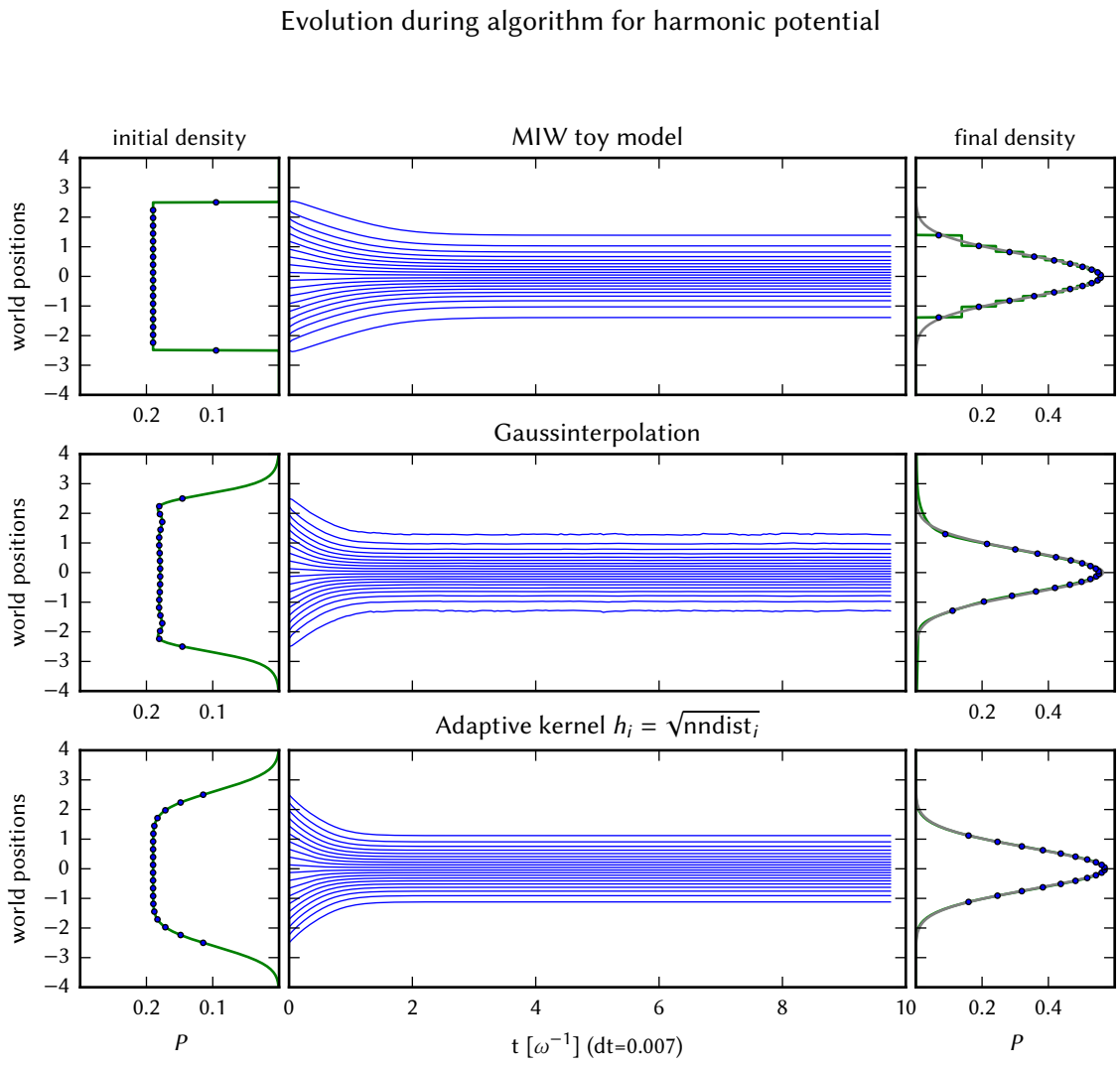

Figure 2.8.: Illustration of the evolution during the ground state algorithm for the harmonic potential $V(x) = \frac{1}{2}x^2$. The initial density estimate is represented by the green line in the left plot, given a uniform distribution of worlds (blue points). The blue lines in the central plots represent the worlds positions during the ground state algorithm. The final density estimate (green line) and world positions (blue points) are shown in the right plots. There, the density of the exact ground state is also drawn as a gray line. The last row shows the result for an adaptive kernel density estimate with an bandwidth function $h_i = \sqrt{\text{nndist}_i}$, where nndist_i represents the nearest neighbour distance of the ith world. Starting from a uniform distribution, worlds move closer to the center at $x = 0$ and converge to the ground state of the harmonic oscillator as the final density plot shows. However, the Gaussinterpolation models shows small fluctuations in the positions of the outer worlds.

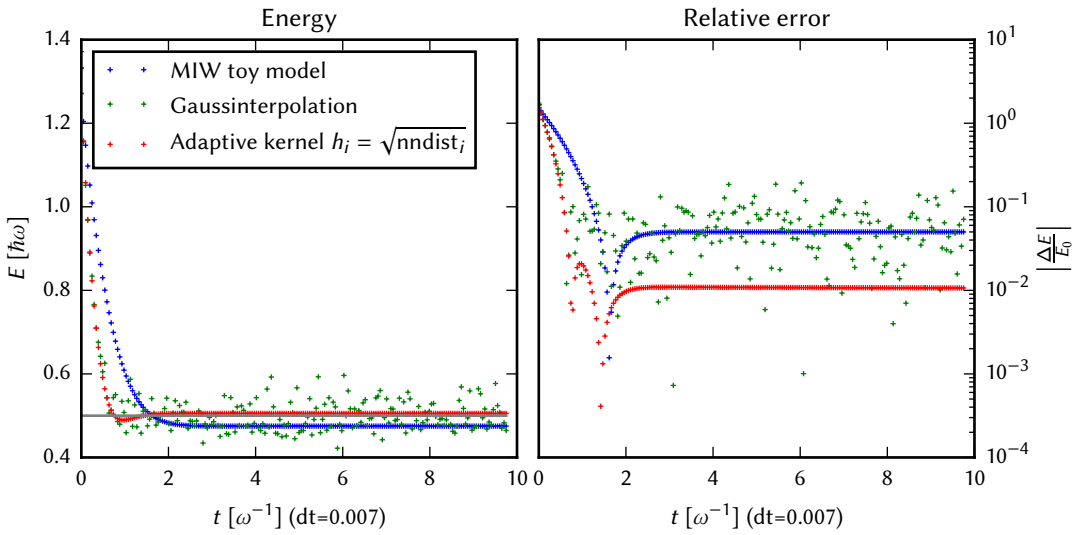

Figure 2.9.: Evolution of the energy expectation value during the ground state algorithm. Absolute energy values are shown in the left plot, whereas the right plot shows the relative error with respect to the analytic solution of the harmonic potential. All considered models reach final energy close to the ground state energy with an relative error below $2 \cdot 10^{-1}$. The best error is achieved by the adaptive kernel model. The worst behaviour is shown by the Gaussinterpolation model, as it also shows huge fluctuations in the energy values.

More details about the Pöschl-Teller potential can be found in appendix A.2.2. For this section we set the parameter λ to $\lambda = 6$. The ground state of the system is then given by the wave function

$$\Psi(x) = \frac{3\sqrt{154}}{32} \frac{1}{\cosh^6(x)}, \tag{2.51}$$

with a ground state energy of $E = -18$.

Figure 2.10 and 2.11 show the results for the Pöschl-Teller potential, similar to the harmonic case. Clearly, all interaction models are capable of reaching the Pöschl-Teller ground state even though it is not of Gaussian form. Both final densities and reached energy expectation values are close to the exact solution of the quantum system. As in the harmonic case, the Gaussinterpolation model shows oscillations around the exact ground state both in the trajectory and the energy pictures. Yet, relative errors are smaller than in the harmonic case.

We will now continue our analysis of our interworld interaction models for excited states, which will lead us to key differences between the different interaction models and to the problem of instabilities in the context of nodes. As a consequence the problem of treating nodes correctly will be thoroughly discussed, and an extension of the ground state algorithm will be developed to also cover the cases of finding higher excited states.

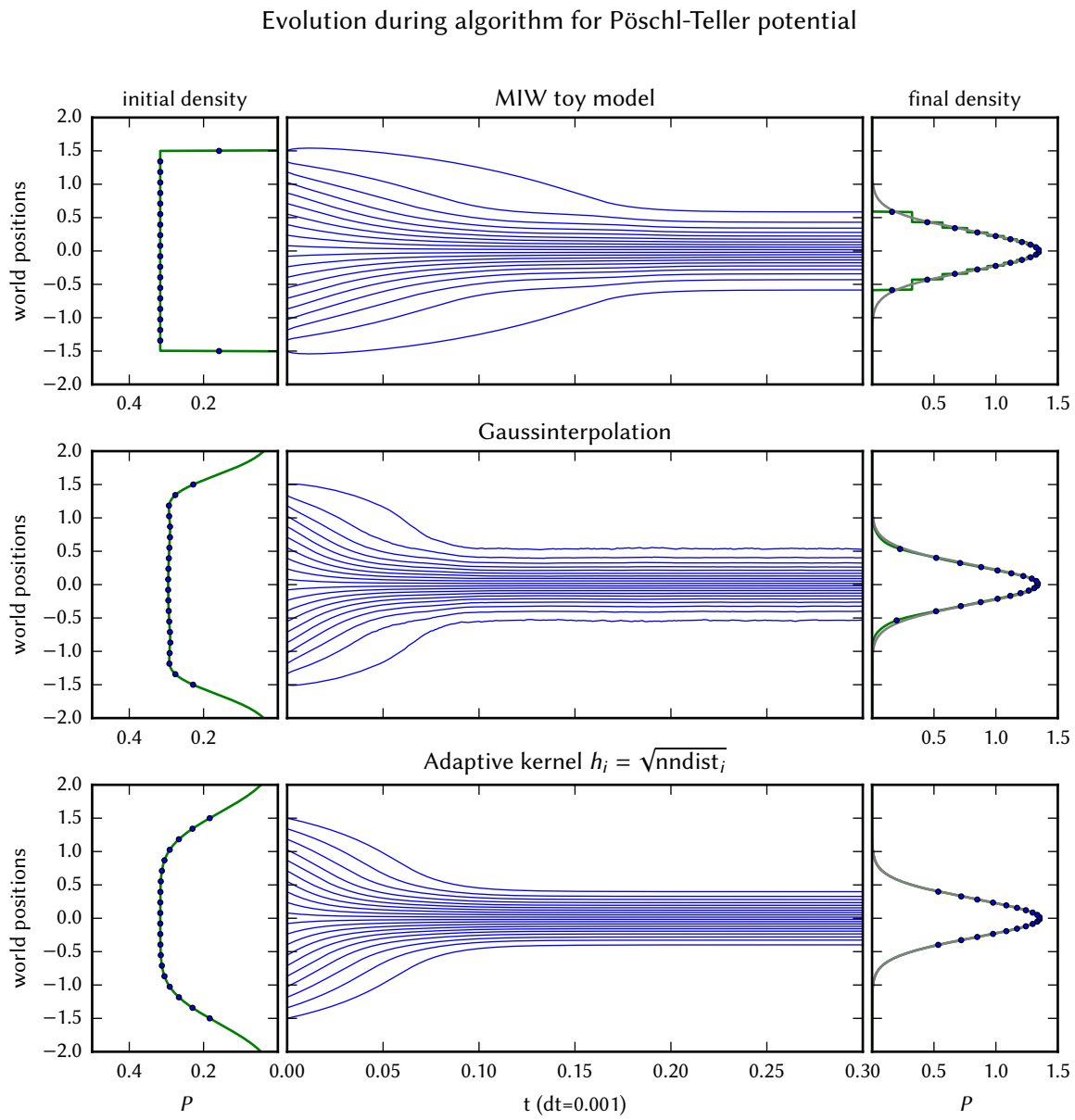

Figure 2.10.: Illustration of the evolution during the ground state algorithm for the Pöschl-Teller potential for $\lambda = 6$ (see A.2.2) similar to the illustration of figure 2.8 The trajectories behave similar to the harmonic case in figure 2.8. Starting from a uniform distribution, worlds move closer to the center at $x = 0$ and converge to the ground state of the Pöschl-Teller potential as the final density plot shows. However, as in the harmonic case, the Gaussinterpolation model shows small fluctuations in the positions of the outer worlds.

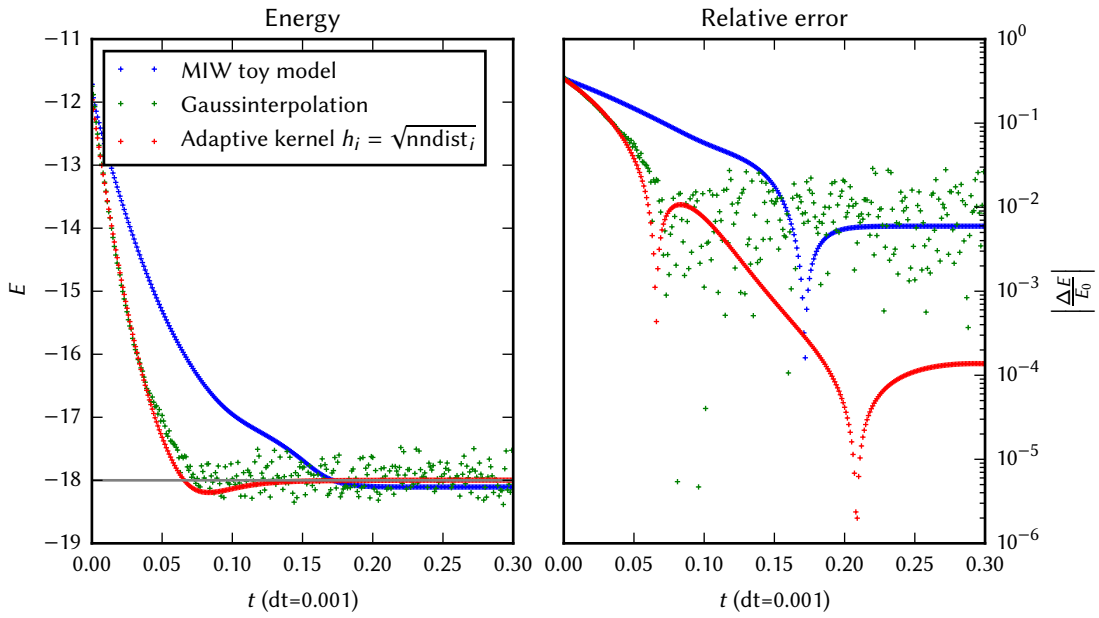

Figure 2.11.: Evolution of the energy expectation value during the ground state algorithm for the Pöschl-Teller potential. Absolute energy values are shown in the left plot, whereas the right plot shows the relative error with respect to the analytic solution of the harmonic potential. All considered models are capable of reaching the ground state energy, although oscillation in the Gaussinterpolation model occur, similar to the harmonic case. In comparison to the harmonic case the relative errors in the energy expectation value are lower and do not exceed values of $3 \cdot 10^{-2}$. The best error is again achieved by the adaptive kernel interaction model. The worst behaviour is shown by the Gaussinterpolation model, as it also shows huge fluctuations in the energy values.

2.5. Excited states

Up to this point we only considered calculating ground states of the harmonic and Pöschl-Teller potential. The interesting question arises, how excited states could be found and if excited states exist with respect to the considered interaction models.

As was discussed in section 1.4, for every energy eigenvalue E of the Schrödinger operator, there exists an eigenfunction Ψ, which is real. For such wave functions the Bohmian vector field also vanishes and worlds do not move. Thus it is plausible that there exist "excited" world configurations, which do not move with respect to our interaction models and are close to the excited states of the exact solution of the quantum system. However, we will see numerical investigations in this section, which suggest otherwise.

2.5.1. Trouble with nodes

In order to search for those excited configurations, we use the probability density $|\Psi_n|^2$ given by an excited state of the stationary Schrödinger equation to generate an initial configuration of worlds according to the definition of the MIW toy model (2.12). Then we apply the ground state algorithm and monitor the world configuration and the corresponding energy during the algorithm. Here we use again the harmonic potential and the MIW toy model as the interaction model and increase the number of worlds to $N = 100$ to be closer to the exact dynamics given by the Bohmian guiding law.

Although it was assumed, that the sampled configuration is close to a possible excited one, it was not expected to be a stable configuration or to reach the "excited" configuration within the algorithm, but rather to decay to the ground state as in the section before. We assumed that if an excited configuration existed, it would probably pose an unstable fixed point in our ground state algorithm with respect to the chosen interaction model. Thus, the sampled configuration should converge to the ground state, since due to numerical inaccuracies we could never hope to hit the suspected "excited" configuration exactly. Instead, it was expected that the sampled configuration would stay close to the initial configuration for a significant amount of iterations and therefore need more iterations to reach the ground state than a uniform distribution of worlds or that at least some distinctive feature in the energy value during the algorithm should be visible.

The damped trajectories of such simulations for the first and second excited state of the harmonic oscillator are shown in figure 2.12. Clearly, both configurations are unstable as expected and converge to the ground state. However, in the beginning there is no apparent timescale, in which the worlds stay close to their initial configurations. On the contrary, the corresponding energy values in figure 2.13 suggest that these configurations converge even faster to the ground state than uniformly distributed initial configurations.

Besides the first and second excited state, additional initial states have been investigated for the energy plot in figure 2.13 including a superposition of ground and first excited state. Clearly, all initial configurations converge to the MIW ground state. Especially the second and third excited state, together with the uniformly distributed initial configuration, show exponential decay with no qualitative difference. Starting from an excited state does not take longer than an uniformly distributed configuration and no distinct feature with respect to the excited energies can be observed even on a short timescale within the algorithm. Starting from the superposed state takes even longer

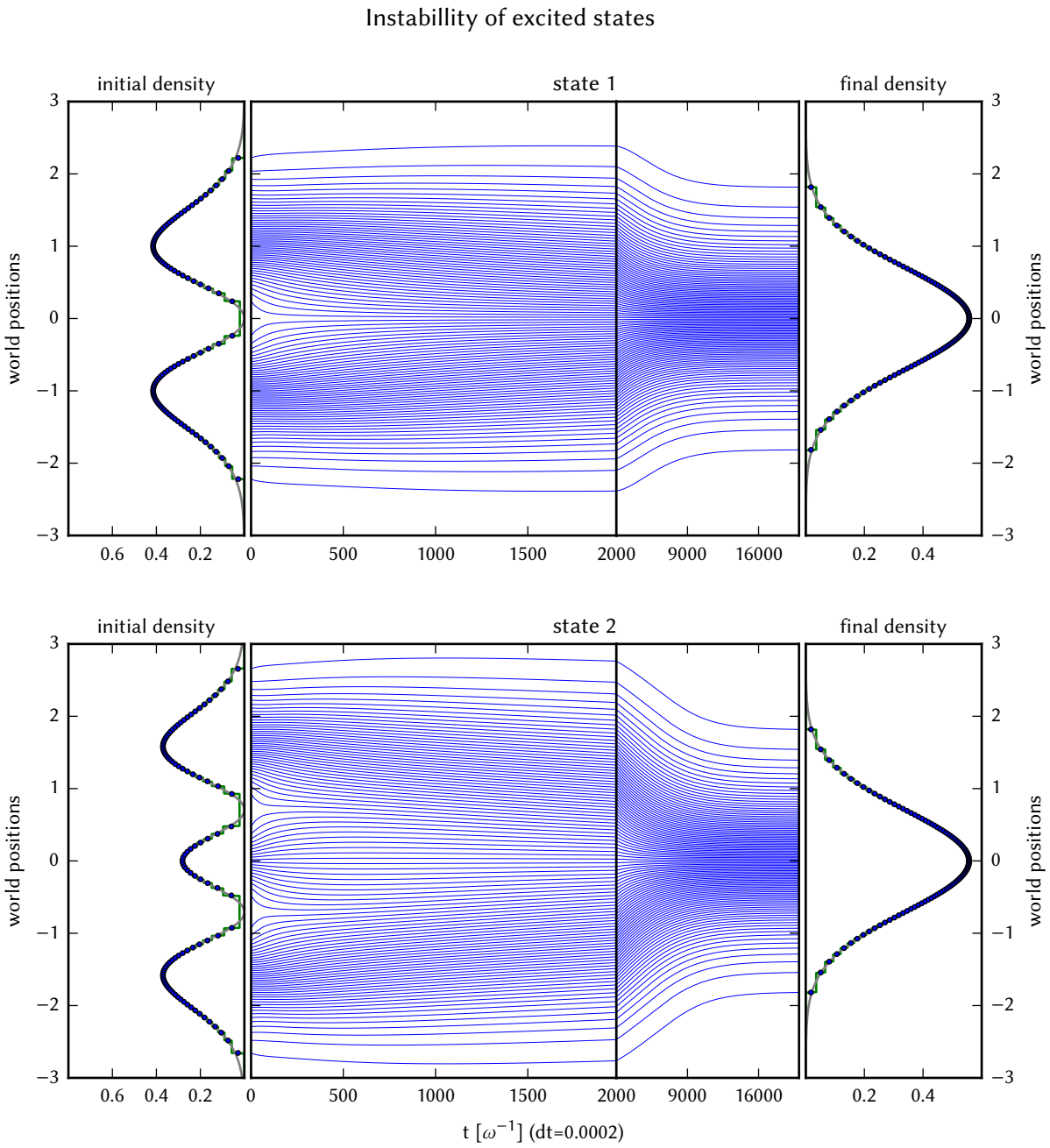

Figure 2.12.: Evolution of $N = 100$ worlds during the execution of the ground state algorithm with 10^8 iterations and time step dt =2e-4 starting from an initial configuration sampled from the first (upper plot) and second (lower plot) excited state of the harmonic oscillator. The left (right) column shows the initial (final) density estimate (green line) given by the world configuration (blue points). Grey lines indicate the corresponding exact analytic probability densities. The centered plot shows the evolution of worlds on two different timescales, the left part focussing on the immediate evolution in the beginning of the algorithm. Both initial configurations are clearly unstable and converge to the ground state as anticipated, but do not stay in the initial configuration for a significant amount of iterations. In the beginning worlds near the nodes of the corresponding excited states move closer together, which then triggers the remaining worlds to also move to the center. In contrast, in regions of high density, far away from the nodes, world positions stay nearly constant in the beginning of the algorithm.

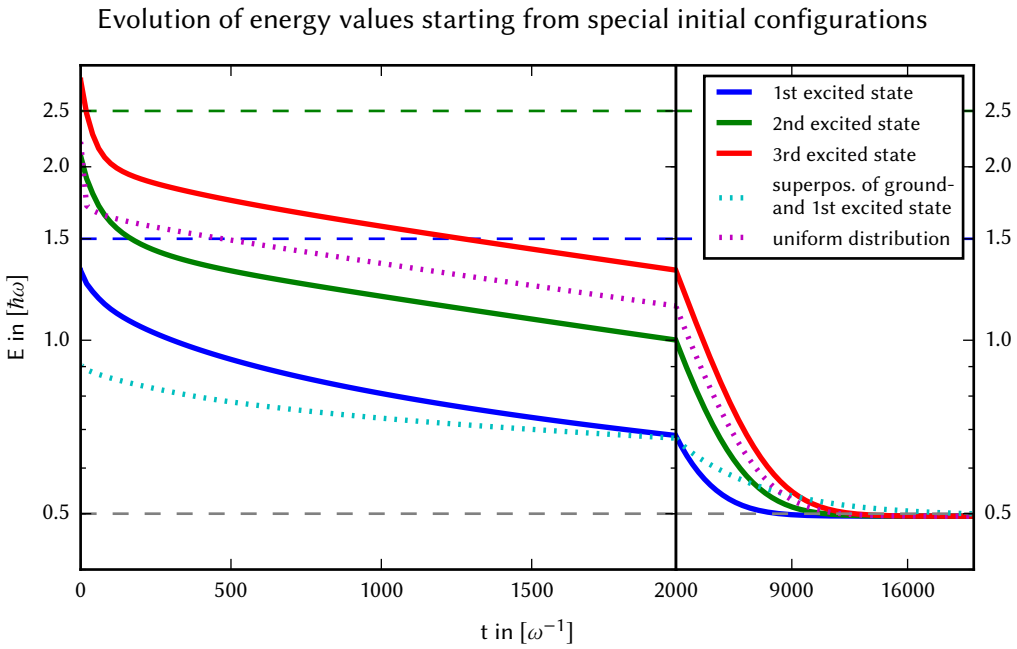

Figure 2.13.: Energy values during the ground state algorithm of the harmonic potential and the MIW toy model for different initial configurations sampled from different excited states of the harmonic oscillator. Dashed lines indicate the exact energy levels of the corresponding excited states. Energy values on the y-axis are scaled logarithmically and the time evolution is divided into two different timescales focusing on the first iterations of the algorithm on the left side.

to reach the ground state. In hindsight this is no surprise, because the world distribution is asymmetrical with respect to the center and the worlds have to move more in total to reach the ground state configuration. Furthermore, energy values of the excited states start significantly below their exact counterparts.

A closer look at the evolution in the beginning reveals that worlds close to the nodes of the corresponding initial wave functions are the origin of the instability of these configurations. In contrast to worlds in regions of high density, worlds around the node do not stay constant, but move closer together, such that the density estimate increases and the approximate feature of a node as a low density estimate gets lost. Similar instabilities could be observed for interaction models which no special treatment for nodes, such as the adaptive kernel density estimate and the Gaussinterpolation model of the section before. Additionally, direct searches for an excited stationary configuration using standard root finding methods have been unsuccessful. This strongly suggests that there is systematic error present in the current formulation of interaction models with respect to nodal regions. Another possibility could be that the number of worlds N was too low and thus the system was too far away from the continuum limit.

In order to rule out the latter, energy values and force of the MIW interworld interaction for a higher number of worlds have been investigated. As before a configuration of worlds was generated given the exact excited states. However, instead of applying the ground state algorithm, the energy and the force of the generated configuration was compared to the exact values directly. This approach

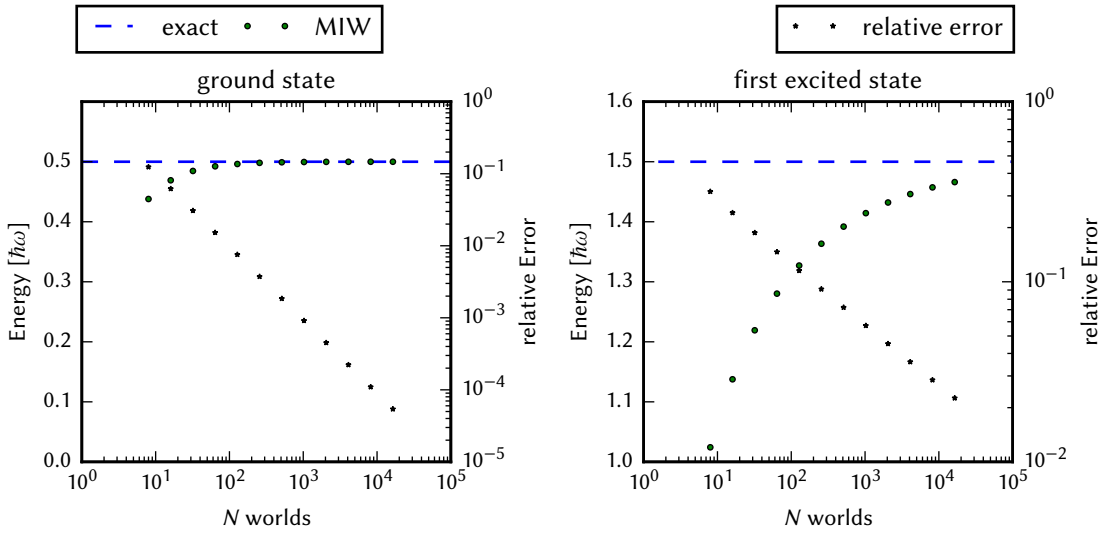

Figure 2.14.: Energy values for the MIW interaction model for increasing number of worlds and different initial configurations. Although the energy is well approximated by the MIW Potential for the ground state even for small N, this is not the case for the first excited state. The energy values lie significantly below the exact values. Admittedly, the energy values seem to converge to the exact values with increasing N, but even in that case the convergence is very slow.

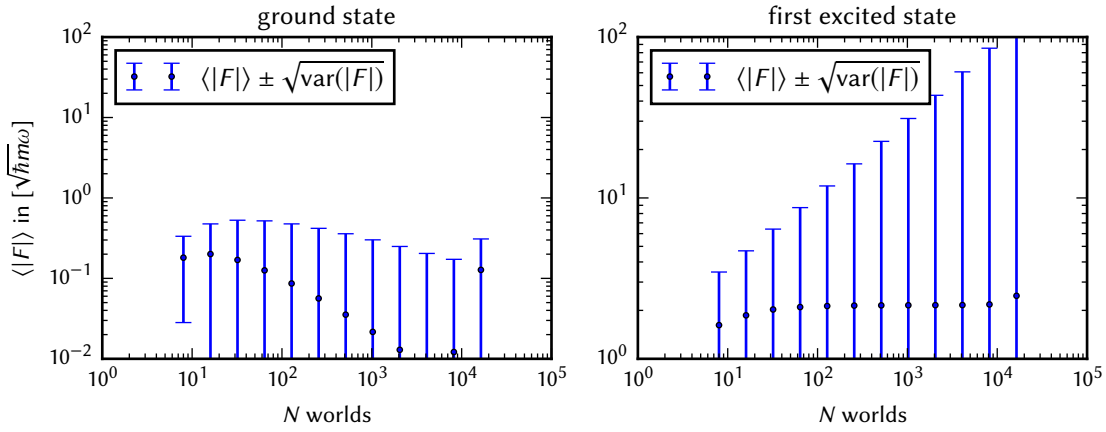

Figure 2.15.: Expectation value of the absolute total force $\langle |F| \rangle = N^{-1} \sum_{i=1}^{N} |F(Q_i)| = N^{-1} \sum_{i=1}^{N} |F_{\text{harmonic}}(Q_i) + r_{\text{miw}}(Q_i; Q)|$ acting on the worlds and the corresponding standard deviation for increasing number of worlds. For increasing number N the total force should point wise (at every world) converge to zero. Although this is the case for the ground state, the mean absolute force values stays constant for the first excited state. For this state the standard deviation also increases with higher number of worlds, which indicates that a systematic error exists for the excited state.

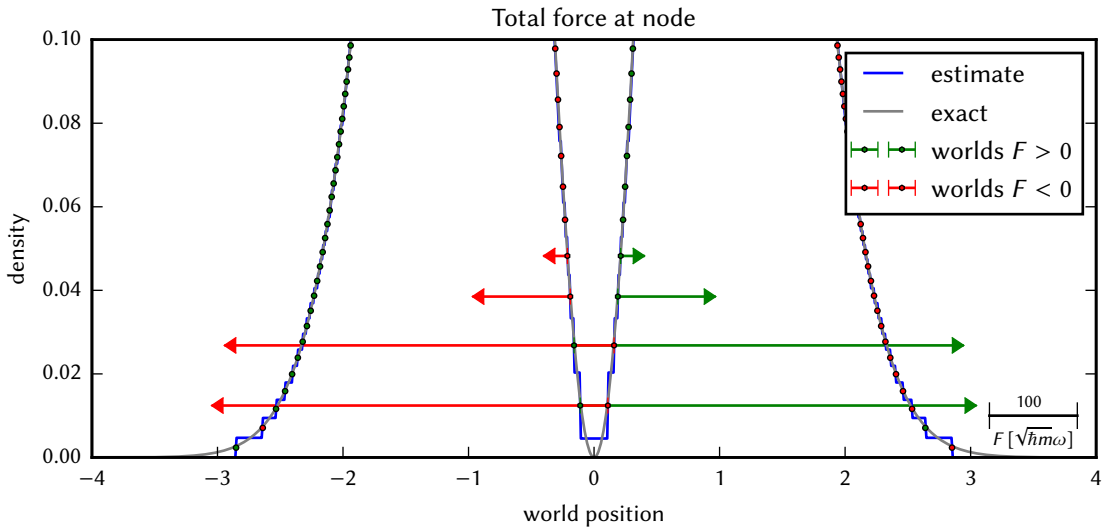

Figure 2.16.: Density estimate of a worlds configuration of 10^3 worlds sampled from the first excited state according to (2.12). Arrows indicate the total force ($F_{MIW} + F_{harm} = F_{MIW} - F_{Bohm}$) acting on each world. In contrast to the Bohmian case the forces do not cancel. Near the node of the wave function at $x = 0$ the force deviates considerably from the exact value. This is the origin of this configurations instability. The error of the 1d MIW force is especially bad in the regions of nodes of the wave function. This could also be observed for higher excited states.

could easily handle a huge number of worlds further approaching the continuum limit.

The results of these investigations are shown in figure 2.14 and 2.15. For increasing N the energy value should approach the analytic value and the interworld interaction force r_{miw} should converge point wise (at every world) to the Bohmian force which cancels the harmonic force for the given states. Thus, the mean absolute force in figure 2.15 should decrease for an increasing number of worlds.

For the ground state this is the case for both the energy and the force values. The sudden jump for N greater than 10^4 in the mean absolute force could be traced back to numerical limitations when sampling the worlds. In contrast, the energy of the first excited state could not be reproduced for even a very high number of words above 10^4, although they appear to converge to the first excited energy value for increasing N. The mean force plot for the excited state highlights the problem more clearly, as the mean force does not decrease and even the variance increases linearly. This indicates that at least at single worlds, the MIW force does not converge to the Bohmian force, thus a systematic error must exist, which cannot be fixed by further approaching the continuum limit.

We have already identified the regions around the node as the origin of the instability of excited states. Figure 2.16 illustrates the region around the node for a sample of $N = 10^3$ worlds. There it becomes clear that the systematic error in the mean absolute force values stems from the worlds surrounding the node at $x = 0$. The two worlds to the left and right respectively are pulled to the center by a strong force. In fact it could be verified that these four worlds pose the main problem in the MIW interaction model, as the forces acting on all other worlds could be reduced to zero by manually fixing the four worlds and applying the ground state algorithm.

Reexamining the interworld force of the MIW toy model (2.28), these four worlds in the vicinity of the node are the only ones which interact with worlds across the node, because the interworld force at Q_i only involves the two neighbouring worlds on either side, i.e.

$$r_{\mathrm{miw}}(Q_i; Q) \equiv r_{\mathrm{miw}}(Q_i; \{Q_{i-2}, Q_{i-1}, Q_i, Q_{i+1}, Q_{i+2}\}) .$$

Clearly the approximations which were used to derive the MIW interaction are unable to capture the correct behaviour when nodes are involved. The corresponding density estimate is strictly positive and cannot reproduce the node in the estimate adequately, and the discrete density values around the node are not sufficient, to estimate the necessary derivatives correctly.

This problem with nodes is actually no surprise, because it is already present on a purely theoretical level when the original Bohmian guiding law

$$\dot{\mathbf{Q}} = \Im \frac{\nabla \Psi_t}{\Psi_t}(\mathbf{Q}) \tag{2.52}$$

is considered, which becomes singular at nodes of the wave function and thus the dynamics for trajectories moving into nodes is not well-defined. Nevertheless from a pure theoretical standpoint these trajectories pose no problem, because they only occur for very special initial configurations. This has been established by Berndl [15], who showed that for physical relevant wave functions and potentials global solutions exist for almost all initial conditions with respect to the $|\psi|^2$-measure; or in other words that the set of bad initial conditions of Bohmian trajectories running into nodes has measure zero.

However, integrating the actual Bohmian trajectories numerically already becomes problematic when worlds only approach the vicinity of the singularity of a node, as Wyatt et al. [4] recognized within their algorithm based on a discretized version of the hydrodynamical field equations (1.13) and (1.14). They resolved this problem by identifying these critical areas on the fly during the algorithm and used the superposition principle to either decompose the wave function into node free components or to introduce an additional wave function to cover up the node. These techniques, however, cannot be adapted to our problem, because the superposition principle is not accessible on the level of the probability density and the quantum potential.

Enforcing nodes

In the last paragraph it was discussed that our simple interaction models are unable to treat nodes correctly. Since any higher excited state involves at least one node, it is clear that we have to modify our interaction models to be capable of treating nodal regions accurately.

If we reconsider the node problem in figure 2.16 and forget about the exact solution given by Bohmian mechanics, the movement of the worlds is actually no surprise. As was stated before, the force given by the quantum potential tends to reduce the “curvature” of the density. From this standpoint, the worlds around the node move exactly how they should, namely to the center. In doing so the density estimate at the node is increased and thus its “tension” is reduced. It is clear that our density estimate only given by our world configuration simply is not capable to contain the information about a node at $x = 0$. That is, the density estimate always remains strictly positive between worlds and thus cannot reproduce the correct behaviour when nodes occur. This applies to all considered density estimators so far.

Consequently, somewhere in the derivation of our interaction model the information must have got lost. In fact, this loss can be traced back to the derivation based upon the hydrodynamic formulation of Bohmian mechanics. The first step of this formulation consist in rewriting the wave function Ψ in polar form with probability density P and phase S, i.e. $\Psi_t = P^{1/2} \exp iS_t$ (see equations (1.6) and (1.7)). Considering the wave function for the first excited state of the harmonic oscillator

$$\psi(x) = \frac{\sqrt{2}}{\sqrt[4]{\pi}} x \, \exp\left(-\frac{x^2}{2}\right), \tag{2.53}$$

this corresponds to

$$\begin{aligned} P(x) &= \frac{2}{\sqrt{\pi}} x^2 \exp\left(-x^2\right) \\ S(x) &= \begin{cases} 0 & \text{for } x > 0 \\ \pi & \text{for } x < 0\,. \end{cases} \end{aligned} \tag{2.54}$$

Thus, the phase jumps discontinuously by π at the node. This information, however, is not available when we only use the density for our interaction model as we did in section 1.3. Here we see that one essential feature of the density is contained in the phase itself, namely the node corresponding to a phase jump.

This gives rise to the idea of reintroducing phase as a field S_i assigned to each world Q_i to retain the information about a node. If the phase then jumped between two worlds, i.e. $S_i = 0, S_{i+1} = \pi$, we would know that a node has to occur between these two worlds and could adjust our density estimate appropriately. Unfortunately this reintroduced field S would also have to be integrated, which we wanted to avoid in the first place when we constructed our interaction models. In addition it contradicts the whole spirit of modeling quantum phenomena without any reference to a field.

Then again, in our case of real wave functions only values $S_i \in \{0, \pi\}$ are valid, which is why the phase itself would not be of interest in any case. The only interesting information is contained in the existence and the location of a node itself. Therefore, instead of additionally integrating the phase, we use it only as a marker where to enforce the node in our density estimate.

2.5.2. Properties of nodes

Before we put this new idea of enforcing nodes in the density estimate into action, we want to have a deeper look at nodes and their connection to excited states. Surprisingly a lot can be said about stationary states and their nodes, or in higher dimensions nodal surfaces, which in today's quantum mechanics courses are not commonly discussed. Yet, it is difficult to make general statements, because such properties strongly depend on the potential chosen.

We start with an old observation, which dates back to Richard Courant [16], who investigated eigenvalue problems in the context of partial differential equations, even before Schrödinger introduced his wave mechanics. Adapted to our case of Schrödinger type differential operators, he states that if the eigenfunctions of a self-adjoint Schrödinger operator on a domain G with homogeneous boundary conditions are ordered according to increasing eigenvalues (counting multiplicity), then the nodes of the n-th eigenfunction divide the domain G into no more than n subdomains. This theorem, sometimes called nodal domain theorem, uses the variational characterization of eigenvalues and is based upon the min-max principle.

There have been more precise proofs of this statement. For example Anconda, Helffer and Hoffmann-Ostenhof proved besides more general inequalities their version of the Courant's nodal theorem in [17], which we shortly want to state here.

Nodal domain theorem: Let $H(\Omega_0) = -\Delta + V$ be a Schrödinger operator on a bounded domain $\Omega_0 \subset \mathbb{R}^d$ ($d \geq 2$) with Dirichlet boundary condition and let $V \in L^\infty(\Omega_0)$ be real valued. If Ω_0 is connected and u an eigenfunction of $H(\Omega_0)$ associated to some eigenvalue $\lambda \in \sigma(H(\Omega_0))$, then

$$\mu(u) \leq \#\{j|\lambda_j < \lambda\} + 1\,, \tag{2.55}$$

where $\mu(u)$ denotes the number of nodal domains of u; i.e. the number of connected components of $\Omega_0 \setminus \overline{u^{-1}(\{0\})}$ and the right side is the number of eigenvalues lying below λ plus one. (For proof see [17].) □

Anconda et al. also indicate that the assumptions on the potential V and the domain Ω_0 can be further relaxed. However, they were more concerned with deriving more general inequalities concerning the spectrum counting functions with respect to different subdomains of Ω_0. This statement also implies that the ground state of such a system does not have any nodes and can be chosen to be strictly positive or negative.

Energy levels and nodal surfaces

Evidently there is a strong connection between nodes and excited states. It turns out that enforcing nodes of the exact solution of the excited state is sufficient to guarantee that world configurations converge to the respective excited states (see section 2.5.4). This can also be proven generally. That is, in order to calculate the excited state's energy it is enough to minimize the energy expectation value with respect to wave functions under the constraint that they have the same nodes as the considered excited state.

Theorem (nodal variational principle): Let $\Omega \subset \mathbb{R}^n$ be connected and let $H(\Omega) := -\Delta + V$ be self-adjoint on $\mathcal{D}(H) \subset L^2(\Omega)$ with Dirichlet boundary condition. Let λ be an eigenvalue of $H(\Omega)$ with eigenfunction ψ and denote the zero set of ψ by

$$N(\psi) := \{x \in \Omega | \psi(x) = 0\}\,. \tag{2.56}$$

Let $\Omega_1, \ldots, \Omega_k$ be the connected components of $\Omega \setminus \overline{N(\psi)}$, called nodal domains, and let $H(\Omega_i) := -\Delta + V$ be the corresponding Hamiltonian with Dirichlet boundary condition on Ω_i. Furthermore for all $i = 1, \ldots, k$ we assume that if $H(\Omega_i)$ has a lowest eigenvalue, it is non-degenerate, i.e. the corresponding eigenfunction is either strictly positive or negative on Ω_i. Then the following holds

$$\lambda_{\text{nodal}} := \inf_{\substack{\varphi \in \mathcal{D}(H(\Omega)) \\ ||\varphi|| = 1 \\ \varphi(x) = 0\ \forall x \in N(\psi)}} \left\langle \varphi, H(\Omega)\varphi \right\rangle = \lambda\,. \tag{2.57}$$

In other words, the same energy eigenvalue can be obtained by minimizing the energy expectation value over all wave function with the same nodal surfaces as the considered eigenfunction ψ.

Proof Clearly it holds that

$$\lambda = \langle \psi, H(\Omega)\psi \rangle \geq \lambda_{\text{nodal}} \,. \tag{2.58}$$

Thus, one has to show that $\lambda_{\text{nodal}} \geq \lambda$. By definition of the nodal domains, the restriction $\psi_i := \psi \big|_{\Omega_i}$ of ψ on one of its nodal domains fulfills the Dirichlet boundary condition $\psi_i \big|_{\partial\Omega_i} = 0$ and therefore $\forall i = 1, \dots, k$ ψ_i lies in the domain of $H(\Omega_i)$.

Furthermore, ψ_i is an eigenfunction of $H(\Omega_i)$ with eigenvalue λ. Since ψ_i is strictly positive or negative by definition of the nodal domains Ω_i and $H(\Omega_i)$ is assumed to be non-degenerate, ψ_i has to be the eigenfunction with the lowest eigenvalue. Hence it holds

$$\inf_{\xi \in \mathcal{D}(H(\Omega_i))} \frac{\left\langle \xi, H(\Omega_i)\xi \right\rangle_{\Omega_i}}{\left\langle \xi, \xi \right\rangle_{\Omega_i}} = \frac{\left\langle \psi_i, H(\Omega_i)\psi_i \right\rangle_{\Omega_i}}{\left\langle \psi_i, \psi_i \right\rangle_{\Omega_i}} = \lambda \,, \tag{2.59}$$

where by $\langle \cdot, \cdot \rangle_{\Omega_i}$ we denote the scalar product of $L^2(\Omega_i)$.

Now let $\varphi \in \mathcal{D}(H(\Omega))$ normalized to one and with the same nodal domains as ψ, i.e. $\varphi(x) = 0 \, \forall x \in N(\psi)$. After plugging φ into the quadratic form of $H(\Omega)$ we can decompose the integral into the nodal subdomains of ψ.

$$\left\langle \varphi, H(\Omega)\varphi \right\rangle = \int_\Omega \varphi^*(x)\, H(\Omega)\, \varphi(x) \tag{2.60}$$

$$= \sum_{i=1}^{k} \int_{\Omega_i} \varphi^*(x)\, H(\Omega)\, \varphi(x) \tag{2.61}$$

Since φ fulfills the boundary conditions on Ω_i, and by $\varphi_i := \varphi \big|_{\Omega_i} \in \mathcal{D}(H(\Omega_i))$ we can rewrite each term with the Hamiltonian $H(\Omega_i)$ on the nodal subdomains

$$= \sum_{i=1}^{k} \int_{\Omega_i} \varphi_i^*\, H(\Omega_i)\varphi_i \tag{2.62}$$

$$= \sum_{i=1}^{k} \left\langle \varphi_i, \varphi_i \right\rangle_{\Omega_i} \frac{\left\langle \varphi_i, H(\Omega_i)\varphi_i \right\rangle_{\Omega_i}}{\left\langle \varphi_i, \varphi_i \right\rangle_{\Omega_i}} \tag{2.63}$$

and with (2.59) it follows

$$\geq \sum_{i=1}^{k} \left\langle \varphi_i, \varphi_i \right\rangle_{\Omega_i} \lambda \tag{2.64}$$

$$\geq \left\langle \varphi, \varphi \right\rangle \lambda = \lambda \,. \tag{2.65}$$

□

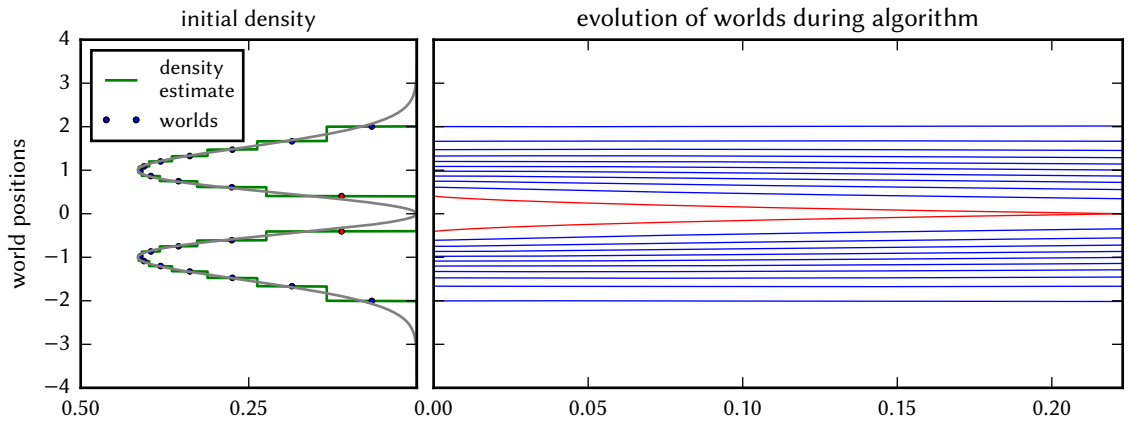

Figure 2.17.: Even if a node is enforced in the density estimate (2.19) of the MIW toy model, the node of the first excited state of the harmonic potential still remains unstable. The two worlds next to the node (red) collide during the ground state algorithm.

2.5.3. Enforcing nodes in MIW

MIW toy model

Our interaction models have to be modified in order to impose nodes in the density estimates manually. For the MIW toy model this can simply be achieved by introducing a function f in the density estimates of equation (2.19), i.e

$$\begin{aligned} P_i^+ &= \frac{1}{N(Q_{i+1} - Q_i)} f(Q_{i+1}, Q_i) \\ P_i^- &= \frac{1}{N(Q_i - Q_{i-1})} f(Q_i, Q_{i-1}) \,, \end{aligned} \tag{2.66}$$

where $f(Q_{i+1}, Q_i)$ vanishes if we impose a node between world Q_i and Q_{i+1} and unity otherwise.

Figure 2.17 shows that only enforcing the node for the MIW model in the density estimate is not enough. In this case the two neighbouring worlds (red) next to the node move to the center until they cross each other, which violates our condition that the order in worlds in one dimension cannot change. On the other hand, compared to 2.12 the dispersion of the overall worlds seems to have improved on short time scales. It turns out that only closest worlds at the node still pose a problem (in contrast to the four neighbouring worlds before). In order to still be able to compare the MIW toy model with the other interaction models, we additionally fix the world positions of the two inner worlds next to the node manually, because this has turned out to be a stable configuration for this model.

Adaptive kernel density estimates

For the adaptive kernel density models more has to be done. Since we use a Gaussian as kernel functions, the resulting density estimate is strictly positive and cannot exhibit a node within in the

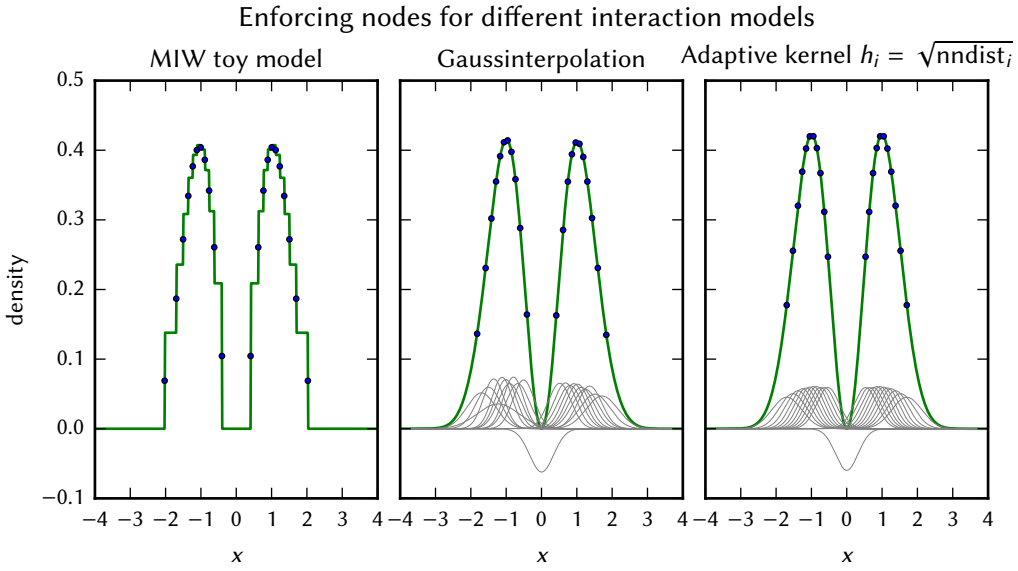

Figure 2.18.: Illustration of density estimates with enforced node at $x = 0$. Gray lines indicate the individual kernel functions, which constitute the density estimate. A negative kernel function has been placed at $x = 0$ in order to impose a node for the kernel density estimates.

model. One method to solve this, is to introduce additional kernel functions at the positions of a node and subtract them from the original kernel density estimate, i.e.

$$P_Q(X) = \frac{1}{C}\left[\sum_{i=1}^{N} \frac{1}{h_i} K\left(\frac{X - Q_i}{h_i}\right) - \sum_{j=1}^{\#\{\text{nodes}\}} \frac{1}{\tilde{h}_j} K\left(\frac{X - \tilde{Q}_j}{\tilde{h}_j}\right)\right], \tag{2.67}$$

where $\tilde{Q}_j$ denotes the corresponding node position. In our case we set the node position $\tilde{Q}_j = (Q_i + Q_{i+1})/2$ in the middle of worlds Q_i and Q_{i+1}, if a node occurs between these worlds. The nodal bandwidths $\tilde{h}_j$ are adjusted in such a way that the density estimate vanishes exactly at the node position. The resulting new density estimate has to be normalized again by adjusting C appropriately.

Unfortunately, this new density estimate is not necessary a probability distribution as P_Q could be negative, but in numerical simulation of the ground state algorithm this has turned out to be negligible.

Gaussinterpolation model

The Gaussinterpolation model allows for a special treatment of nodes. As kernel functions are placed between the worlds, there is already a kernel function present at the location of a node, which can be modified directly by allowing negative bandwidth h_i. As we use a Gaussian function as kernel function this is equivalent to subtracting a kernel function at the node position.

If we then modify the a-priori density estimate of equation (2.46) similar to the MIW toy model, the condition (2.48) results in a negative bandwidth of kernel function at the node. Yet, the recursion

(2.49) has to be replaced in order to deal with vanishing a-priori density estimates. A possible choice is given by

$$h_i \leftarrow \frac{K(0)}{p_{i+1/2} - P(x_{i+1/2}) + \frac{1}{h_i} K(0)} \,. \tag{2.68}$$

This modification is more appealing than the modifications for the adaptive kernel density estimate, since the node can be treated more naturally in the already established framework. Figure 2.18 summarizes the modification in the density estimate of the three models under consideration. For the kernel density models the single kernel functions have been drawn separately in order to indicate the negative kernels, which enforce the node at $x = 0$.

2.5.4. Calculating stationary states

Harmonic potential

With these modifications in place we are ready to test the modified interaction models in the case of the first excited harmonic state. As in figure 2.12 we start with a world configuration sampled from the first excited state of the harmonic oscillator according to equation (2.12), because we assume this world configuration to be close to the stationary excited world configuration of the respective interaction models. We then apply the ground state algorithm in the hope that an enforced node in the density estimate prevents the configuration from decaying to the ground state energy.

Figure 2.19 shows the respective evolution of the worlds during the ground state algorithm. With the enforced node at $x = 0$ the interaction models are capable of reproducing the density of the first excited state of the harmonic oscillator. Yet in contrast to the MIW toy model the inner worlds of the kernel density estimation models do not need to be fixed in order to achieve a stable configuration. Considering the corresponding energy values in figure 2.20 the MIW toy model clearly is unable to reproduce the correct energy values, as its final energy value lies significantly lower than the exact energy value compared to the other models. This indicates that the model still exhibits a systematic error, although the world configuration is stable. This is probably due to the fact that the corresponding potential (2.29) is still unable to capture the correct behaviour at the node, even with an enforced node in the density estimate. In general, fixing worlds manually is quite unsatisfactory, because the exact positions of the corresponding worlds have to be already known in advance.

In contrast, the Gaussinterpolation model and the adaptive kernel density estimate can reproduce both the density and the energy values of the analytic solution at least qualitatively. Overall the Gaussinterpolation shows the best behaviour. Although it also oscillates slightly around the exact state, which manifests itself in the energy values, it lies closer to the exact energy value, whereas the adaptive kernel density estimate reaches an energy value slightly above. Comparing the final density estimates, it is noticeable that in the adaptive kernel estimate the two inner worlds next to the node reach positions further apart from the node than it is the case in the Gaussinterpolation model. This shows that the enforced node of the adaptive kernel density model must exhibit a stronger repellent force that the Gaussinterpolation model. This also explains the higher energy value, because worlds at greater distance to the origin correspond to higher energies for the harmonic potential.

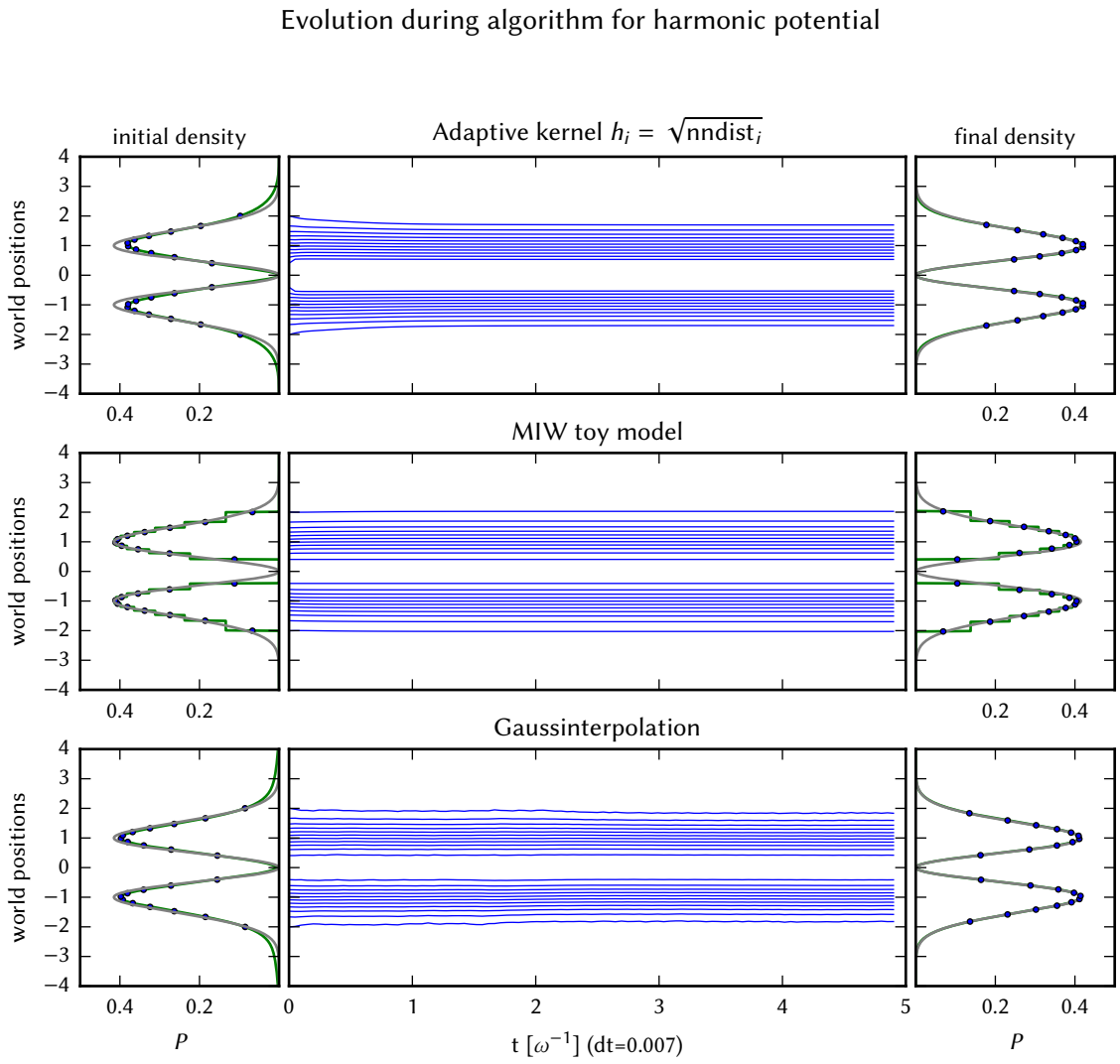

Figure 2.19.: Ground state algorithm applied to worlds with enforced node in the density estimates of the respective interaction models described in section 2.5.3. The initial world configuration was drawn from the exact first excited state of the harmonic oscillator. For the MIW toy model the inner two worlds next to the node were kept fixed to ensure stability (see figure 2.17). The world configurations now converge to the first excited state and do not decay further to the ground state as in figure 2.12 without an enforced node. Similarly in the case of no enforced node, the Gaussinterpolation model oscillates slightly around the stable configuration. Yet, all considered models are capable of reproducing the density of the first excited state.

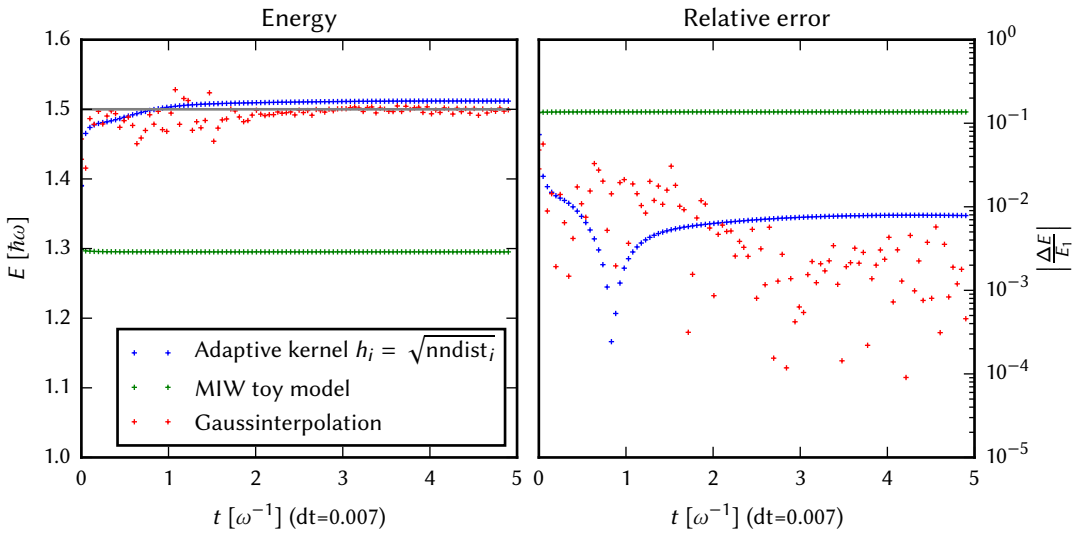

Figure 2.20.: Energy values of the corresponding world configurations of figure 2.19. The MIW toy model reaches a final configuration with an energy value significantly deviating from the analytic solution. In contrast both kernel density models reach the analytic energy at least qualitatively. Although the Gaussinterpolation shows oscillatory behaviour it approximates the analytic energy value best, whereas the adaptive kernel density estimate overestimates the analytic value slightly.

For higher excited states in principle the same procedure can be applied. With higher numbers of nodes, however, we have to use an increasing number of worlds to be able to resolve the density correctly; i.e. numerical errors due to the discretization by finitely many worlds increase.

Pöschl-Teller potential

At last we use the Pöschl-Teller potential to benchmark the algorithm for the first excited state, when only the position of nodes is known. I.e. instead of drawing our initial world configuration from the analytic solution we start from an uniform symmetric distribution of worlds as we did for the ground states, enforce a node at the origin and use the ground state algorithm to find an approximation to the first excited state. As before we have to fix the two inner worlds in the MIW toy model to guarantee stability, which implies that those worlds are fixed arbitrarily by our initial configuration.

The results for these initial conditions can be found in figures 2.21 and 2.22. The MIW toy model reaches a final configuration with a density estimate that resembles the analytic solution. Yet, the two arbitrarily fixed inner worlds distort the final density estimate notably. In this case, those worlds were placed too close to the origin, such that outer worlds also have to come closer to the center in order to be repelled enough by the interworld force in order to cancel the classical force. As in the case for the harmonic potential, the energy values for the MIW toy model are also significantly smaller than the analytic value. Since the whole configuration is closer to the center, this adds another negative contribution to the energy of the configuration.

The Gaussinterpolation model behaves similarly to the cases before. Although the oscillatory be-

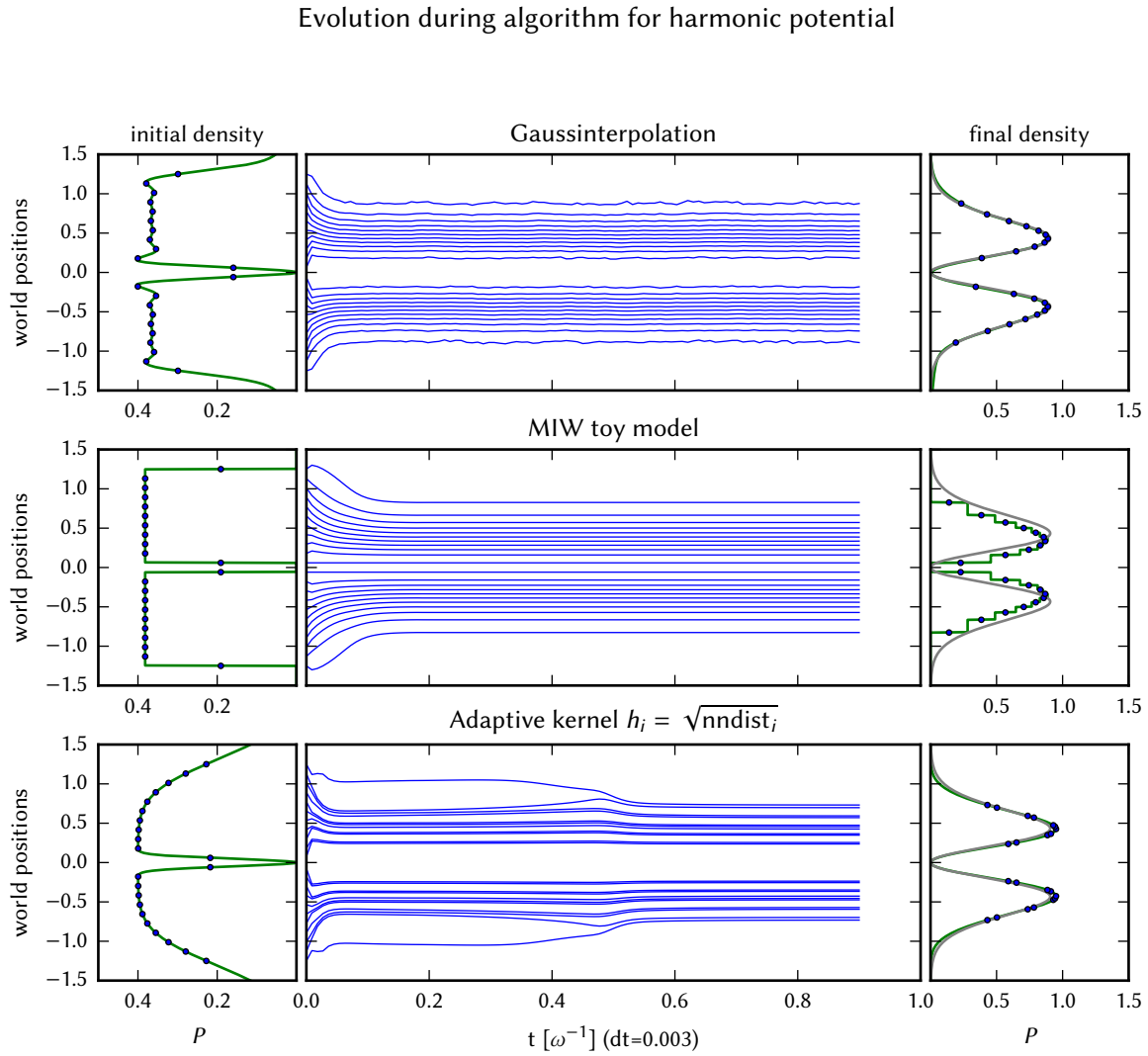

Figure 2.21.: Calculating first the excited state of the Pöschl- Teller potential. In contrast to figure 2.19 the initial world configuration was drawn from a uniform distribution. For the MIW toy model the inner two worlds next to the node were kept fixed to ensure stability (see figure 2.17). Only the kernel density estimate models are capable of approximating the density, whereas the MIW estimate is distorted by the arbitrarily chosen position of the inner two worlds. Interestingly, the worlds of the adaptive kernel density estimate form pair clusters during the algorithm, which do not repel each other as desired for an interworld interaction.

haviour remains, it reaches the correct density estimate and can also approximate the correct energy value. In contrast, the adaptive kernel estimate reveals some interesting shortcomings. While the final energy value and density estimate are capable of approximating their analytic counterpart in a similar quality as in the cases before, the worlds do not repel each other enough and form clusters during the evolution of the ground state algorithm. This results in a worse sampling of the exact density, and henceforth any expectation value, which is approximated by the worlds' configuration alone. This indicates that the adaptive kernel estimate is not capable of modeling the repulsiveness

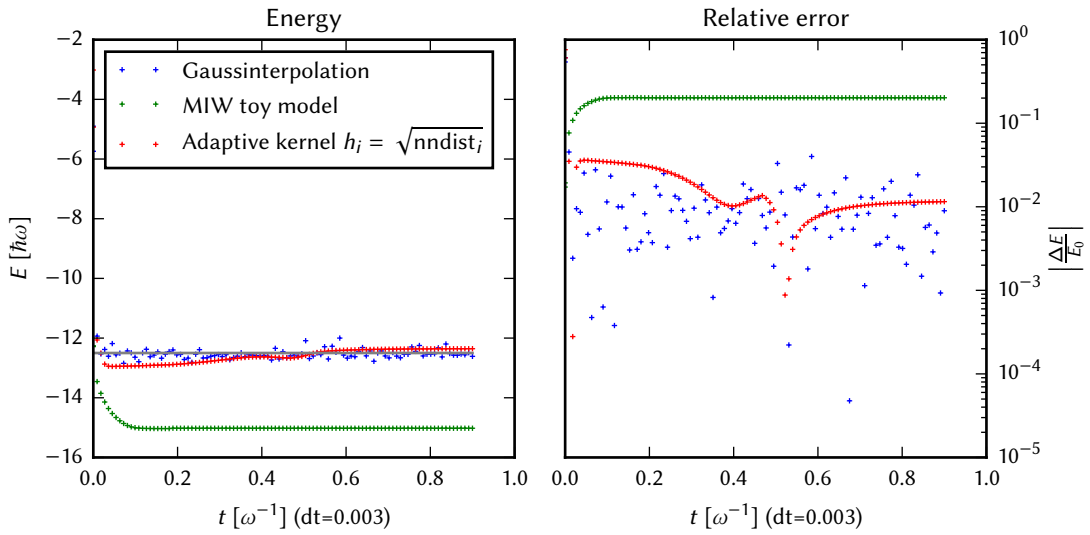

Figure 2.22.: Energy values of the corresponding world configurations of figure 2.21. The MIW toy model reaches a final configuration with an energy value significantly deviating from the analytic solution. In contrast, both kernel density models reach the analytic energy at least qualitatively. In this case, the oscillatory behaviour of the Gaussinterpolation model seems to be more severe, such that both kernel density model can predict the correct energy level similarly well. Yet, the adaptive kernel density estimate is again above the analytic solution.

of the quantum potential correctly.

2.6. Discussion and open questions

In summary, all three models considered were capable of finding the ground states of the considered one dimensional quantum systems. From a computational perspective the MIW toy model was most efficient, whereas both the adaptive kernel density estimate and Gaussinterpolation model were computationally more expensive due to their more costly density estimate. The Gaussinterpolation required additional computational effort for the recursive calculation of its bandwidths.

In contrast, the kernel density based models were more reliable in the situation of excited states with manually imposed nodes. There, the MIW toy model proved to be insufficient and could not reproduce the correct behaviour at the node, even if one was enforced manually. Since the Gaussian model uses the same a-priori density estimate and is capable of dealing with nodes, it is clear that the origin of the problems for the MIW model must lie within the discrete approximations to the density derivatives. Models similar to the MIW toy model with higher order approximation for the discrete derivatives (2.25) have been considered. Although they lead to an improved and more stable behaviour in the vicinity of nodes, new problems arise at the boundary worlds resulting in a globally unstable system. Unfortunately, these problems could not be reconciled satisfactorily, which is why those models have been rejected.

Comparing both kernel density based estimates, the adaptive kernel density estimate is more con-

vincing by design due to its explicit bandwidth function. Yet, the observed clustering of worlds indicates that the model could not guarantee a repulsive enough interworld force between the worlds to guarantee uniform spreading of worlds in configuration space with respect to the represented density estimate. This is the main strength of the Gaussinterpolation model, which retains the uniform spreading similar to the MIW toy model and can estimate derivates sufficiently accurate to handle nodes correctly. Unfortunately, the Gaussinterpolation exhibited small oscillations around the stationary states. These oscillations could originate from an interplay between discrete time integration steps and the recursion relation to calculate the bandwidths. Future investigation could focus on a better way of specifying the bandwidths in both the Gaussinterpolation model and the adaptive kernel density estimate to overcome these shortcomings.

In addition to the harmonic and the Pöschl-Teller potential preliminary investigation of the hydrogen atom and respective radial wave functions have been carried out, which have not been included in this thesis. Unfortunately new problems appeared when implementing the correct boundary condition at $x = 0$, which could not be reconciled easily. In general the question of boundary conditions for a confined quantum system has not been thoroughly investigated and could be interesting for future investigations.

Another future research question could be, whether excited states can be calculated without the explicit knowledge of the location of their nodes. That is, whether it is possible to construct a search algorithm for excited states which only enforces a certain amount of nodes and also incorporates a search mechanism for their location. This could possibly be achieved by incorporating the nodes' locations into the energy minimizing principle.

From a broader perspective, the problems in nodal regions are rather discouraging for the solution of full dynamical quantum systems. In typical dynamical situations nodes develop on the fly due to interference effects and cannot be guessed beforehand as it is possible for excited states. Thus, it is highly questionable whether a many worlds approach solely based on a density estimate can handle these situations.

Nevertheless, the one-dimensional interaction models have been capable of finding both ground and higher excited states, at least conceptually. Therefore we will continue with the interesting question, whether it is possible to construct two-dimensional models interworld interaction models, which can be used to find ground states of two-dimensional quantum systems.

3. Generalisations to higher dimensions

Up to this point we only tried to model scalar one dimensional quantum systems, which provide a first proof of concept. Yet, the question of how to generalize this approach to higher dimensions is still open. Despite the mixed results in the one dimensional case it is still interesting to know, whether a higher dimensional interworld interaction model can be developed in principle. In order to keep things simple, we only consider the two-dimensional case and try to calculate very simple ground states. This is sufficient to reveal some key difficulties when trying to construct higher dimensional interactions.

This chapter is intended to discuss some natural generalisations to the models in the one-dimensional case and difficulties arising in their construction. Corresponding to the one-dimensional models, we investigate two categories: Adaptive kernel density estimates with different bandwidth functions and a generalization of the Gaussinterpolation model to two dimensions.

As in the one-dimensional case, the construction of two-dimensional interworld interaction models strongly depends on the chosen procedure (1.15) of estimating the density from a given world distribution. Although this problem of density estimation has already been addressed in paragraph 2.3.1, there are some important differences between the one-dimensional case and higher dimensional systems, which make it difficult to define an a-priori density estimate necessary for the construction of a Gaussinterpolation type model.

Hence, we will focus on two-dimensional a-priori density estimates first, which will lead us to the problem of finding a partition of configuration space into cells associated to the given worlds distribution. Then, we will use these methods to construct different two-dimensional interworld interaction models, and use both harmonic and Pöschl-Teller potential to benchmark those models.

3.1. Differences compared to one dimensional systems

The one dimensional system is distinguished from the higher dimensional systems by the non-crossing property of world trajectories. This non-crossing of worlds guarantees that the order of worlds is fixed and cannot change during the dynamics. In two dimensions this is no longer the case, because worlds can simply move *around* each other. Thus the constraint of non-crossing is a much weaker condition in any higher dimensional system and there is no longer a preserved ordering of worlds.

However, all one dimensional models, except the adaptive kernel density estimates, used this property at some point in their derivation. In particular this concerns the a-priori density estimates of the MIW toy model and the Gaussinterpolation model of the form $P \sim 1/(Q_{i+1} - Q_i)$. Furthermore there is no canonical way of defining a cumulative distribution function, which can be used to define the

worlds positions as a discretization of configuration space, as it was the case in the MIW toy model (see equation (2.12)).

Additionally, models with discrete approximations of spatial derivatives are also considerably more difficult in higher dimensions. This is especially problematic for our case of world trajectories which form an unstructured grid. That is why the MIW toy model is so problematic to generalize to higher dimensions, for which no two dimensional analog could be found.

3.2. Density estimation in two dimensions

3.2.1. A-priori density estimates via partition

Since in one dimension the a-priori density estimate (2.19) based on a partition of configuration space into intervals has proven most reliable, we try to construct a similar method in two dimensions. Thus, we try to find a partition of configuration space into connected subsets when the only information available is encoded in the world position.

Given such a partition of $\mathbb{R}^2$ into open connected cells $G_{i=1,\dots,M} \subset \mathbb{R}^2$

$$\begin{aligned} G_i \cap G_j &= \emptyset \quad \forall\, i \neq j \\ \bigcup_{j=1}^{M} \overline{G_j} &= \mathbb{R}^2 , \end{aligned} \tag{3.1}$$

we can form an a-priori density by assigning

$$P_i = \frac{1}{M|\mathrm{Cell}_j|} \tag{3.2}$$

to each of the cells, analogously to the interval based estimate in one dimension.

Each cell should be of simple geometric shape, such that the area of each cell is simple and fast to calculate. This immediately leads to the idea of using triangles, as they have the most simple shape in two dimensions. Such a partition into triangles with a given point set as vertices is called a triangulation.

There are many different possible triangulations of a point set Q, but we will only examine the Delaunay triangulation. Yet, alternative triangulations could be interesting for future considerations, since they might allow for a triangulation better adapted to our problem of two dimensional density estimation. De Loera et al. [18] give a thorough introduction into this topic.

Delaunay triangulation

A very common triangulation used in many numerical methods is given by the Delaunay triangulation. There exist efficient algorithms and according to [18] it is considered to be one of the most uniform triangulations, since its triangles are on average close to equilateral triangles, which will be specified below.

Definition Consider $\mathbb{R}^d$ as a metric space with respect to the euclidean metric and a finite point set $Q := \{Q_1, \dots, Q_N\} \subset \mathbb{R}^d$ with $Q_i \neq Q_j \, \forall i \neq j$. We denote by conv(Q) $\subset \mathbb{R}^d$ the *convex hull* of Q, i.e. the intersection of all convex sets containing Q.
The Delaunay triangulation is then defined by the (weak) empty sphere property: A subdivision of conv(Q) into simplices (triangles in $d = 2$) with vertices in the point set Q is called a Delaunay triangulation if for every simplex its corresponding circumsphere (circumcircle) does not contain any points of Q inside.

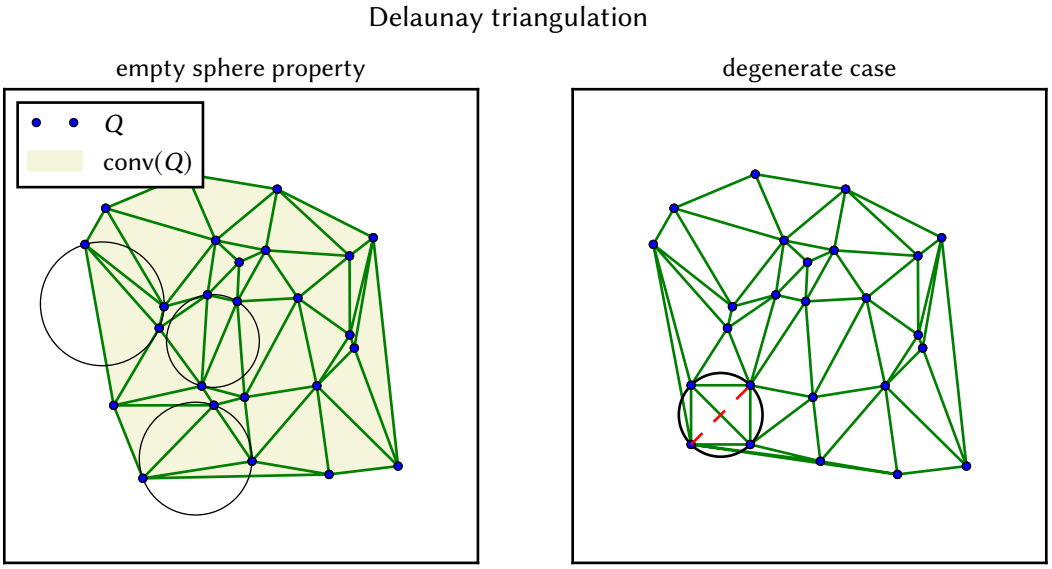

Figure 3.1.: The left hand side illustrates the empty sphere property of the Delaunay triangulation. The triangulation ensures that no point is inside of any circumcircle. The right hand side illustrates the degenerate case, where more than three points lie on a circumcircle. In this case, there are two possible Delaunay triangulation, indicated by a red line.

This definition is called weak, because as pointed out by [18] there exist degenerate point configurations, in which such a Delaunay triangulation is not unique. In these cases there exists at least one circumsphere which passes through more than $(d + 2)$ points, which allows for different subdivisions into simplices fulfilling the above definition. However, we will ignore these degenerate cases, since the numerical library used just picks one of the possible candidates. An illustration of a Delaunay triangulation and the empty sphere property can be seen in figure 3.1, which also illustrates a degenerate case.

The resulting Delaunay triangulations have fairly regular properties.

- They minimize the maximum circumradius of triangles in the triangulation.
- They maximize the minimum circumradius of triangles in the triangulation.
- They maximize the minimum angle in the triangulation.
- All nearest neighbour pairs in the point set are valid facets in the triangulation.

Yet, it does not necessarily minimize the maximum angle. A proof can be found in [18, p. 101].

Voronoi diagrams

Instead of using a triangulation of a point set to subdivide configuration space, there is another very natural subdivision, called Voronoi diagram. It is the dual graph of the Delaunay triangulation and very naturally incorporates a notion of spatial proximity. However, the partition is made up from irregular polygons, which are more difficult to handle computationally.

Definition Consider $\mathbb{R}^d$ as a metric space with respect to the euclidean metric and a point set $Q := \{Q_1, \dots, Q_N\}$ with each $Q_i \in \mathbb{R}^d$ and $Q_i \neq Q_j \, \forall i \neq j$, then for each point the Voronoi cell is defined by

$$\mathrm{VorCell}_i := \left\{ X \in \mathbb{R}^d : \|X - Q_i\| < \left\|X - Q_j\right\| \ \forall j \neq i \right\} , \tag{3.3}$$

i.e. the set of all points X, which are closer to Q_i than to any other point of the point set Q. We call $\mathrm{VorCell}_i$ an *inner cell* if it is bounded, an *outer cell* if it is unbounded. The Voronoi cells form a partition

$$\begin{gathered} \bigcup_{i=1}^{N} \overline{\mathrm{VorCell}_i} = \mathbb{R}^d \\ \mathrm{VorCell}_i \cap \mathrm{VorCell}_j = \emptyset \quad \forall i \neq j \, , \end{gathered} \tag{3.4}$$

and it's dual graph is given by the Delaunay triangulation (for a proof see [18]). Here duality means, that two points are connected within the Delaunay triangulation if their corresponding Voronoi cells have a common edge. Furthermore, the line in the Delaunay triangulation is perpendicular to the corresponding common edge of the Voronoi cells. This is illustrated in the right hand side of figure 3.2.

Nearest neighbour estimate

As an alternative to a partition of configuration space we will also consider the much simpler nearest neighbour estimate introduced in section 2.3.1 as an a-priori density estimate. In fact the estimate given by a partition and nearest neighbour estimate in one dimension were essentially the same estimates.

In two dimensions the corresponding density estimate is given by

$$P_Q(X) = \frac{k}{N \pi r_k(X; Q)} \, , \tag{3.5}$$

where in most cases we will use $k = 2$.

Although it avoids the more complicated calculations of forming an a-priori density estimate via a partition, it is a rather crude estimate and can introduce discontinuities in the derivatives, when the nearest neighbour structure changes during the ground state algorithm.

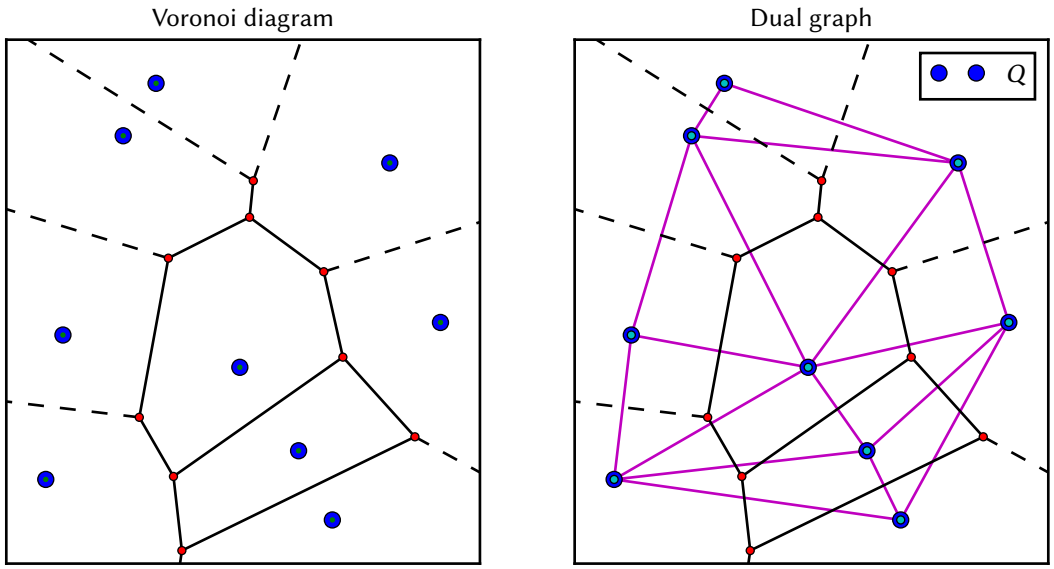

Figure 3.2.: Illustration of a Voronoi diagram in two dimensions. For each point Q_i, there is an associated Voronoi cell, which contains all points in the plain nearest to this point Q_i. Dashed lines expand to infinity and indicate unbounded Voronoi cells. The right plot illustrates the duality between Delaunay triangulation and Voronoi cells.

3.2.2. Kernel density estimates

The adaptive kernel density estimation of section 2.3.1 can be easily generalized by using a product of two kernel functions, each for one dimension. As in one dimension we choose a normalized Gaussian for each dimension, which forms a spherical symmetric kernel function

$$K(X) = \frac{1}{2\pi} \exp\left(-\frac{1}{2} X^T X\right). \tag{3.6}$$

An adaptive kernel density estimate is straightforward to construct:

$$P_Q(X) = \frac{1}{N} \sum_{i=1}^{N} \frac{1}{h_i^2} K\left(\frac{X - Q_i}{h_i}\right) \tag{3.7}$$

$$= \frac{1}{N} \sum_{i=1}^{N} \frac{1}{2\pi h_i^2} \exp\left(-\frac{1}{2} \frac{(X - Q_i)^T (X - Q_i)}{h_i^2}\right). \tag{3.8}$$

As in the one dimensional case a bandwidth function h_i has been introduced. The resulting estimate is smooth and the interworld interaction force can be readily calculated with equation (1.19).

In principle we could also choose individual bandwidth functions for each dimension or even introduce a positive definite two by two matrix $\mathbf{A}$ to replace $X^T X \to X^T \mathbf{A} X$. On the one hand this could be used to have more flexible smooth density model, on the other hand this would also increase the number unspecified parameters, which is unclear how to handle if only world positions are given as a source of information. Additionally, since we will only consider spherically symmetric classical potentials as a test scenario, this simplification seems to be reasonable.

3.3. Discussion of different approaches

In this section different models for the two dimensional approach are discussed. To benchmark the models both the harmonic potential and Pöschl-Teller potential have been used, for which the corresponding one dimensional potentials were added for both dimensions each. Thus, the exact ground state is given by a product state of the corresponding one dimensional ground state in each dimension.

3.3.1. Gaussinterpolation

For a two dimensional Gaussinterpolation type model, several different models have been considered. All of these models use some a-priori density estimate in combination with a smooth density model in form of an adaptive kernel estimator. Exactly like in the Gaussinterpolation model, the a-priori density estimate is enforced in the smooth estimator with choosing appropriate bandwidths h_i, which can be calculated from the same recursion relation (2.49).

Triangle centered estimate

For this first model, we use a Delaunay triangulation and assign to each triangle its corresponding a priori density estimate as per (3.2). In order to combine this with the smooth kernel estimator, the

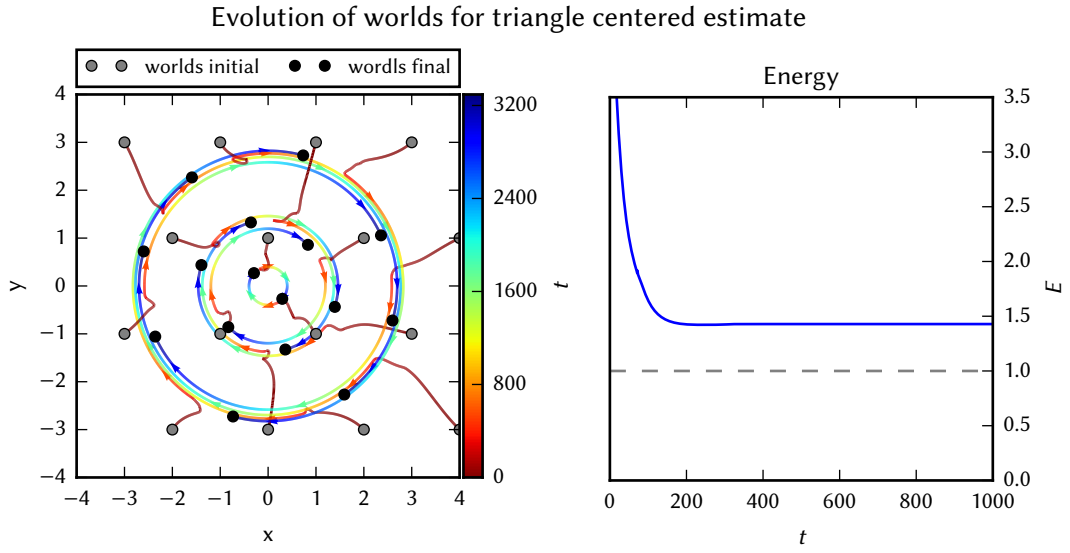

Figure 3.3.: Evolution of worlds during ground state algorithm for the harmonic potential. The corresponding trajectories haven been drawn into the two dimensional plane, where the color changes along the lines represent their time parameterisation. After an initial movement to the center, the worlds begin to circle around the center. The corresponding energy plot on the right shows that the configuration stays at a higher energy level and does not decay to the ground state.

question arises where to put the corresponding kernel functions within the triangle. Following the one dimensional Gaussinterpolation model, it is natural to place the Gaussians at the center of the corresponding triangles.

A further question is, whether the triangulation should be recalculated after each iteration of the ground state algorithm or whether one should calculate the triangulation at the beginning and use the same mesh structure during the algorithm. The latter, however, proved to be inappropriate in simulations. This is due to the fact that the Delaunay structure is not guaranteed to be conserved during the ground state algorithm. That is, worlds can move in such a way that the empty sphere property is violated. This becomes worse when single lines of the mesh cross each other and no longer form a partition of configuration space and the whole algorithm breaks down.

In contrast, refining the Delaunay triangulation after each iteration step showed better results, but this model still remained to be too stiff and a corresponding ground state could not be reached. As an example figure 3.3 illustrates such a situation. Instead of converging to some final configuration, the worlds begin to circle around the origin. The corresponding energy values in figure 3.3 show that this rotating configuration corresponds to an energy value above the exact ground state energy.

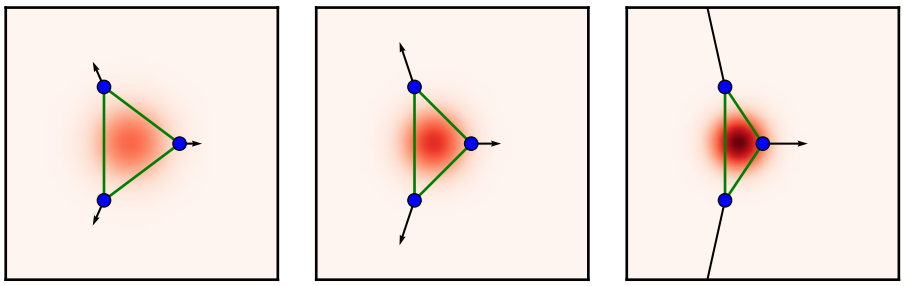

Figure 3.4.: Stiffness of the triangle centered estimate. Red color indicates the density estimates and arrows reflect the corresponding repulsive force. With the right world approaching from the left, the area of the triangle decreases and causes the a-priori density estimate to increase. Since the kernel function is placed in the center of the triangle, a bump develops in the center causing a strong repellent force. Thus the world is unable to pass through the left worlds.

One possible reason for the stiffness of the triangle centered estimate is shown in 3.4. Since the a-priori density values are enforced in the center of a triangle, worlds moving to the center cannot cross the triangle although this should be allowed. Worlds moving to the center reduce the area of the triangle, which leads to an increasing a-priori density estimate. Consequently a bump at the center of the triangle builds up thus strongly repelling the approaching worlds.

As an alternative to the partition based triangle estimate, also a nearest neighbour type estimate has been investigated. In order to overcome the rigidness of the triangle centred estimate, kernel functions were not placed at the center of the triangle, but at the edges of the Delaunay triangulation. The a-priori nearest neighbour estimate was essentially given by the inverse squared length of the triangles' edges. The idea was to model the repulsiveness directly on the edges and thus allowing crossing between worlds. Yet, the damped trajectories of the ground state algorithm fluctuated heavily, such that no convergence was achieved at all.

Worlds centered Voronoi estimate

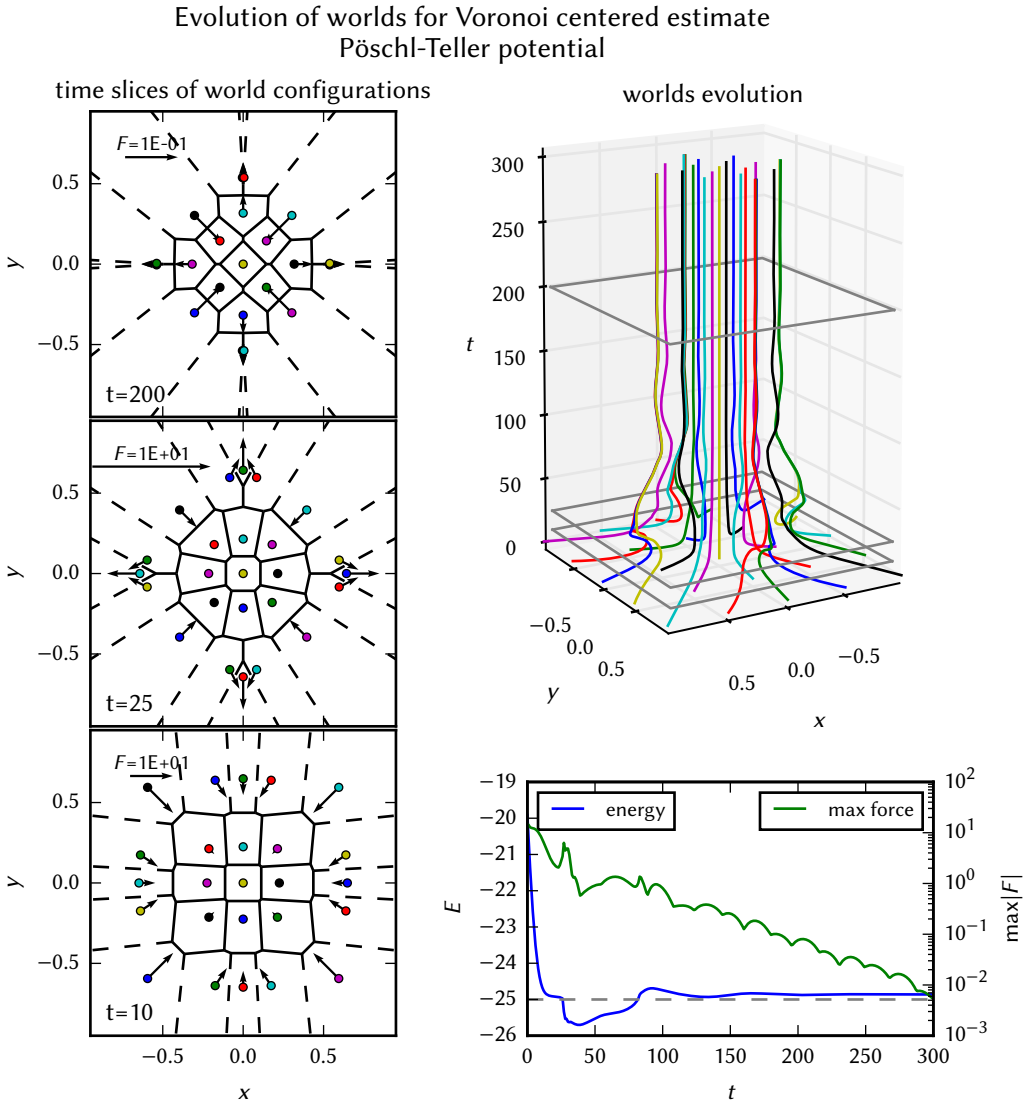

Figure 3.5.: Upper right plot shows the damped world trajectories of the ground state algorithm. Snapshots of the world distribution for different times are shown on the left. Voronoi cells and forces have been added. Additionally to the energy values the maximum of the total force acting on the worlds has been added. Although outer worlds run into each other, the system converges to the ground state at least qualitatively as the energy values and the vanishing total force indicates.

Similarly to the previous model, this model also is composed out of a partition based a-priori density estimate in combination with a smooth density estimator. Instead of Delaunay triangles, it uses Voronoi cells as a partition of configuration space. Since there is one Voronoi cell associated to each world, it is natural to assign the corresponding density (3.2) also to the worlds themselves. The kernel functions are then simply placed at the worlds and the iterative scheme of 2.49 is used to calculate the respective bandwidths.

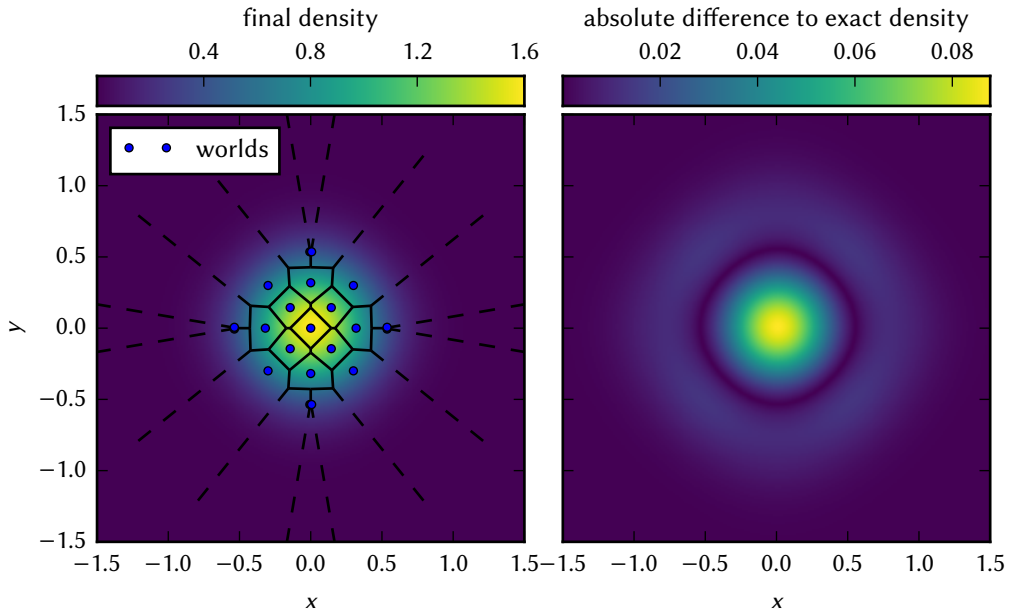

Figure 3.6.: Final density of the worlds centered Voronoi estimate for the Pöschl-Teller potential. The density is fairly close to the exact Gaussian distribution with a relative error below 10%.

There is however one subtlety. The outer Voronoi cells are of infinite size, which corresponds to a vanishing density. This problem already exists in the one dimensional Gaussinterpolation model, although less prominent, because it only concerns the outer two worlds, which are stabilized by the conserved order of worlds. Following the one dimensional model, we apply the kernel functions only to worlds with non-vanishing density and use the recursion relation to enforce the a-pirori density only at these points. Worlds with non-vanishing Voronoi cells only contribute to the kernel density estimate indirectly by delimiting the neighbouring inner Voronoi cells. The idea is to "smear out" the discrete density estimate as in the one dimensional case.

Results of the ground state algorithm for the Pöschl-Teller system can be found in figure 3.5. In contrast to the previous model, the situation has improved significantly. In fact it seems to converge to the ground state of the exact system. The energy value reached is close to the exact solution and even the final reached density in figure 3.6 is fairly close to the exact solution. However, some of the outer worlds with unbounded Voronoi cells run into each other, clearly not exhibiting a repulsive enough effect between each other.

The situation is worse for the harmonic potential, which is illustrated in figure 3.7. For this system, worlds show some severe fluctuations, run into each other, and do not converge to some final state. Also both energy values and forces fluctuate heavily.

For both system the boundary worlds seem to be the most problematic. The fact that they can run into each other can be traced back to the fact that outer worlds with unbounded Voronoi cells do not carry a kernel function in the smooth density estimate. Thus, when two outer worlds approach each other, there is no cumulative effect in the density estimate to form a bump and hence a repelling effect between these worlds.

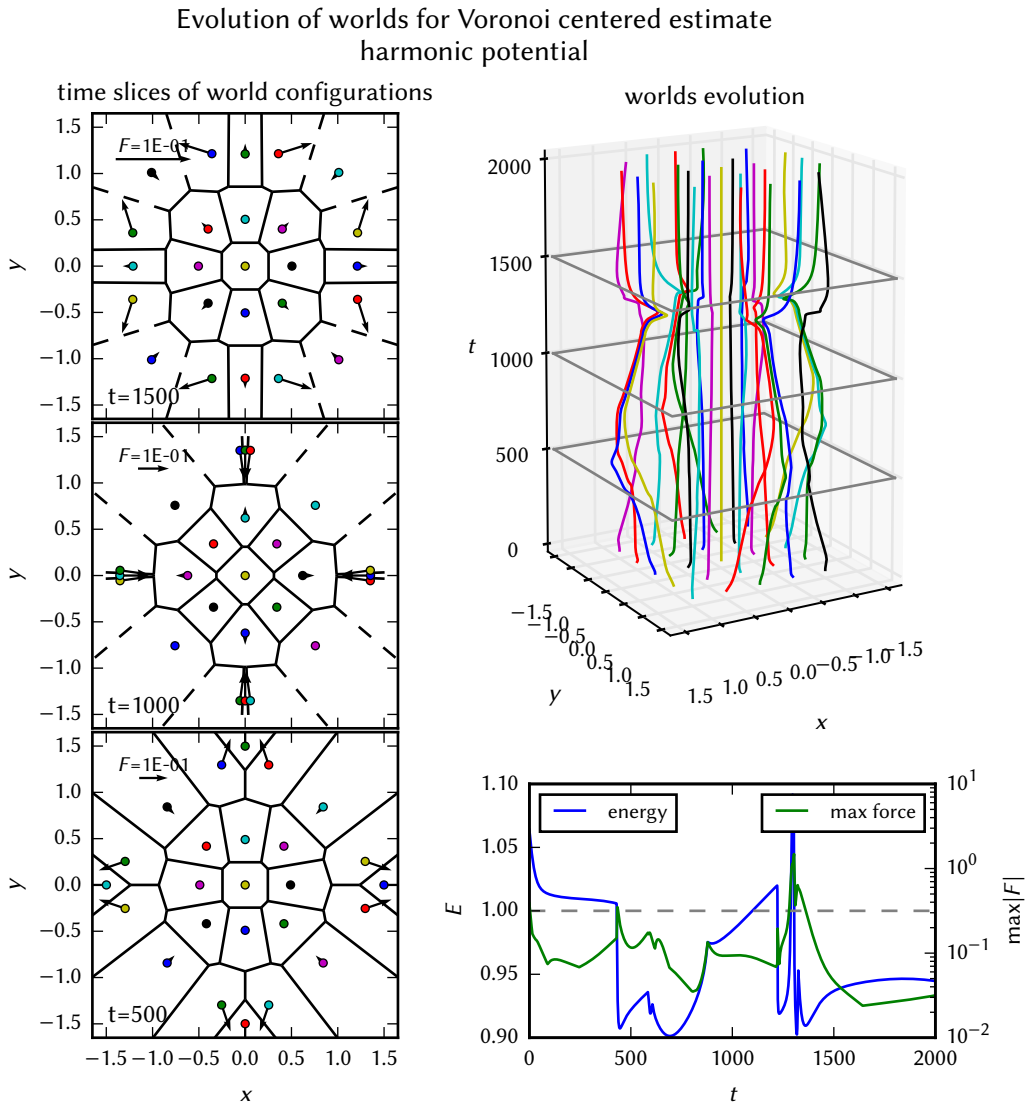

Figure 3.7.: In contrast to figure 3.5, the worlds centered Voronoi estimate behaves worse for the harmonic potential. Worlds oscillate heavily and a final configuration is not reached. This can be observed in both the trajectories and the corresponding energy values.

In order to mitigate the instabilities and fluctuations of the outer worlds a set of fixed worlds surrounding the center with a great distance can be used to ensure that each world carries a bounded Voronoi cell and thus stabilizes the boundary. However, the final configuration reached for such approaches deviated greatly from the exact solution with respect to its density estimate. Alternatively, the symmetry of the worlds which run into each other suggests that the initial world configuration should also respect the spherical symmetry of the potentials. In other words, the collision of outer worlds is conceivably driven by a process to restore the spherical symmetry. A possible solution to this problem could be achieved by allowing outer worlds to merge when they collide into each other.

3.3.2. Adaptive kernel density estimates

In comparison to all other models, the adaptive kernel density estimates are straightforward to generalize to two dimensions. Only the bandwidth function has to be specified. Various bandwidth functions have been investigated, that is, bandwidths as a polynomial of the nearest neighbour distance. Unfortunately no choice has lead to stable convergence to the ground state for both the harmonic and the Pöschl-Teller potential.

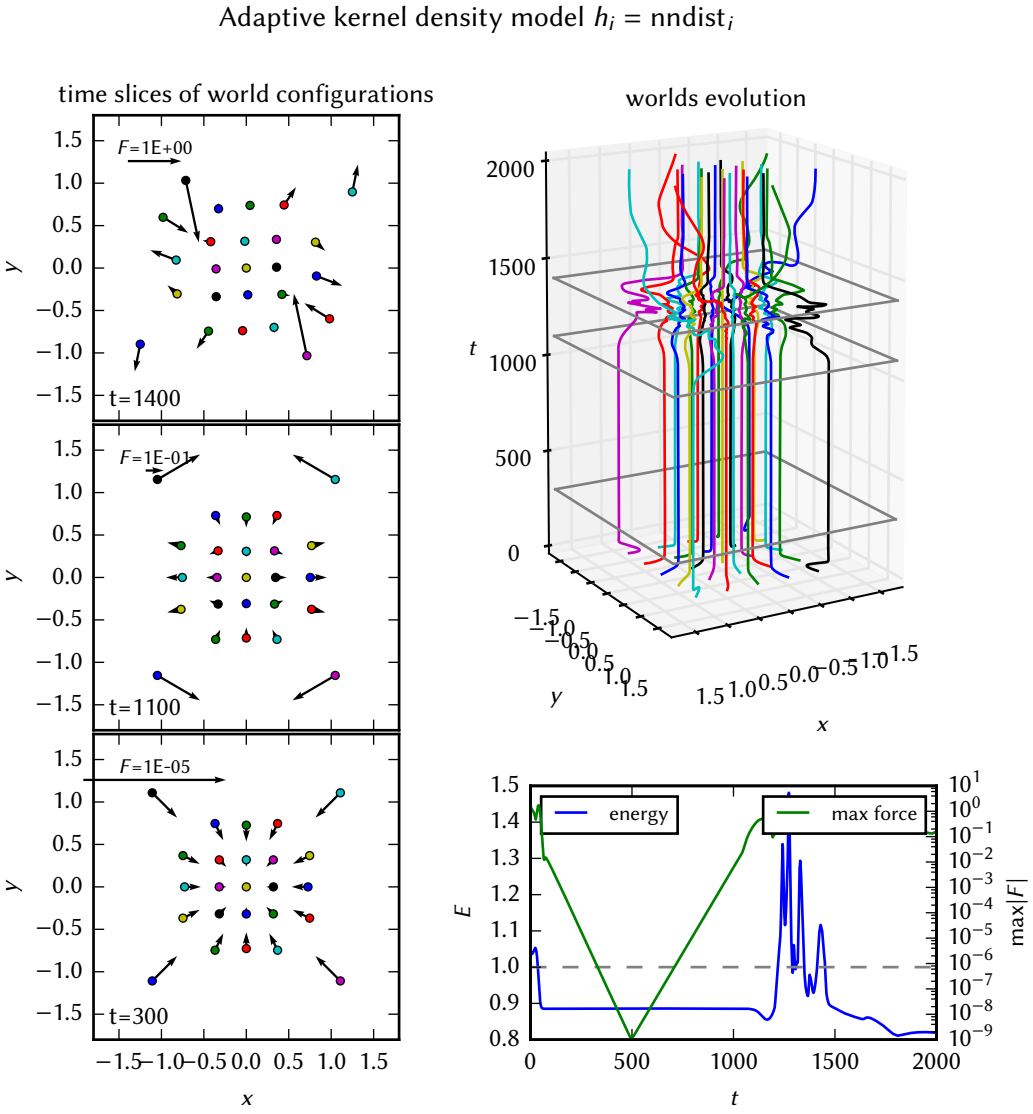

Figure 3.8.: Results of the ground state algorithm for an adaptive kernel density estimate with a linear dependence on the nearest neighbour distance applied to the harmonic potential. The system quickly reaches a seemingly stable configuration, in which it remains for a long time while reducing the maximal force. However, the force at the four outer worlds increases again and rotates outwards away from the center, which leads the system to a state of unstable fluctuations.

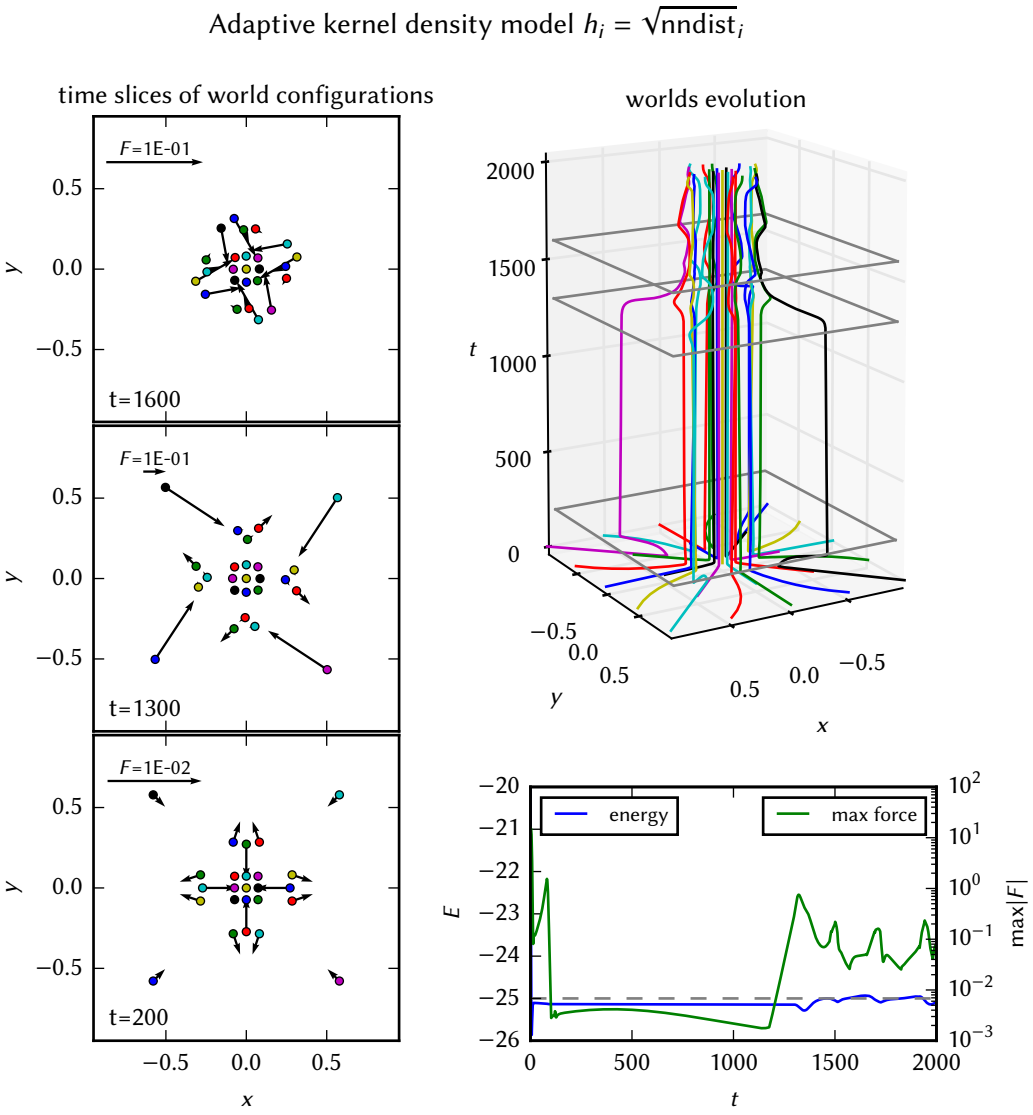

Figure 3.9.: Results of the ground state algorithm for an adaptive kernel density estimate with bandwidths given by a square root law applied to the Pöschl-Teller potential. Similar to figure 3.8 the system remains in a seemingly stable configuration until huge forces in the four outer worlds lead the system to unstable fluctuations. In contrast to figure 3.8, the energy expectation value remains close to the analytic value despite the fluctuations in the world positions.

As an example, figure 3.8 and 3.9 show two evolutions of an adaptive kernel density estimate for two different bandwidth functions. Although both systems seem to converge at first, the configuration reached in the beginning proves to be unstable. After several time integration steps and a decrease in the total force acting on the worlds, they exhibit a sudden increase shaking up the whole configuration of worlds. Consequently, this leads to fluctuations, in which the system remains and does not converge to a final state. Notably the problem seems to arise first in the four outer worlds at the corners.

Unfortunately, the origin of these fluctuations could not be tracked down conclusively. One guess is that the fluctuations are caused by an interplay between the discrete time integration and the bandwidths' dependence on the nearest neighbour distance. Although the nearest neighbour distance changes continuously, it is conceivable that the new worlds' position after a discrete time integration step results in a severe change in the nearest neighbour structure and thus also in the density estimate. This could lead to an opposing repellent effect to the movement before pushing the worlds back into the direction of their original position. Repeating these steps, the worlds could bounce back and forth between different configurations. However, this cannot explain the sudden change of the worlds configuration after having already settled down to an intermediate configuration. Since all worlds carry a kernel function, boundary effects should play a minor role. Yet, the rotating forces in the outer worlds seem to indicate a spatial origin of this behaviour.

3.4. Conclusion

The situation in two-dimensions has proven to be quite challenging and various different two dimensional models showed rather unsatisfactory results. The density estimates of the considered models were either too stiff as for the triangle centered estimate or too flexible resulting in fluctuations in the worlds positions, and could not reach an appropriate estimate of the ground state of the two dimensional quantum system.

The best two dimensional model is the generalization of the Gaussinterpolation model to the worlds centered Voronoi estimate in 3.3.1. Although it also exhibited fluctuating world configurations, it was able to reach the ground state of some quantum systems at least qualitatively. Furthermore, the model's fluctuations seem to arise from problems with the boundary worlds. The question of handling the boundary correctly could be addressed in future investigations to further stabilize the model and improve its energy estimates.

If the boundary situation could not be improved, one would be forced to think about alternative approaches to an interworld interaction model. Though, without new theoretical insight into the question of how to construct a good density estimate in higher dimensions, it is highly questionable that this can be achieved.

4. Summary and outlook

In this thesis various interworld interaction models based upon the many worlds approach of Hall et al. [1] have been investigated. The main objective was to find a new method to solve the stationary Schrödinger equation. To this end both one-dimensional and two-dimensional systems have been investigated with the aim to identify interworld interaction models with good agreement with ordinary quantum mechanics.

In the one-dimensional case three different models haven been analyzed. In addition to the original MIW toy model introduced by Hall et al. [1], two new models have been constructed based upon standard kernel density estimation techniques: the adaptive kernel density estimate (see 2.3.1) with bandwidths given by a square root law, and the Gaussinterpolation model (see 2.3.3).

All three models were capable of approximating the ground states and their respective energy levels of simple one-dimensional quantum system such as the harmonic and Pöschl-Teller potential. For the calculation of excited states instabilities could be traced back to an inappropriate treatment of nodes in the density estimate. This problem could be solved by manually imposing nodes in the density estimate, thus providing a new variational principle for calculating excited states. This principle was successfully applied to the calculation of excited states for the harmonic oscillator and Pöschl-Teller potential.

In this context, the kernel density based models were more reliable, whereas the MIW toy model proved to be insufficient and could not reproduce the correct behaviour at the node, even if one was enforced manually. Yet, both kernel density based models showed other shortcomings. Instead of fully converging, the Gaussinterpolation model reached the exact stationary states with small oscillations around the corresponding exact solution. Conversely, the adaptive kernel density exhibited the formation of world clusters, thus failing to reproduce the correct repulsiveness of the interworld interaction. From a computational perspective the MIW toy model was identified as the most efficient model, whereas both the adaptive kernel density estimate and in particular the Gaussinterpolation model were computationally more expensive due to their more costly density estimate based on Gaussian kernel functions.

In the two-dimensional case various generalizations to the kernel density based models have been constructed. Yet, none of the constructed models could produce reliable estimates for the ground states of the considered test cases. The density estimates of the models were either too stiff, such that they could not reach the ground state, or too flexible resulting in fluctuations in the worlds' positions. The worlds centered Voronoi estimate of 3.3.1 showed the most promising results of a two-dimensional model. Although it also exhibited fluctuating world configurations, it was able to reach the ground state of some quantum systems at least qualitatively. Furthermore, the partition of configuration space into Voronoi cells seems to be the best candidate of constructing a partition based density estimate, since it incorporates the nearest neighbour structure of the worlds distribution in very natural way.

Further investigations of the many worlds approach should focus on this type of two-dimensional models and in particular address the boundary problem, since it seems to be the cause for the fluctuations observed in the worlds centered Voronoi estimate. This could also be beneficial for the calculation of higher excited states, because a method similar to the one-dimensional case has to be developed for the purpose of imposing nodal surfaces, which can be seen as a special kind of boundary condition.

Another future research question could be, whether excited states can be calculated without the explicit knowledge of the location of their nodes. That is, whether it is possible to generalize the nodal variational principle used in one dimension to a new method, for which only the number of nodal surfaces has to be specified without knowing their explicit location. This could possibly be achieved by incorporating the nodes' locations into the energy minimizing principle of the ground state algorithm.

Although some of the difficulties in one dimension could be overcome and simple quantum systems can in principle be solved, the results for the two-dimensional case are rather discouraging. It seems to be very difficult to construct a density estimate in higher dimensions, which can be used for a reliable interworld interaction. Unfortunately, treating high dimensional systems is exactly the main interest for the development of a new algorithm for solving the stationary Schrödinger equation. Thus, without any new theoretical insight into the problem of higher dimensional density estimates, it is highly questionable that the approach of many interacting worlds can significantly improve the treatment of such high dimensional system.

Considering the time-dependent Schrödinger equation, the problems in the nodal regions identified in chapter 2 clearly show that the current many interacting worlds approach will not be able to approximate dynamical situations correctly. In typical dynamical situations nodes develop on the fly due to interference effects and cannot be guessed beforehand as it was possible for the calculation of stationary states. Thus, it is highly questionable whether a many worlds approach solely based on a density estimate will be able to handle these situations in a general setting.

A. Appendix

A.1. Proof of Equivariance

Here we follow the argument presented by Dürr et al. [5]. There also a more detailed discussion of equivariant measures can be found.

Suppose Ψ_t solves the Schrödinger equation, with initial normalized wave function Ψ_0. Let $\Phi_t : \mathbb{R}^{dn} \to \mathbb{R}^{dn}$ be the flow on configuration space, generated by the vector field (1.3), i.e. $\Phi_0(\mathbf{Q}_0) = \mathbf{Q}_0$ and $\frac{\mathrm{d}}{\mathrm{d}t}\Phi_t(\mathbf{Q}_0) = \mathbf{v}^{\Psi}(\Phi_t(\mathbf{Q}_0))$.

Then for any smooth function $f : \mathbb{R}^{nd} \to \mathbb{R}$ with compact support

$$\mathbb{E}^{\Psi_0}[f \circ \Phi_t] \coloneqq \int f \circ \Phi_t(\mathbf{X}) \, |\Psi_0(\mathbf{X})|^2 \, \mathrm{d}X = \int f(\mathbf{X}) \, |\Psi_t(\mathbf{X})|^2 \, \mathrm{d}X =: \mathbb{E}^{\Psi_t}[f] \,. \tag{A.1}$$

In other words, given an ensemble of worlds $\mathbf{Q}_1, \dots, \mathbf{Q}_N$ distributed according to the $|\Psi|^2$-measure, i.e.

$$\mathbb{E}^{\Psi_0}[f] = \int f(\mathbf{X}) \, |\Psi_0(\mathbf{X})|^2 \, \mathrm{d}X \approx \frac{1}{N} \sum_{i=1}^{N} f(\mathbf{Q}_i) \tag{A.2}$$

then $\forall t \in \mathbb{R}$ we can recover the $|\Psi_t|^2$ statistics from the time evolution of the corresponding world trajectories

$$\mathbb{E}^{\Psi_t}[f] = \mathbb{E}^{\Psi_0}[f \circ \Phi_t] \approx \frac{1}{N} \sum_{i=1}^{N} f(\Phi_t(\mathbf{Q}_i)) = \frac{1}{N} \sum_{i=1}^{N} f(\mathbf{Q}_i(t)) \,. \tag{A.3}$$

Proof First we only consider the left hand side of equation (A.1) and apply the simple substitution $\mathbf{X} \to \Phi_t^{-1}(\mathbf{X})$

$$\int f \circ \Phi_t(\mathbf{X}) \; |\Psi_0(\mathbf{X})|^2 \, \mathrm{d}X = \int f(\mathbf{X}) \; (|\Psi_0|^2 \circ \Phi_t^{-1})(\mathbf{X}) \left| \frac{\partial \Phi_t^{-1}(\mathbf{X})}{\partial \mathbf{X}} \right| \mathrm{d}X \tag{A.4}$$

$$=: \int f(\mathbf{X}) \rho_t(\mathbf{X}) \, \mathrm{d}X \,, \tag{A.5}$$

defining the probability density ρ_t, which should not be confused with the $|\Psi_t|^2$-distribution. Instead one should read equation (A.5) as a definition for ρ_t, which is the probability distribution transported along the Bohmian flow Φ. However, we will now see that the transported probability density ρ_t is identical to $|\Psi_t|^2$.

Since $\Phi_0 = id$, clearly $\rho_0(\mathbf{X}) = |\Psi_0(\mathbf{X})|^2$, we can rewrite equation (A.5) as

$$\int f \circ \Phi_t(\mathbf{X})\ \rho_0(\mathbf{X})\,\mathrm{d}X = \int f(\mathbf{X})\ \rho_t(\mathbf{X})\,\mathrm{d}X\,. \tag{A.6}$$

Taking the derivative with respect to time

$$\int \nabla f \cdot \mathbf{v}_t^{\Psi}(\Phi_t(\mathbf{X}))\ \rho_0(\mathbf{X})\,\mathrm{d}X = \int f(\mathbf{X})\ \partial_t \rho_t(\mathbf{X})\,\mathrm{d}X\,. \tag{A.7}$$

Now there exists a very nice trick [5, p. 22]. By replacing $f \longrightarrow \nabla f \cdot \mathbf{v_t}^{\Psi}$ in equation (A.6), and integrating the right hand side by parts, we see that

$$\int \nabla f \cdot \mathbf{v}_t^{\Psi}(\Phi_t(\mathbf{X}))\ \rho_0(\mathbf{X})\,\mathrm{d}X = \int \nabla f \cdot \mathbf{v}_t^{\Psi}(\mathbf{X})\ \rho_t(\mathbf{X})\,\mathrm{d}X \tag{A.8}$$

$$= -\int f\,\nabla(\mathbf{v}_t^{\Psi}(\mathbf{X})\rho_t(\mathbf{X}))\,\mathrm{d}X\,. \tag{A.9}$$

Plugging this into equation (A.7) it follows

$$\int f(\mathbf{X})\ \left[\partial_t \rho_t(\mathbf{X}) + \nabla(\mathbf{v}_t^{\Psi}(\mathbf{X})\rho_t(\mathbf{X}))\right]\mathrm{d}X = 0\,, \tag{A.10}$$

and since this holds for every compact smooth function f, ρ has to fulfill the continuity equation

$$\partial_t \rho_t + \nabla(\mathbf{v}_t^{\Psi}\rho_t) = 0 \tag{A.11}$$

with $\rho_0 = |\Psi_0|^2$.

Furthermore, it can easily be calculated that the same equation holds for $|\Psi_t|^2$, as it fulfills the Schrödinger equation and by using the explicit form of $\mathbf{v}_t^{\Psi}$.

Since both $|\Psi_t|^2$ and ρ_t fulfill the same continuity equation and coincide for $t = 0$ and solutions to these partial differential equations are unique, it follows that $\rho_t = |\Psi_t|^2\ \forall t \in \mathbb{R}$ and therefore equation (A.1) holds. □

A.2. Quantum systems in one dimension

A.2.1. Harmonic potential

The harmonic potential is given by

$$V(x) = \frac{1}{2}x^2 \tag{A.12}$$

and corresponds to a linear force

$$F(x) = -x\,. \tag{A.13}$$

The nth stationary solutions is given by

$$\Psi_n(x) = \left(\frac{1}{\pi}\right)^{1/4} \frac{1}{\sqrt{2^n n!}} H_n(x) \exp\left(-\frac{1}{2}x^2\right), \tag{A.14}$$

with energy values

$$E_n = n + \frac{1}{2}, \tag{A.15}$$

and Hermite polynomials H_n.

A.2.2. Pöschl-Teller potential

The Pöschl-Teller potential is given by

$$V(x) = -\frac{\lambda(\lambda+1)}{2} \frac{1}{\cosh^2(x)}, \tag{A.16}$$

with the force

$$F(x) = -\lambda(\lambda+1) \frac{\tanh x}{\cosh^2 x}. \tag{A.17}$$

It exhibits the stationary solutions

$$\Psi_\lambda^\mu(x) = P_\lambda^\mu(\tanh x), \tag{A.18}$$

where P_λ^μ are the associated Legendre polynomials and $\lambda \in \mathbb{N}^+$, $\mu = 1, 2, \ldots, \lambda - 1, \lambda$. Energy eigenvalues are given by

$$E_\lambda^\mu = -\frac{1}{2}\mu^2. \tag{A.19}$$

The ground state is given by Ψ_λ^λ.

Bibliography

[1] M. J. Hall, D.-A. Deckert, and H. M. Wiseman, "Quantum Phenomena Modeled by Interactions between Many Classical Worlds," *Physical Review X*, vol. 4, Oct. 2014.

[2] J. Crank and P. Nicolson, "A practical method for numerical evaluation of solutions of partial differential equations of the heat-conduction type," *Advances in Computational Mathematics*, vol. 6, no. 1, pp. 207–226, 1996.

[3] "LRZ: SuperMUC Petascale System Description." (see webpage). Accessed: 2016-11-23.

[4] R. E. Wyatt, *Quantum dynamics with trajectories: introduction to quantum hydrodynamics*, vol. 28. Springer Science & Business Media, 2006.

[5] D. Dürr and S. Teufel, *Bohmian mechanics: the physics and mathematics of quantum theory*. Berlin ; London: Springer, 2009. OCLC: ocn302080513.

[6] D.-A. Deckert, D. Dürr, and P. Pickl, "Bohmian grids and the numerics of schrödinger evolutions," in *Quantum Trajectories* (P. Chattaraj, ed.), Atoms, Molecules, and Clusters, ch. 22, CRC Press, 2010.

[7] D.-A. Deckert, D. Dürr, and P. Pickl, "Quantum Dynamics with Bohmian Trajectories †," *The Journal of Physical Chemistry A*, vol. 111, pp. 10325–10330, Oct. 2007.

[8] D. Bohm, "A Suggested Interpretation of the Quantum Theory in Terms of "Hidden" Variables. I," *Physical Review*, vol. 85, pp. 166–179, Jan. 1952.

[9] P. J. Davis and P. Rabinowitz, *Methods of Numerical Integration*. Academic Press, 1984.

[10] B. W. Silverman, *Density Estimation for Statistics and Data Analysis*. CRC Press, Apr. 1986.

[11] A. J. Izenman, "Review Papers: Recent Developments in Nonparametric Density Estimation," *Journal of the American Statistical Association*, vol. 86, pp. 205–224, Mar. 1991.

[12] D. W. Scott, *Multivariate density estimation: theory, practice, and visualization*. Hoboken, New Jersey: John Wiley & Sons, Inc, second edition ed., 2015.

[13] I. S. Abramson, "On Bandwidth Variation in Kernel Estimates-A Square Root Law," *The Annals of Statistics*, vol. 10, pp. 1217–1223, Dec. 1982.

[14] A. Elgammal, R. Duraiswami, and L. S. Davis, "Efficient Kernel Density Estimation using the Fast Gauss Transform with Applications to Color Modeling and Tracking," *IEEE Transactions on Pattern Analysis and Machine Intelligence*, vol. 25, pp. 1499–1504, 2003.

[15] K. Berndl, "Global existence and uniqueness of Bohmian trajectories," *arXiv:quant-ph/9509009*, Sept. 1995. arXiv: quant-ph/9509009.

[16] R. Courant and D. Hilbert, *Methoden der mathematischen Physik*. Springer-Verlag, 1924.

[17] A. Ancona, B. Helffer, and T. Hoffmann-Ostenhof, "Nodal domain theoremsa la Courant," *Documenta Mathematica*, vol. 9, pp. 283–299, 2004.

[18] J. A. De Loera, J. Rambau, and F. Santos, *Triangulations*, vol. 25 of *Algorithms and Computation in Mathematics*. Berlin, Heidelberg: Springer Berlin Heidelberg, 2010.

List of Figures

Ich versichere, die Arbeit selbstständig angefertigt und dazu nur die im Literaturverzeichnis angegebenen Quellen benutzt zu haben.

München, den 22. Dezember 2016